



HAL
open science

Rheology and migration of deformable particles in dense suspensions

Mehdi Maleki

► **To cite this version:**

Mehdi Maleki. Rheology and migration of deformable particles in dense suspensions. Classical Physics [physics.class-ph]. Université Grenoble Alpes [2020-..], 2021. English. NNT : 2021GRALI043 . tel-03628805

HAL Id: tel-03628805

<https://theses.hal.science/tel-03628805v1>

Submitted on 3 Apr 2022

HAL is a multi-disciplinary open access archive for the deposit and dissemination of scientific research documents, whether they are published or not. The documents may come from teaching and research institutions in France or abroad, or from public or private research centers.

L'archive ouverte pluridisciplinaire **HAL**, est destinée au dépôt et à la diffusion de documents scientifiques de niveau recherche, publiés ou non, émanant des établissements d'enseignement et de recherche français ou étrangers, des laboratoires publics ou privés.

THÈSE

Pour obtenir le grade de

DOCTEUR DE L'UNIVERSITÉ GRENOBLE ALPES

Spécialité : MEP : Mécanique des fluides Energétique, Procédés

Arrêté ministériel : 25 mai 2016

Présentée par

Mehdi MALEKI

Thèse dirigée par **Hugues BODIGUEL**, Professeur, Université Grenoble Alpes

et codirigée par **Marc LEONETTI**, chercheur CNRS, CNRS et **Clément DE LOUBENS**, Chargé de Recherche, CNRS

préparée au sein du **Laboratoire Laboratoire Rhéologie et Procédés**

dans l'**École Doctorale I-MEP2 - Ingénierie - Matériaux, Mécanique, Environnement, Energétique, Procédés, Production**

Rhéologie et migration de particules déformables dans les suspensions denses

Rheology and migration of deformable particles in dense suspensions

Thèse soutenue publiquement le **30 mars 2021**, devant le jury composé de :

Monsieur Hugues BODIGUEL

PROFESSEUR, Université Grenoble Alpes, LRP UMR 5520, Directeur de thèse

Monsieur Guillaume Ovarlez

DIRECTEUR DE RECHERCHE, Université de Bordeaux, Laboratoire de futur (LOF), UMR 5258, Rapporteur

Madame Annie Colin

PROFESSEUR, Université Paris sciences et lettres, ESPCI Paris UMR 8231, Rapportrice

Monsieur Laurent Orgéas

DIRECTEUR DE RECHERCHE, Université Grenoble Alpes, 3SR Lab UMR 5521, Président

Monsieur Frédéric Blanc

MAITRE DE CONFERENCE, Université Côte d'Azur, INPHYNI UMR 7010, Examinateur



Abstract

Deformable particles migrate in a sheared suspension. A source of this phenomena would be the collective interactions between particles which rheologically means the emergence of normal stresses generated by direct contact between particles. In this thesis the particle normal stress has been experimentally investigated as an origin of migration of deformable particles. Non-Brownian droplets and microcapsules were used as a model system of deformable particles. A membrane emulsification process was adapted to produce uniform suspensions of microcapsules at high throughput. Then an automatic microfluidic system was developed to measure the elasticity of their shell. In microcapsule suspensions, it was found that the contact viscosities show a shear-thinning behavior. In high volume fraction, the contact viscosity, which originate from normal stress, is the principal contributor to the apparent viscosity. Migration and normal stress of buoyant particles were inferred by measuring the vertical concentration profile in viscous resuspension experiments in a vertical Couette cell. The normal stress varies linearly with the Shields number for droplets and non-linearly with a 0.7 power law for microcapsules as rigid particles. The dependency of the normal stress on the volume fraction is in agreement with the models proposed in the literature for solid particles. All of these results suggest that the migration of deformable particles in dense suspension under shear can be explained by the same rheological laws as for rigid particles, regardless of their deformability (for $Ca < 0.4$). Furthermore, in the case of capsules, these rheological laws are governed by the solid contacts between the particles.

Key words: Microcapsule, Emulsion, Normal stress, Interfacial properties, Viscous resuspension, Shear-induced migration

Résumé

Les particules déformables migrent dans une suspension cisailée. Une source de ce phénomène serait les interactions collectives entre particules ce qui signifie rhéologiquement l'émergence de contraintes normales générées par le contact direct entre les particules. Dans cette thèse, la contrainte normale des particules a été étudiée expérimentalement comme une origine de migration de particules déformables. Des gouttes et des microcapsules non browniennes ont été utilisées comme système modèle de particules déformables. Un procédé d'émulsification membranaire a été adapté pour produire des suspensions uniformes de microcapsules à haut débit. Puis un système microfluidique automatique a été développé pour mesurer l'élasticité de leur coque. Dans les suspensions de microcapsules, il a été trouvé que la viscosité de contact présente un comportement de rhéofluidification. Pour des fractions volumiques élevées, la viscosité de contact, qui provient de contraintes normales, est le principal contributeur à la viscosité apparente. La migration et la contrainte normale des particules non-isodenses ont été déduites en mesurant le profil de concentration vertical dans des expériences de resuspension visqueuse dans une cellule de Couette verticale. La contrainte normale varie linéairement avec le nombre de Shields pour les gouttes et non-linéairement avec la puissance 0.7 comme les particules solides. La dépendance de la contrainte normale à la fraction volumique est en accord avec les modèles proposés dans la littérature pour des particules solides. L'ensemble de ces résultats suggère que la migration de particules déformables en suspension dense sous cisaillement s'explique par les mêmes lois rhéologiques que pour des particules rigides, indépendamment de leur déformabilité (pour $Ca < 0.4$). De plus, dans le cas des capsules, ces lois rhéologiques sont gouvernées par les contacts solides entre les particules.

Mot clés: Microcapsule, Emulsion, Stresse normale, Propriétés interfaciales, Resuspension visqueuse, Migration des particules induites par l'écoulement

Contents

Abstract	2
Résumé	3
Introduction	6
1 State of the art and objectives	8
1.1 Rheology and migration in suspensions of hard particles	8
1.1.1 Migration observations in suspensions	8
1.1.2 Rheology of suspensions of rigid spheres	9
1.1.3 Connecting migration and rheology	11
1.2 Rheology and migration in suspensions of soft particles	13
1.2.1 Migration of soft particles: the blood	13
1.2.2 Dynamics of isolated soft particles in flow	14
1.2.3 Suspension of soft particles in flow: highlights from numerical simulations	15
1.3 Objectives	16
2 Materials and Methods	17
2.1 Introduction	17
2.2 Chemicals and solutions	17
2.3 Droplet and Microcapsule synthesis	18
2.3.1 Microfluidics for droplets	18
2.3.2 Membrane emulsification for microcapsules	19
2.4 Characterization of physical properties of suspensions	19
2.4.1 Size variation	19
2.4.2 Volume fraction	20
2.4.3 Microcapsules shell elasticity G_s	20
2.4.4 Rheometry and details about the rheometer	24
2.5 Resuspension experiments	24
2.5.1 Transparent Taylor-Couette cell	24
2.5.2 Visualization and parallax issue	25
2.5.3 Concentration profile measurement by light absorption	26
2.5.4 Tuning refractive index of droplets	27

3	Production and characterization of microcapsules	29
4	Rheology of attractive suspensions of microcapsules	41
4.1	Introduction	42
4.2	Materials and Methods	42
4.2.1	Chemicals and Solutions	42
4.2.2	Production and Preparation of suspensions	42
4.2.3	Characterization of physical properties	43
4.2.4	Rheometer and the measurement method	44
4.3	Results	45
4.3.1	Steady State Rheology	45
4.3.2	Shear-reversal rheology	51
4.3.3	Discussion	56
4.4	Conclusion	58
5	Viscose resuspension of droplets	59
6	Viscous resuspension of attractive microcapsules	74
6.1	Introduction	74
6.2	Materials and methods	74
6.3	Results	75
6.4	Discussion and concluding remarks	77
7	Conclusion and Perspectives	79
	Bibliography	82

Introduction

Suspensions of particles dispersed in a liquid are omnipresent in nature, in industry and in biology. Their flow properties are rich and complex and depend both on the particles constituting them, on their volume fraction and on the shear rate.

As soon as the particle size exceeds the micrometer scale, the Péclet numbers are generally high and the suspensions are then considered non-Brownian. The flow of this type of suspension has long been considered to be essentially governed by hydrodynamic forces in the fluid in which they are dispersed, today we know that contact interactions as well as colloidal interactions also play a role, which becomes major when the volume fraction exceeds 35-40%. Rheology can then exhibit various behaviors such as shear thinning, shear thickening (which is sometimes very sudden), and tends towards jamming when approaching a concentration where congestion prevents the flow.

The other characteristic of non-Brownian suspensions is that spatial repartition of the particles can be non-uniform and is influenced by the flow. This is particularly the case with heterogeneous flows, where particles migrate from highly sheared areas to less sheared ones. Due to the strong dependence of the rheological properties of suspensions on the concentration, this shear-induced migration is crucial in order to understand and predict the properties of the flows.

In this thesis, we focus on deformable particles. In fact, in various industrial sectors (agro-food, cosmetics, etc.) but above all in biology, there are suspensions of particles which can be easily deformed. These may be made of drops (emulsions), soft solid particles, vesicles, cells, etc. In all these systems, the easily deformable nature of the particles leads to additional phenomena. At very high volume fraction, the rheology becomes that of a yield stress fluid. Indeed, if rigid particles can no longer flow beyond a certain size, these softer particles can deform and can be sheared if the stress is sufficient.

Regarding the spatial distribution of the particles in the flow, the coupling between the shape of the particle and the hydrodynamic forces leads to migration phenomena (i.e., the trajectory of the particles deviates from that of the streamlines), even for isolated particles. This phenomenon has been studied in detail for vesicles and red blood cells, as it is probably the cause of the Fåhræus – Lindqvist effect: the red blood cells concentrate in the center of the blood vessels, leaving a layer of depletion near the walls, which significantly facilitates blood circulation. The description of these effects, even for isolated particles, is complex and has been the subject of numerous studies: it is necessary to account for the coupling between the shape of the particle, its mechanical properties, those of its surface, and the hydrodynamic constraints of the suspending fluid.

In addition to these fluid-structure-type mechanisms, we can also expect collective effects similar to those existing in the case of solid particles: interactions between particles (hydrodynamic, contact, colloidal), exacerbated by shear, should lead to shear-induced migration, which has been little studied in the case of deformable particles. In recent years, experimental approaches have been developed to manufacture and characterize elastic capsules. These objects, made up of an elastic membrane enveloping a liquid, are intermediate between vesicles which

have negligible bending modulus, drops for which there are no contacts, and solid particles. These systems are considered to be adequate models for red blood cells. It therefore seems interesting to study the rheological properties and the migration properties under flow of these systems, in order to extend the knowledge acquired on solid particles to this type of deformable objects.

One of the major bottlenecks for this type of study lies in our ability to produce capsules in large quantities. Indeed, the approaches developed so far are essentially based on micro- or millifluidic methods, which have many advantages, but can only with difficulty be implemented to produce sufficient quantities for the study of collective effects, both on rheology and on migration phenomena. The mass production of elastic particles has been the subject of a specific development during this thesis, and will be detailed in this manuscript.

In order to study the migration induced by the shearing of deformable objects, we have chosen to decouple the multiple origins of migration phenomena, by avoiding the effects linked to the migration due to the proximity of a wall, and to that induced by a shear rate gradient, those two mechanisms being at work even for isolated objects. For this, we propose to use a Couette geometry to study the viscous resuspension of deformable and buoyant particles. This approach, which has been already used for solid particles, makes it possible to precisely determine the normal stresses at the origin of the shear-induced migration. We have chosen to start with a system that is in principle simpler than capsule suspensions, namely emulsions. One of the experimental advantages of these systems is the possibility of making them completely transparent to light, and of using an absorption measurement to simply and precisely determine the local volume fraction. Then, we extended this approach to suspensions of deformable capsules.

In parallel, and because the capsule suspensions constitute an original system, we have specifically studied the rheology of these suspensions by standard rheometric approaches (flow curves in particular), but also by using a shear reversal protocol. The latter allows in the case of solid particles to dissociate the hydrodynamic contribution to the stress from that of contacts.

This manuscript is organized as follows: In Chapter 1, I summarize the state of the art relating to the questions raised above, concerning the rheological and migration properties of suspensions of non-Brownian particles, solid or deformable. In Chapter 2 "Materials and methods", I detail the choices and the developments made both on the different systems used to conduct the study, and both on the experimental methods used. The Chapter 3 is taken from a scientific article, entitled "Membrane emulsification for the production of suspensions of uniform microcapsules with tunable mechanical properties", which describes the methodology we have specifically developed to produce large quantities of elastic capsules. The Chapter 4 concerns the rheological properties of capsule suspensions. It will also be the subject of a publication, and is presented as an article in preparation. The last part of the manuscript is Chapter 5 shows the results obtained on the viscous resuspension of emulsions, which is also the subject of a scientific article. Finally, we present the results obtained on the resuspension of capsules, before concluding and presenting some perspectives.

Since part of this thesis manuscript consists of articles, and since these are the result of a collective work, it seems important to me to clarify my contribution to these articles:

- Chapter 3: I performed all the experiments and analyzes, and prepared the figures.
- Chapter 4: I performed all the experiments and analyzes, prepared the figures and wrote the first version of the manuscript.
- Chapter 5: I performed all the experiments and analyzes, prepared the figures and wrote the first version of the manuscript.

Chapter 1

State of the art and objectives

1.1 Rheology and migration in suspensions of hard particles

1.1.1 Migration observations in suspensions

The question of how suspensions of particles flow in tubes is a rather old problem that has been the focused of many studies for 50 years. It has been early observed that when flowing in a tube, particles do accumulate in the center, leading to a nearly plug flow [1, 2]. More recent work quantified more accurately the velocity and concentration profiles [3, 4]. In a slit channel, the same phenomenon is observed and has been well characterized [5, 6], see Figure 1.1. Extension to Brownian particles has also been reported by some authors [7, 8]. Although diffusion in this case has to be considered, it is not sufficient to suppress particle migration.

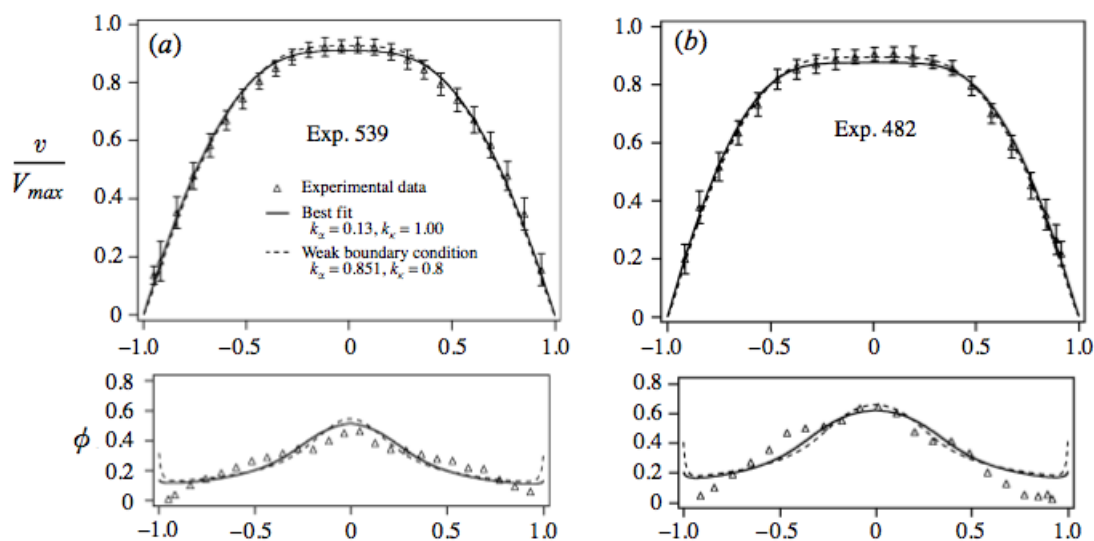


Figure 1.1: Migration and velocity field in straight channel (from [5])

The work of Leighton and Acrivos brought essential observations to this problem [9]. By observing and analyzing the migration phenomenon in a Couette cell, they show that particles migrate towards low shear zones of the flow, consistently with the observations in tubes. These observations have been refined by several authors [10, 11].

In plane-plane configuration however, no migration is observed [12, 13], although a rather important gradient of shear rate exists in this geometry. This paradox has been partly resolved by the a tensorial and mechanical description of the migration [14], even though it remains a phenomenological issue. Let us point out that some more recent experiments report that there is

an outward migration at a volume fraction lower than 0.2 [15]. In square geometry, it seems that secondary currents are rather important [16, 17]. The shear-induced migration mechanism is also responsible for the resuspension that is observed when a suspension undergoing sedimentation is sheared [18].

Migration from low to high shear zone in non-homogeneous flows such as Couette flow or pressure driven tube flow is a rather generic feature. Indeed, it has been evidenced in many systems, not restricted to solid particles. For instance, it also exists emulsions [19], in polymer solutions [20, 21], DNA solutions [22] and in more complex systems such as blood [23]. Although some specific systems features should be taken into account, such as particle anisotropy, surface roughness, and particle deformation (e.g. in the case of droplets or polymers) and Brownian motion. The fact that this phenomenon appears to be general is rather striking. For example, semi-dilute emulsions made of droplets that are 6 orders of magnitude more viscous than the continuous phase exhibits an axial migration towards the center [24], as shown in figure 1.2. This result might be interpreted as an indication that the shear-induced migration also exists without contact forces neither deformable objects. A possibility is that this migration is coming from second order hydrodynamic interactions that can be large in confinement.

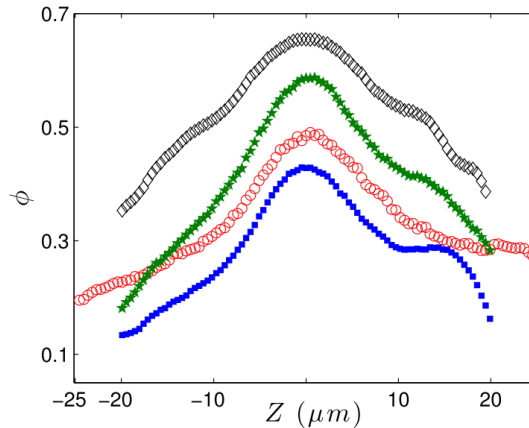


Figure 1.2: Concentration profile of a semi-dilute emulsion made of highly viscous droplets flowing in a straight channel (preliminary result from [24]).

1.1.2 Rheology of suspensions of rigid spheres

Presence of suspended particles generates non-Newtonian effects in suspension flows even with a Newtonian suspending fluid. Behavior of the suspensions in macroscopic scale is strongly influenced by microscopic configuration of particles inside the suspension, which is generally referred as the microstructure. The complex rheological behavior of sheared suspensions is in part driven by the deviation from an equilibrium microstructure of the particles [25, 26, 27].

For the same volume fraction of the particles, the suspension shows different viscosity relative to the particle shape [28, 29]. Figure 1.3 represents an example of suspensions with different particle shapes. In general, increase of the suspension viscosity relative to the particle shape is in the following fashion: rods > plates > cubes/grains > spheres. In low volume fractions $\phi < 0.05$ where the particles are completely isolated, the increase in the viscosity comes from the viscous dissipation of deviated streamlines passing around the particles. When the particles are not spherical, this viscous dissipation increases and the result is the growth of suspension viscosity [30]. In large ϕ the impact of the particle shape on the rheology can be captured through its effect on ϕ_m which is highest for spherical particles and decreases systemically for particles that are increasingly prolate or oblate. Consequently, a suspension of spherical particles has a lower viscosity compared to that of prolate or oblate particles [28].

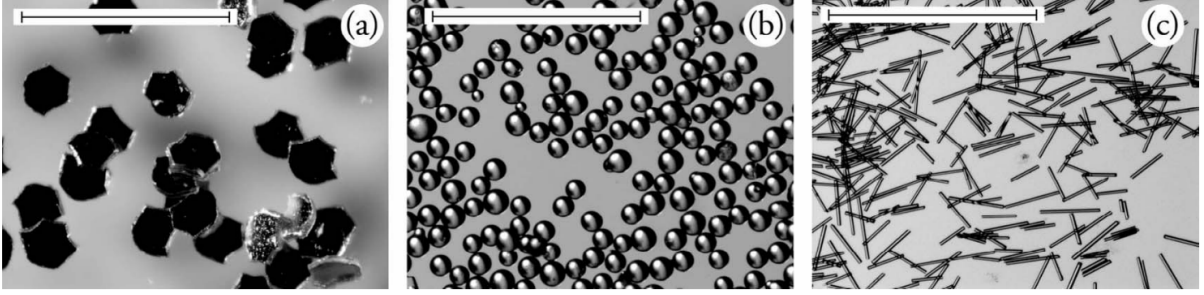


Figure 1.3: Example of different particle shapes in a suspension: **a:** Oblate polyacrylic glitter, **b:** Spherical glass beads, **c:** Prolate glass fibers. Length of scale bar is 1 mm. Image from Mueller *et al.* [28].

A wide size distribution of particles increases ϕ_m which is an important variable to understand and control the behavior of suspension [31, 32]. This means that if the particles are monodisperse, then the mixture of particle sizes can reduce the viscosity in high volume fractions. Actually, the small particles can fit to the space left between the large ones in contact. This fact is useful in concrete manufacturing where as possible as aggregate materials should be added by keeping the concrete quiet flowable [30].

Increasing the volume fraction of the particles causes a growth in the suspension viscosity. By increasing ϕ , the viscous dissipation due to hydrodynamic interactions increases and as a consequent, the suspension viscosity growth. At larger ϕ the particles come to direct mechanical solid contact and frictional dissipation increases drastically the viscosity. For further ϕ the viscosity diverges and becomes infinite and consequently the suspensions cease to flow at ϕ_m . However, the value of ϕ_m depends to predominant circumstances.

The impact of flow on the inter-particle interactions and also the evolution of microstructure should be considered in a microscopic scale. However, the whole suspension in a macroscopic scale can be considered as a continuous fluid. A suspension of monodisperse, solid, spherical, non-Brownian and buoyant particles in a Newtonian fluid is the simplest example of a suspension. In the absence of inertial effects, only hydrodynamic and frictional forces governs inter-particle interactions. The linearity of Stokes flow asserts that the scaling of the shear stress is viscous $\tau = \eta_r \eta_f \dot{\gamma}$, where η_r is the relative viscosity and η_f is the viscosity of suspending fluid. The only remaining independent variable is the volume fraction of particles ϕ which determines the relative viscosity η_r of the suspension. Thus η_r is independent of the shear rate $\dot{\gamma}$ and it is only a function of volume fraction $\eta_s = \eta_s(\phi)$ [33].

Early theoretical investigations of the rheological behavior of a suspension started by the classical paper of Albert Einstein [34] (1906,1911) for dilute-limit regime of ϕ :

$$\eta_s = \eta_f \left(1 + \frac{5}{2}\phi\right) \quad (1.1)$$

Rigid particle resists to the straining and creates a disturbance flow which increases the viscous dissipation rate. In the other words, the viscosity is increased because of the resistance of the non-deforming particle to the straining component of the shearing flow [33]. By increasing ϕ the distance between the particles becomes shorter and the interaction between them is no longer negligible. The particles are affected by the long-range flow disturbance which is generated by the neighbors. Batchelor & Green [35, 36] in 1972 derived the second-order correction in volume fraction to the viscosity by considering two-body hydrodynamic interactions:

$$\eta_s = \eta_f \left(1 + \frac{5}{2}\phi + 5\phi^2\right) \quad (1.2)$$

The experimental data validate this correlation in the dilute regime of particles ($\phi < 0.15$). However, it fails to predict the sharp rise of the viscosity in the larger volume fractions [33]. A

theoretical approach to the viscosity of the suspensions for larger ϕ is an extreme challenge. The many-body hydrodynamic interactions between the particle through the suspending fluid should be considered and a detailed description of the microstructure is required [25]. Another complexity is that the particles can interact by direct mechanical contacts which increases the anisotropy of the microstructure [37].

Many empirical equations have been developed which relates the suspension viscosity to volume fraction of particles. Generally they followed Einstein’s analytical effort to extend the volume fraction into a more practical region and aim to account for the divergence of the viscosity at ϕ_m . The most popular one is known as the Kreigee-Dougherty equation:

$$\eta_s = \eta_0 \left(1 - \frac{\phi}{\phi_m}\right)^{-2} \quad (1.3)$$

Surprisingly, the only real variable is ϕ_m . This variable depends on the size distribution of particles, deformability and also the flow condition [30].

Numerous studies show that in concentrated regime the contact forces become dominant and overcome the long-range hydrodynamic interactions [38, 39, 40, 41]. In order to understand this mechanism, some experimental approaches have been developed to connect the rheology of dense suspensions to the rheology of dry granular media [42, 43, 44]. In the suspension both frictional contacts and long-range hydrodynamic interactions present and in the granular media the rheological behavior is determined only by direct frictional contacts [33, 44].

1.1.3 Connecting migration and rheology

Two different classes of models have been proposed to describe migration in non-Brownian suspensions. The first one is based on scaling arguments and on the concept of shear-induced diffusion [9, 45], and has been referred to in the literature as “diffusive models”. The second class is on the contrary based on mass and momentum conservation of the suspension components and has been referred to as the “suspension balance model” [46, 14]. Though diffusive models have been occasionally used [15, 47], the suspension balance model has the merit to relate the migration to the rheological properties that could be independently measured [48]. We will thus limit ourselves in this state of art to the latter.

The suspension balance model was introduced two decades ago in order to relate the migration properties to the rheology of the suspensions [46, 14, 49]. Its formalism allows to predict the migration in various geometries [50]. Although the model has been recently questioned by several authors [51, 52], it is however worthwhile starting by describing the initial version of the model, since it may still apply in some cases, and since it has been widely used to interpret experimental and numerical results.

Although the model could be detailed in the presence of buoyancy forces [49], we present here for the sake of simplicity the governing equations for the particular case of density-matched particles, where the buoyancy force is neglected.

It relies on the decomposition of the stress into a particle stress σ_p and a fluid stress σ_f so that the total stress σ is the sum of these two stresses. Note that these stresses are ensemble averaged ones. This decomposition allows to write the momentum balance for the two subsystems and thus to relate the particle stress to the mean force f_I exerted by the fluid on the particles, i.e. $\nabla \cdot \sigma_p + f_I = 0$ (and similarly, $\nabla \cdot \sigma_f - f_I = 0$). The main interest of this stress decomposition is then to be able to relate the interaction force to velocity differences. With a mean-field description and for density-matched particles, this force is given by

$$f_I = -\frac{9\eta_f}{2a^2} \frac{\phi}{f(\phi)} (u_p - u) \quad (1.4)$$

where η_f is the viscosity of suspending fluid, a is the radius of particles, u_p is the mean velocity of the particles, u is the volume average velocity of the whole suspension, and $f(\phi)$ is the decreasing

function of the particle volume fraction, similar to the sedimentation hindrance function [53]. Refinements have been proposed for this function, e.g. in [54], where

$$f(\phi) = \left(1 - \frac{\phi}{\phi_m}\right)(1 - \phi)^m \quad (1.5)$$

The fluid stress is in the case of a Newtonian surrounding fluid and simply given by

$$\sigma_f = -P_f I + \eta_f \dot{\gamma} \quad (1.6)$$

where $\dot{\gamma}_{ij} = \partial_{x_j} u_i + \partial_{x_i} u_j$ and P_f is the fluid pressure. Note that the fluid pressure could be rather different from the pressure itself.

The particle stress has been modeled using the following semi-empiric expression [14]:

$$\sigma_p = \eta_f \left[\eta_p(\phi) \dot{\gamma} - \eta_n(\phi) \bar{\gamma} \begin{pmatrix} 1 & 0 & 0 \\ 0 & \lambda_2 & 0 \\ 0 & 0 & \lambda_3 \end{pmatrix} \right] \quad (1.7)$$

where the first term is the particle contribution to the shear viscosity, while the second one reflects the anisotropy of the normal stress. In the second term, $\bar{\gamma} = \sqrt{2\dot{\gamma} : \dot{\gamma}}$ is the amplitude of the shear rate. Since $\eta_p(\phi)$ is directly deduced from the suspension viscosity, it is rather well established and well approximated by the form proposed by Krieger, i.e. $\eta_p(\phi) = (1 - \phi/\phi_m)^{-2}$ in the semi-dilute regime. Let us mention that many variants of this function have been proposed [14, 55, 56].

The anisotropic part of the normal stress tensor (second term of equation 1.7) has been a matter of debate during the last years. In the framework of the suspension balance model, it is indeed possible to measure it more or less directly, since the anisotropy of particle normal stress tensor coincides with the total stress one (given the form of the fluid stress in equation 1.6, only the particle stress could exhibit non-zero normal stress differences). In this framework, the particle stress is thus closely linked to the global rheology of the suspension. Measurements of the normal stress differences N_1 and N_2 have thus been conducted to determine empirically the particle stress variations with the volume fraction. Parallel plate rheometry [55, 57], rotating rod experiments [11, 55], tilted trough [58], Couette cell [59]. These experiments are rather difficult, but agree on two main facts : the second normal stress coefficient is negative and increases when the volume fraction is higher than 0.2, with no divergence at the maximum packing fraction ϕ_m , and the first normal stress coefficient is also negative but much lower than the second one. A set of parameters in equations that appear to be compatible with these observations is [58]: $\lambda_2 \approx 0.8 - 1$, $\lambda_3 \approx 0.5$, and $\eta_n(\phi) = 3.3(\phi - 0.22)$ for $\phi > 0.22$, and $\eta_n(\phi) \approx 0$ otherwise. Note that the value of 0.5 for λ_3 is coming from the observation that there is almost no migration in rotating parallel plate geometry [14]. However, many quantitative discrepancies arise from different experiments and simulations (see e.g. [59]), so that the problem of global normal stresses of a sheared suspension remains an open issue.

The isotropic contribution could be measured similarly to the osmotic pressure of a colloidal suspension, i.e. by measuring the pressure difference between the sheared suspension and the surrounding liquid separated by a grid smaller than the particles [60, 59].

The migration flux, which is given by the velocity difference between the particles and the surrounding fluid thus directly involves the particle stress. Indeed, the particle flux \mathbf{j} defined by $\mathbf{j} = \phi(u_p - u)$, under the assumption of validity of equation 1.4, $\mathbf{j} = (2a^2/9\eta_f) f(\phi) \nabla \cdot \sigma_p$. Particle conservation then allows to close the problem and reads

$$\frac{\partial \phi}{\partial t} + u \cdot \nabla \phi = -\nabla \cdot \mathbf{j} = \frac{2a^2}{9\eta_f} \nabla \cdot (f(\phi) \nabla \cdot \sigma_p) \quad (1.8)$$

Thus the particle migration is directly linked to the variations of the particle stress tensor. It is thus possible to compare the concentration profiles determined experimentally with the

predictions of the suspension balance model. Depending on the geometry, although a qualitative agreement is always found, a good quantitative agreement is found for the Couette geometry [11], but rather poor agreement in the case of tube channels [54, 7].

Equation 1.8 provides an understanding of important features of the migration, especially concerning the time scale of the migration (e.g. in the case of Couette flow) or the entrance length (in the case of tube flows). The time scale of the migration is given by $h^2/a^2\bar{\gamma}$, where h is the characteristic size of the flow (i.e. the channel height, or the cell gap) and a the particle size. For small particles compared to the gap (and corresponding to the limit where a continuum theory could apply), the migration is thus very slow. Similarly, the entrance length is given by h^3/a^2 , and could thus be very long expect in confinement. These time and length scales underline the crucial role played by the confinement (i.e. the aspect ratio between the channel size and the particle diameter). We expect fast migration and short entrance length in confinement.

In a channel, several attempts have been made to validate this theory. Though qualitatively acceptable, it seems that a quantitative agreement is not reached [5, 7], as could be seen in figure 1.1. The model usually underpredicts the migration close to the wall and overpredicts it in the center. In the center, the fact that the shear rate vanishes leads to a divergence in the concentration. It is thus necessary to smooth the center part of the profile. This issue is supposed to come from the limit of an effective continuum medium, which should not apply at the scale of a particle.

1.2 Rheology and migration in suspensions of soft particles

1.2.1 Migration of soft particles: the blood

A well-documented case of migration in suspensions of soft particles concerns the blood [23]. Blood can be considered as a dilute suspension of macromolecules (fibronectin, 100 nm length) and deformable particles of different sizes and stiffness: red blood cells (RBC, 7 μm), leukocytes (10 μm) and platelets (2 μm). On the macroscopic scale, this leads to a highly non-linear rheology of the blood: the resistance of blood to flow in capillaries (i.e. its apparent viscosity) shows a non-linear dependence with the flow confinement, the Fåhræus–Lindqvist effect [61, 62]. The apparent viscosity of the blood shows a minimum for a typical size of the capillaries of the order of RBC size (figure 1.4). These effects are closely related to the spatial organization of the different constituents of this suspension. On the microscopic scale, blood exhibits segregation, as the volume fraction of the different particles depends on the lateral position in the vessel: red blood cells are concentrated in the center of the channel, leaving a depletion layer near the wall (also referred as cell-free layer), where rigid particles are more likely to be found figure 1.5. The process by which platelets and leukocytes migrate from the center of the vessel towards the wall is called margination [63, 64, 65]. Recent theoretical and numerical simulations show that the deformability of RBCs is probably the salient physical ingredient to explain this phenomenon [66, 67, 68].

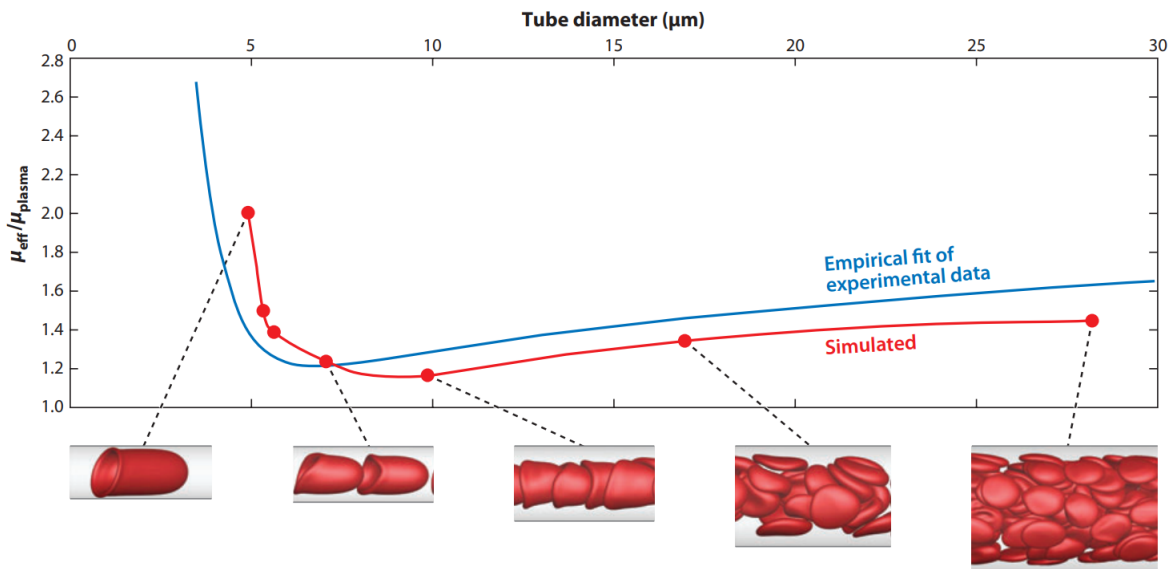


Figure 1.4: Non-Newtonian effects for suspensions of soft particles, here RBC's, related to the microstructure, Ref [66]. The effective viscosity depends on the diameter of the capillary where model RBC's flow.

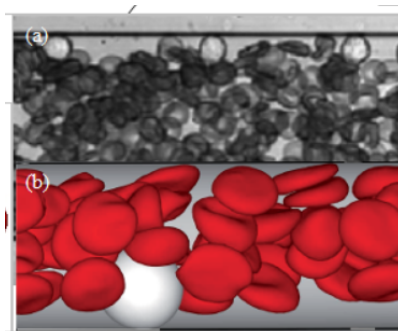


Figure 1.5: Segregation in the blood. Red blood cells (gray) occupy the center of the flow, whereas leukocytes (white) are near the wall.

1.2.2 Dynamics of isolated soft particles in flow

Migration in suspensions of soft particles is considered a complex problem [23], since the particles not only interact with each other, but also are deformable objects and thus modifies their shape as a response to the external flow [69, 70]. The dynamic of deformation of the shape becomes a time dependent unknown of the problem as shown in figure 1.4. Indeed, the shape of a single vesicle in a linear flow, a well-studied case of a soft particle, can be stationary with a rotation of the membrane (tank-treading), oscillates as a solid body (tumbling) or oscillates with a coupling between rotation and axis length [71, 72]. The conjunction of experimental, theoretical, and numerical studies gives a quite clear insight into the dynamics of an isolated vesicle in flow.

For microcapsules, another kind of soft particles made from an elastic shell, numerous theoretical and numerical [73, 74, 75] investigations attest that analogue dynamics are expected but controlled by other geometrical (shape at rest) or interfacial rheological properties. Recently, comparison of experiments [76] with numerical simulations [77] has shown that shell viscoelastic properties govern the tank-treading motion in shear flow, due to the localized and cyclic deformation of the membrane figure 1.6. Moreover, the transition between two dynamics depends on the local shear (capillary number). It means that in some flow configurations, we could expect

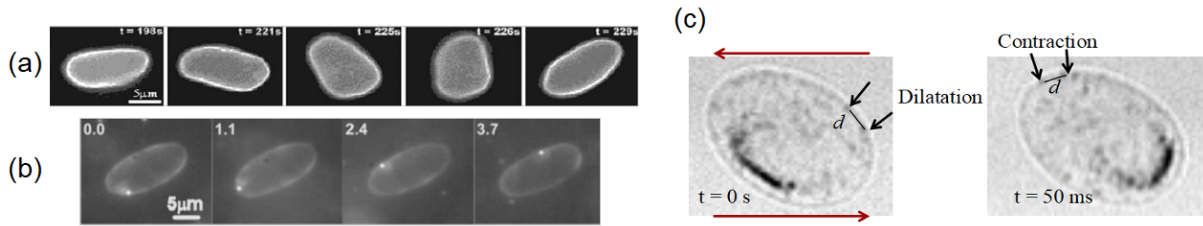


Figure 1.6: Dynamics of soft particles in shear flow. (a) Rotation of the membrane of a vesicle with a fluorescent marker. (b) Solid oscillation of a vesicle. From Ref. [71]. (c) Rotation and deformation of the membrane of a microcapsule, from Ref. [76]

some regions where one dynamics dominates. Finally, the softness of microcapsules modifies deeply short-range interactions, as the lubrication interactions become shape dependent. It is expected that these dynamics modify not only the global properties of the suspension (rheology), but also the transport properties of an individual particle: a tank-treading particle might migrate perpendicularly to the streamlines, while a tumbling particle would not.

1.2.3 Suspension of soft particles in flow: highlights from numerical simulations

Concerning the collective dynamics of soft particles in flow, there are two complementary approaches in literature: (i) full numerical simulations of a large number of particles [73, 66] and (ii) experimental, theoretical, and numerical studies considering the hydrodynamic interactions between two soft particles [78, 72, 79]. This last approach has the advantage to highlight the salient physical ingredients to understand the behavior of a suspension in flow [23]. If a smooth sphere (blue in figure 1.7-a) is immersed in shear flow near a fixed solid sphere (gray), the reversibility of the Stokes equation (low Reynolds number) together with the symmetry of the object imposes that the streamline is only changed at the neighboring of the fixed sphere. However, short range interactions (electrostatic, localized surface deformation in the lubrication film) or surface roughness can introduce interactions that break the symmetry and induce a deviation between both hard spheres [80, 81]. For soft microcapsules, there is no longer a fore-aft symmetry due to the deformation of the capsule, and in this case the soft particles will be pushed away from the fixed sphere (figure 1.7-b). Similar effects are present near a wall effect known as lift velocity (figure 1.8) and in a Poiseuille flow with a normal migration velocity. For suspensions, these hydrodynamic interactions are referred to homogeneous for particles with the same stiffness or size and heterogeneous if the first particle is soft and the second rigid or larger (figure 1.9). These two key phenomena, hydrodynamic migration and hydrodynamic pair collisions, generate flow structuration as the formation of a depletion layer near the wall or segregation in suspensions of particles of different stiffness. According to the properties of the microcapsules (shape at rest, size, viscoelasticity), complex spatio-temporal organization can be expected.

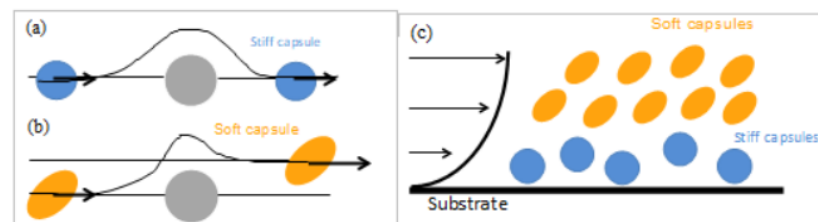


Figure 1.7: Interactions between stiff and soft capsules: (a) for stiff capsules, (b) for soft capsules, (c) segregation in binary.

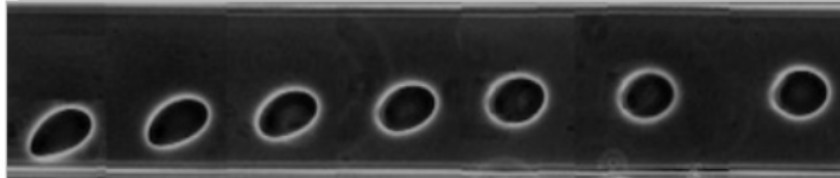


Figure 1.8: Soft microparticles (vesicle) in the vicinity of interfaces experienced hydrodynamic interactions that push them away from the wall. Image from Ref. [78]

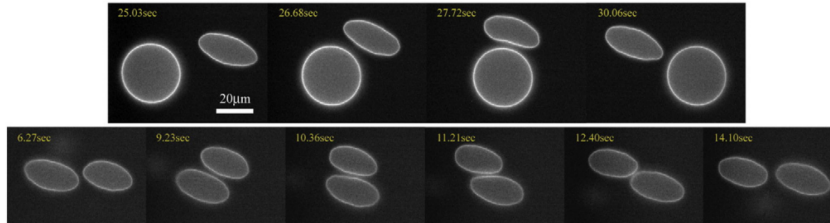


Figure 1.9: Dynamics of soft particles (vesicles) is altered when interacting with a second particle. **(Top)** The interaction is heterogeneous for particles of different properties (size, stiffness) and **(Bottom)** homogeneous for similar particles. Image from Ref [82]

1.3 Objectives

The main objective of this thesis was to study the rheology and migration phenomena in suspensions of soft microparticles.

The first objective of this thesis was to fabricate well-controlled suspensions of soft particles. In fact, one of the major bottlenecks for this type of study lies in our ability to produce soft microparticles in large quantities. We used two kinds of soft microparticles: droplets and microcapsules. A microcapsule is a droplet protected by an elastic shell. Therefore, it can be considered at first sight as the intermediate object between the droplet and the solid particle: it is deformable, but can interact also by friction. In Chapter 3, we present a process to produce homogeneous suspensions of droplets and microcapsules.

The second objective was to quantify the collective mechanisms leading to migration in suspension of soft particles. We started with a system that is normally simpler than microcapsules, namely an emulsion. We measured normal stress, which leads to migration, in resuspension experiments in a Couette flow cell thanks to the measurement of the profile of concentration.

The third objective was to study the rheology of suspensions of microcapsules with standard rheometric techniques and also shear-reversal experiments to dissociate the contribution from the contact between the capsule to the hydrodynamic interactions on the rheological signature.

Finally, we explored the resuspension of suspension of microcapsules to measure normal stress effects and conclude about the mechanisms who drive collective effects in such suspensions of deformable objects.

Chapter 2

Materials and Methods

2.1 Introduction

In this chapter we will discuss general materials and methods employed in this study. Here we will give the description of the tools and techniques essential for this study and common between different experiments conducted in this work. Specifics and details of the employed techniques will be given for each study individually in the following chapters. First we will list and elaborate on the products used and preparation protocols of the essential solutions in this study. We will briefly describe the different methods employed in microcapsule fabrication and highlight the important differences between them. In the next section we will talk about the mass production of microcapsules via membrane emulsification process. Then we will describe the capsule characterisation and parameter control. In this section we will disclose the methods used to quantify the mechanical properties of the capsule elastic shell. We will present as well the microfluidic chamber used for the capsule characterisation and explain choice of microfluidic design. The last section of this chapter is dedicated to the resuspension experiments. Here we will describe all the essential details of experimental setup. Special accent will be made on the metrological analysis required in order to ensure the accuracy and scientific validity of experimental results.

2.2 Chemicals and solutions

Microcapsules are made by two different physicochemical processes:

- interfacial complexation of chitosan (CH) with phosphatidic fatty acid (PFacid)[83, 84]
- interfacial cross-linking of bovine serum albumin (BSA) with terephthaloyl chloride (TC)[85]

CH / PFacid microcapsules

PFacid was used in a form of a commercial lecithin known as lecithin YN (Palsgaard 4455, food-grade, E442) which was kindly provided by Palsgaard. PFacid was dissolved in food-grade rapeseed oil (Géant Casino) at a concentration of 20% at 35 °C during the night to create a stock solution. Then PFacid solution was centrifuged at 3500 g to remove the insoluble residuals. The stock solution was further diluted with rapeseed oil at the required concentrations (0.1 or 5 % w/w).

Chitosan (CAS n° 9012-76-4, Sigma-Aldrich) with medium molecular weight and 75-85% deacetylation was dissolved in Millipore water (Resistivity > 18.2 mΩ.cm) at a concentration of 1 % w/w by adjusting the pH with hydrochloric acid (1 mol/L) to 3.0. The chitosan solution was then filtered to remove undissolved particles through Minisart syringe filters (pore size 5.0

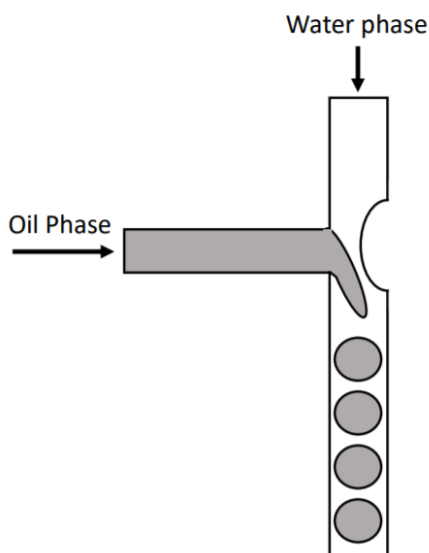


Figure 2.1: Microfluidic T-junction chip to produce monodispersed droplets.

μm). The solution was diluted to 0.25 % w/w with water and glycerol (99.5 % purity, VWR) mixture. The water to glycerol ratio was adjusted when needed in order to control the density of the microcapsules.

BSA / TC microcapsules

To synthesize BSA / TC microcapsules, BSA (CAS n° 9048-46-8, Sigma-Aldrich) is dissolved in phosphate buffered saline solution (Fisher Scientific) and TC (CAS n° 100-20-9, Sigma-Aldrich) dissolved in a mixture of chloroform (CAS n° 67-66-3, Sigma-Aldrich) : cyclohexane (CAS n° 110-82-7, anhydrous, 99.5%, Sigma-Aldrich) at a ratio of 4:1 by volume. Sorbitane trioleate 85 (SPAN 85, CAS n° 26266-58-0, Sigma-Aldrich) were used to stabilize albumin drops during emulsification.

To adjust the density and refractive index of the microcapsules, glycerol (CAS n° 56-81-5, VWR) was added to CH and BSA solutions. To stop membrane formation after a given time, microcapsules were rinsed by a big volume of cyclohexane for several times. Additionally, this allows us to evacuate nonused PFacid and TC molecules. Then the microcapsules were suspended in silicon oil (AP1000, AK1000 from Wacker) which are nontoxic for the microcapsule's membrane and have highly thermal and chemical stability.

2.3 Droplet and Microcapsule synthesis

2.3.1 Microfluidics for droplets

Monodisperse oil-in-water emulsions were produced with a custom-made PMMA T-junction microfluidic chip with a cross-section 1×1 mm. The inside of the chip was treated with acetone in order to render the surface hydrophilic. As shown in figure 2.1, the continuous aqueous phase was injected through the main channel while the dispersed oil phase was introduced through the perpendicular branch via a round glass capillary (CM Scientific Ltd) of $300 \mu\text{m}$ inner diameter. The flow rates were controlled by two syringe pumps (neMSYS, CETONI). To improve the production rate, T-junction chip was modified by narrowing the intersection area to strength shear forces. Two monodisperse emulsions with different droplet sizes were generated at volumetric flow rates of oil phase 0.2 and 0.3 ml/min while the flow rate of aqueous phase 2 ml /min in both cases.

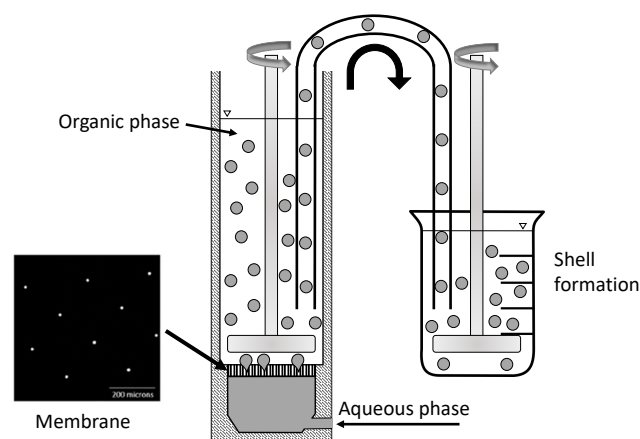


Figure 2.2: Sketch of the membrane emulsification system and microscopic image of the micro-engineered membrane. Aqueous droplets of BSA or CH were dispersed in the oil phase through the micro-engineered membrane. The droplets were sucked-up in a beaker that contained TC or PFacid and stirred for several minutes in order to build the BSA/TC or CH/PFacid shell.

2.3.2 Membrane emulsification for microcapsules

Microcapsule suspensions were prepared with a lab-scale membrane emulsification system, commercialized by Micropore Technologies Ltd (UK) under the commercial name Micropore LDC-1. As shown in Figure 2.2, it includes a microengineered emulsification membrane under a paddle-blade stirrer. The stirrer is driven by a DC motor, which controls the rotational velocity ω . The emulsification membrane is a thin flat nickel membrane which is chemically treated to have an hydrophobic or hydrophilic surface for w/o or o/w emulsions and is provided by Micropore Technologies Ltd (UK). The cylindrical pores are made by laser beam with a diameter of $10 \mu\text{m}$. The pore spacing and porosity of the membrane are $200 \mu\text{m}$ and 0.23% respectively. The arrays of the pores are located in an annular narrow ring shape region on the membrane to limit the variation of shear rate and minimize the polydispersity [86].

For CH / PFacid microcapsules, PFacid solution is agitated by the paddle with a rotational speed of 400 to 1200 rpm. The chitosan solution is injected by a syringe pump (Nemesys) through the membrane. The droplets are sucked up from the dispersion cell with a tube and collected in a beaker. The capsules are kept under gentle stirring in the PFacid solution to stiffen the membrane.

For BSA / TC microcapsules, solution of vegetable oil with span 85 is agitated by the paddle with a rotational speed of 400 to 1200 rpm. The BSA solution is injected by a syringe pump through the membrane. The droplets are sucked up from the dispersion cell and collected in a beaker containing the solution of TC. The capsules are kept under gentle stirring in the beaker to stiffen the membrane.

For both encapsulation systems, the membrane growth is stopped by diluting the oil phase with a large amount of cyclohexane. The microcapsules are then suspended in silicon oil (AP1000, AK1000, Wacker) for subsequent analysis.

2.4 Characterization of physical properties of suspensions

2.4.1 Size variation

Size distribution of microcapsules and droplets was measured by bright field microscopy. Particles were dispersed on a glass slide and scanned by an inverted microscope Olympus IX-

73 equipped with a 4, 10, or 20 times objective, a Marzhauser motorized stage, and a camera Hamamatsu ORCA-Flash 4.0. The sizes of the particles were measured with an home-made algorithm based on the image processing toolbox of Matlab (Mathworks) with several thousands of microcapsules for each batch.

2.4.2 Volume fraction

To determine the volume fraction of the particle suspensions, firstly the suspension was mixed well to be homogenized, and then at least three samples with precise volumes were retrieved from different places. The samples were diluted in the suspending fluid and entirely scanned under the microscope to find the total volume of particles.

2.4.3 Microcapsules shell elasticity G_s

We work under an assumption that microcapsules at rest have a spherical shape with a radius R . In the stagnation point, the major axis of the deformed microcapsule align with the direction of elongational flow in cross-slot branches. The projection of the deformed microcapsule profile in $x - y$ plane forms an ellipsoid with semi-principal axes L and S . The deformation is characterized by Taylor parameter

$$D = \frac{L - S}{L + S} \quad (2.1)$$

Based on the theory of Barthès-Biesel [87, 88] we can relate the steady state deformation of microcapsules D_∞ and the surface elasticity modulus G_s . In the regime of small deformations $D_\infty < 0.1$ and for Capillary number $Ca \ll 1$,

$$G_s = \frac{25 \eta \dot{\epsilon} R}{6 D_\infty} \quad (2.2)$$

where η is viscosity of the continuous phase.

Microfluidic device

In short, the microfluidic device is comprised of a 2D flow-focusing geometry in series with a cross-slot chamber, Figure 2.3-b. The flow-focusing geometry is used to center the capsules in the middle of the channel. The cross-slot with two opposite inlets and two opposite outlets is used to generate an extensional flow in which microcapsules are deformed and analyzed. The microfluidic design with a square cross section (1×1 and 0.5×0.5 mm²) was milled in PMMA mold that was further glued to a glass slide and connected to four syringe pumps (Nemesys). Microcapsules are injected in the central channel of the flow focusing and are centered by the two perpendicular jets (Figure 2.3-c). They travel with the flow to the center of the cross-slot chamber to be deformed in the region where hydrodynamic stress is constant and controlled with precision (Figure 2.3-d).

The microfluidic device is placed on an inverted microscope (Olympus IX-71) which is equipped with 20 and 40 fold objectives. A fast camera (Photron Fastcom SA3) allows us to take images up to 2000 frames per second. In order to minimize the transient time in the microfluidic system the usage of deformable tubings should be avoided as well as the air pockets in the system.

Cross-slot chamber

To determine the mechanical properties of a microcapsule's membrane, we should study the response of the membrane to exerted hydrodynamic stress. A planar extension flow in a cross-slot chamber allows us to impose the desired hydrodynamic stress on microcapsule's membrane in a controlled way. Figure 2.3-d shows a microcapsule brought by a flow to the center of elongational region. If the microcapsule passes through the center of the cross, it deforms as response to the

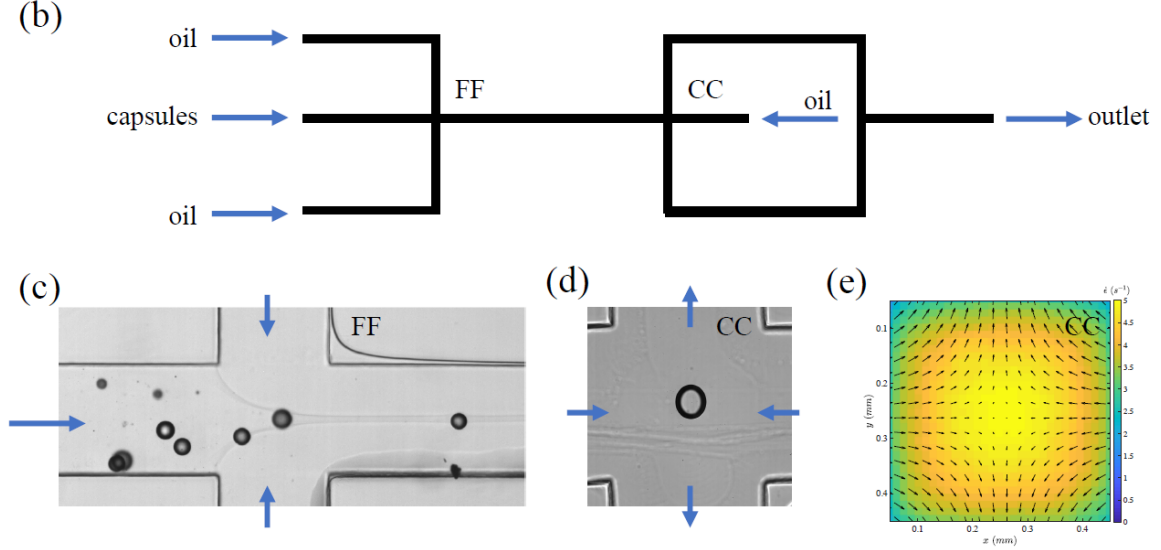


Figure 2.3: Mechanical characterization of suspensions of microcapsules. **b:** Flow chamber for the characterization of microcapsules elasticity. Capsules and oil are injected in a flow focusing geometry (FF) to center the capsules in the channel. Capsules are then stretched in the center of the cross-slot chamber (CC). **c:** Microcapsules being injected in the FF geometry. **d:** Deformation of a capsule in the center of the cross by extensional flow, see 2.4.3 for details. **e:** Colormap of the rate of elongation $\dot{\epsilon}$ in the center of the cross junction.

hydrodynamic stress exerted by the extension flow. The principle of our measurement is based on the fact that if the capsule is centered in the cross, we can measure its deformation in a steady state for a given extension rate. In this way, we can determine the mechanical properties of the membrane via a theoretical relation given by the equation 2.2. For the same purposes, this approach was already used and verified by [89, 84, 90] for microcapsules with different membrane formulations.

At the stagnation point of a planar extension flow when deformation of microcapsule reaches an equilibrium state, the membrane and the internal liquid are both motionless. This originates of symmetrical flows in cross-slot chamber. This means that the viscosity ratio between internal and external fluids of microcapsule has no influence on steady state [91].

For an ideal planar extensional flow of a Newtonian fluid in Stokes flow, the velocity field \vec{u} in Cartesian coordinates is described as

$$u_x = \dot{\epsilon}_0 x, \quad u_y = -\dot{\epsilon}_0 y \quad \text{and} \quad u_z = 0 \quad (2.3)$$

where the extension rate $\dot{\epsilon}_0$ is constant everywhere around the stagnation point. Note that the origin of Cartesian coordinates $O(0, 0)$ for Equation 2.3 is located at the stagnation point at the center of cross-slot chamber.

The Reynolds number (Re) in our experiments is calculated by

$$Re = \frac{\rho U D_h}{\eta} \quad (2.4)$$

where ρ and η are the density (1.08 g/mL) and viscosity (1 Pa.s) of suspending fluid (AP1000, Wacker) at 20 °C respectively. The Reynolds number in our experiments $Re < 1$ which means the flow is in Stokes regime.

We used home written (Matlab) particle tracking velocimetry (PTV) to obtain the velocity field \vec{u} and the extension rate $\dot{\epsilon}$ in cross-slot chamber. PMMA particles with an average diameter of 6 μm (Microbeads) were suspended in the Silicon oil AP1000 (Wacker) at a concentration of

0.2 gr/mL . PTV was performed when the suspension was completely homogeneous and there were no particle aggregations. We recorded an image sequence up to 4000 fps for every injection flow rate of particle suspension.

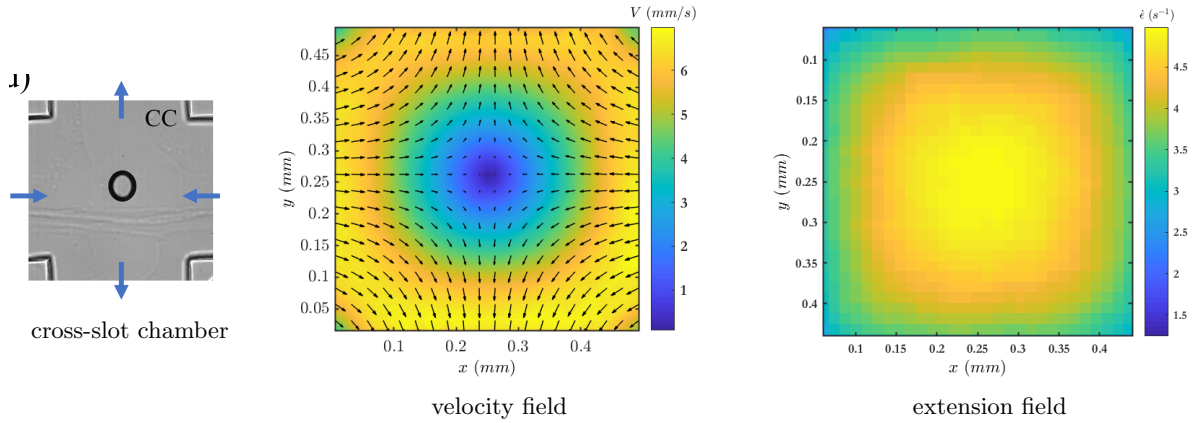


Figure 2.4: Velocity field \vec{u} and extension field ϵ at $z = 0$ plane of cross-slot chamber ($0.5 \times 0.5 \text{ mm}^2$).

Figure 2.4-b shows the velocity field \vec{u} inside the cross-slot chamber at the middle plane $z = 0$. As expected velocity of flow at the center of cross vanishes and causes a stagnation point $u_x, u_y = 0$. Here is the place where microcapsule is trapped, deformed and analyzed. As Figure 2.4-c illustrates, extension rate ϵ at the stagnation point is maximum. This value decreases by moving away from the center. In a region with $200 \mu\text{m}$ diameter around the stagnation point, the extension rate ϵ changes by 10 %. All measurements is done within this region.

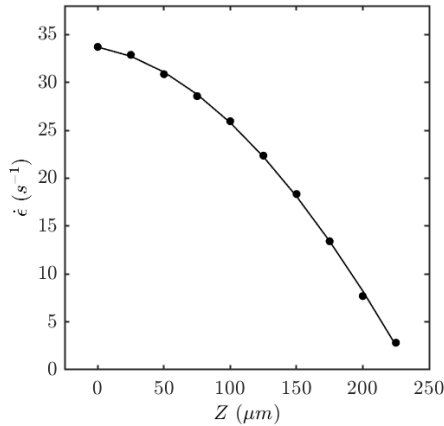


Figure 2.5: Parabolic profile of extension rate ϵ as a function of half depth of elongation chamber ($0.5 \times 0.5 \text{ mm}^2$)

As figure 2.5 illustrates, extension rate ϵ in $x - y$ plane decreases because of channel walls. We do our measurements in a depth of $z = \pm 100 \mu\text{m}$ where the extension rate changes by 8%.

Figure 2.6 shows the calibration of elongation rate and injection flow rate for both sizes of channel. We find that the extension rate around the stagnation point increases linearly by injection flow rate. This calibration allows us to apply a big range of extension rate on the microcapsules.

Flow focusing

Measuring membrane elasticity of microcapsules with a planar extension flow has already been studied and well established in [89, 84, 90]. To our knowledge it is the only simple, reliable and statistically relevant measurement method of microcapsule's membrane elasticity.

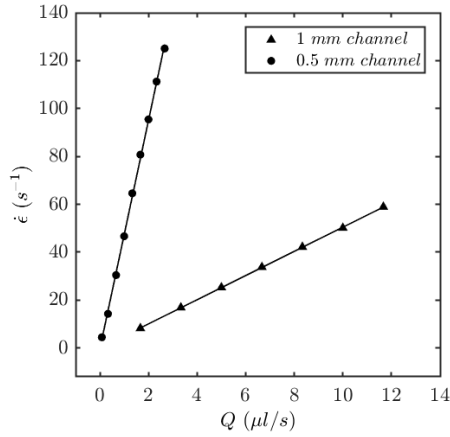


Figure 2.6: Extension rate at $z = 0$ around the stagnation point as a function of injection flow rate for both channels.

Otherwise, there is an issues with this method which lead us to improve measurement device: To implement this technique, the microcapsules should reach a steady deformation at stagnation point which is located at the center of cross-slot chamber. It means that the microcapsules should be brought individually to the stagnation point in a manual way. Therefore this technique remains completely hand-operated which requires a sophisticated know-how of the system and does not allow to process a large number of microcapsules.

To overcome this issue, first we should automatize the measurement process in order to analyze a considerable number of microcapsules. In this way we can have membrane elasticity distribution of a microcapsules suspension which is statistically reliable. Then we should adapt the process for high throughput continuous measurement. By a continuous flow, once steady state is established we can have a reliable estimation of exerted hydrodynamic stress on microcapsule's membrane.

The measurement process is improved thanks to the coupling of planar extension flow with a system for centering the microcapsules in an automated and continuous way. This centering system is a microfluidic flow focusing placed a few millimeters before the cross-slot chamber. As shown in 2.7, it is composed of a central channel into which a diluted suspension of microcapsules is injected. Then the microcapsules are centered by two adjacent flows of the suspending fluid.

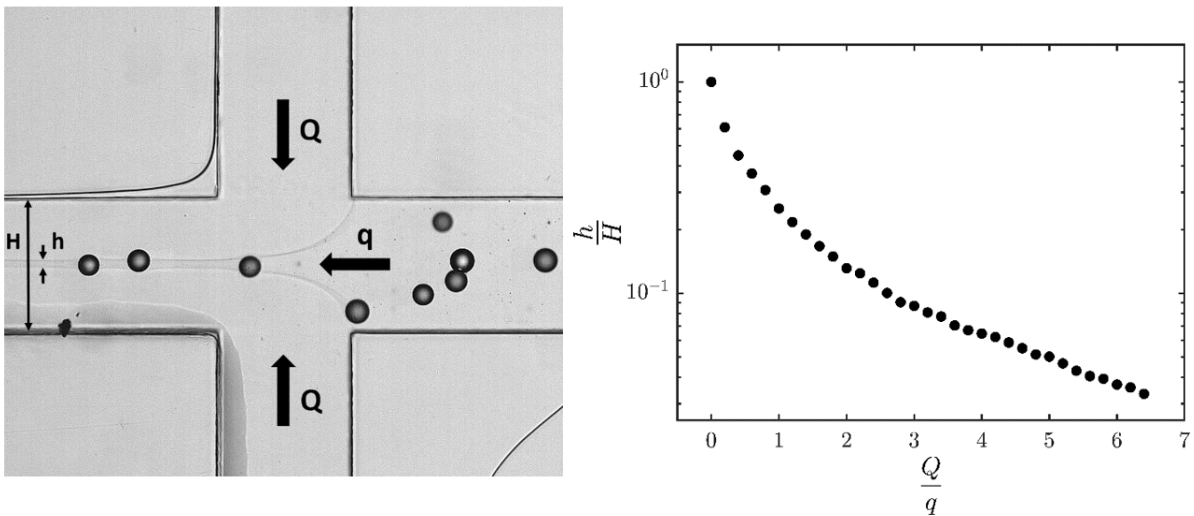


Figure 2.7: **a:** Flow focusing for centering microcapsules. **b:** Relative width of centered flow of microcapsules as a function of $\frac{Q}{q}$.

Using a flow focusing geometry allows us to have a chain of microcapsules which goes directly and continuously to the stagnation point of cross-slot chamber to be deformed and analyzed. For a microcapsules suspension with variable sizes and mechanical properties, automation of the measurement system makes it possible to determine the probability distribution function of the mechanical properties of these objects. The whole procedure of high frequency photography and image processing is done at real time based on a home made algorithm in Matlab (Mathworks). By this approach, all manual interventions is unnecessary and we can automatically measure the membrane elasticity of a large amount of microcapsules. The manual measurement of elasticity of a single microcapsule generally took 5 min [89, 84, 90] . Here, we can analyze about 1000 microcapsules in 90 min.

2.4.4 Rheometry and details about the rheometer

The rheological measurements were carried out with a stress-controlled rheometer (DHR3, TA) with a rotating parallel plate disk geometry. The gap and the diameter of the geometry were 1.5 mm and 60 mm respectively. This gap value was chosen to accommodate 10 to 15 microcapsules in the gap. Moreover, we observed that the apparent viscosity of the suspension was independent of the gap, if the latter was larger than 1 mm. Smooth and rough surfaces were used, without any incidences on the results, meaning that there was non evidence of wall slip effects. Since in a parallel plate geometry the shear rate is not constant and varies from the center to the rim, we corrected the measured viscosity with the Mooney-Rabinovitch correction [92]:

$$\eta_s = \eta_{app} \left[1 + \frac{1}{4} \frac{d}{d} \frac{\ln(\eta_{app})}{\ln(\dot{\gamma})} \right] \quad (2.5)$$

where η_{app} is the apparent viscosity measured by the rheometer, d the diameter of the geometry and $\dot{\gamma}$ the shear rate at the rim. The temperature was controlled with a Peltier system at 25°C.

Shear-Reversal experiments were carried out to the study the micro-structure of the suspension under a given shear stress, as proposed by Galda-Maria *et al.* [93]. The suspensions were pre-sheared with a shear stress σ of 10 Pa for 30 s. Then as shown in figure 4.3, a constant shear stress (ranging from 0.1 to 100 Pa) was imposed on the suspension until the measured viscosity achieved a steady state. Then, the imposed stress was set to zero during two seconds. The last step consisted in shearing the suspension with the same stress but in the opposite direction. The relaxation time of 2 s was chosen after different tests to have no effects of the inertia of the motor and the geometry on the measurement. then the viscosity shown a sudden drop up to increased and reach a steady state value.

2.5 Resuspension experiments

2.5.1 Transparent Taylor-Couette cell

A home-made transparent Taylor-Couette cell shown in figure ?? was carved from a PMMA (Poly(methyl methacrylate)) block with an inner and outer radius of $R_1 = 20$ mm, $R_2 = 24$ mm respectively. With a such a small gap ($R_2 - R_1 = 4$ mm), the radial variation of shear stress $\tau_{xy}(R_1)/\tau_{xy}(R_2) = R_2^2/R_1^2 = 1.44$ can be considered weak enough to provoke a significant radial shear-induced migration of droplets. Despite this small gap, at least $(R_2 - R_1)/2a = 10$ particles can be accommodated within the gap, where a is the radius of largest droplet. The Taylor-Couette cell was fixed on a stress-controlled rheometer (DHR3, TA) and the rotor had a constant angular velocity. The exerted shear rate for a given angular velocity of the rotor can be calculated as

$$\dot{\gamma} = 2\Omega \frac{R_1^2 R_2^2}{R_2^2 - R_1^2} \frac{1}{R_0^2} \quad (2.6)$$

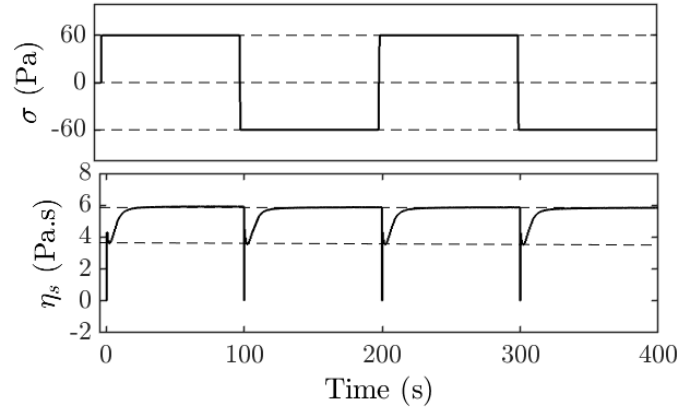


Figure 2.8: An example of Shear-Reversal experiment for a suspension of particle executed by a stress-controlled rheometer in a parallel plate geometry. **Top:** Shear stress as a function of time. **Bottom:** Apparent viscosity as a function of time.

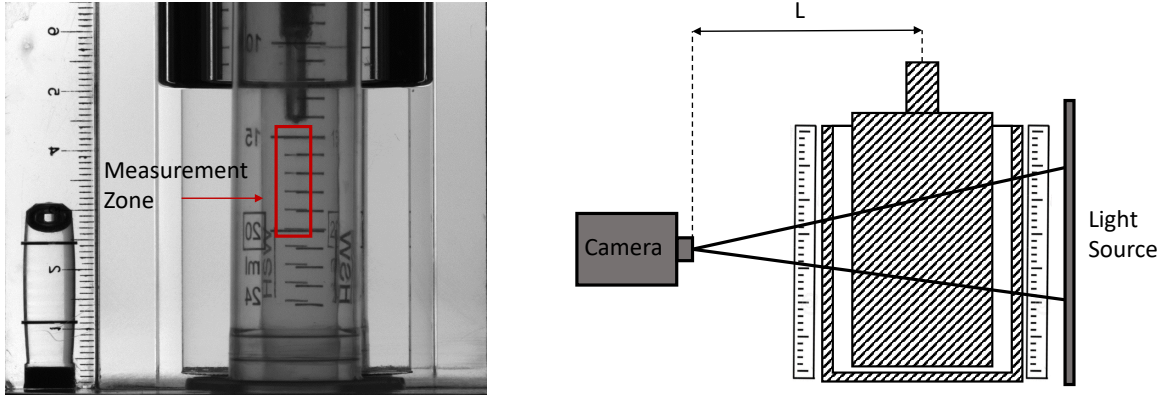


Figure 2.9: Parallax issue along the vertical direction solved by increasing the distance L between the camera and Taylor-Couette cell up to five meters. To have high resolution pictures of measurement zone a lens with a large focal length has been used. A ruler behind and front of the Taylor-Couette cell indicates a negligible parallax issue.

where $R_0 = (R_1 + R_2)/2$. The experiments were carried out in the range of $\dot{\gamma} = 6$ to 260 s^{-1} .

2.5.2 Visualization and parallax issue

In this section, we analyze the parallax issue raised by the finite distance between the camera and Taylor-Couette geometry. In the experimental setup, the light source was a 2D LED panel with a homogeneous and stable light intensity. It was placed parallel to the Taylor-Couette geometry with 10 cm of distance. As shown in figure 2.9-right, light beams traveled through the suspension and geometry, then they were collected by a camera (Basler, acA2500-14gc), located at a distance of L from the geometry.

By considering a finite value of L , the camera receives the incident light beams within an angle of 0 to α relative to the horizontal direction. This leads to a smoothing effect on the concentration profile in the vertical direction x_3 through a length of l (figure 2.9-right). This means that the measurement of the droplet concentration is vertically averaged in this length. Consequently, the errors induced by smoothing can be considerable where the vertical concentration sharply shifts to zero at the nose of the suspension as shown in figure ???. Note

that, measurement of normal viscosity $\eta_{n,3}$ and determining exponent n in SBM model depends strongly on the provided precision to detect the curvature of the concentration transition to zero.

By increasing the distance L between the camera and geometry, the angle α and the vertical averaging length l reduce. Consequently, the spatial smoothing of the concentration profile in the vertical direction becomes less effective. The experiments were performed with a distance of L up to 5 m, whereas the height of the suspension in the measurement zone was 2 cm. To have high resolution images (5 pixels for a droplet diameter) we used a lens with a large focal length. Figure 2.9-left represents an image of the geometry with two similar rulers placed at two sides of the geometry. We can observe that the parallax in the measurement zone is negligible however by approaching to the bottom of geometry, it becomes more decisive. In such configuration of the experimental setup, we estimate $\alpha = 0.11$ degree and vertical averaging length $l = 96 \mu\text{m}$. The ratio of l to the diameter of monodisperse and polydisperse droplets is $l/a = 1/3$ and 1 respectively. These small ratios indicate a negligible effect of the parallax on the concentration profile measurement where it experiences a sharp transition to zero. Consequently, the parallax does not impact the comparison of our measurements with SBM model.

2.5.3 Concentration profile measurement by light absorption

Vertical concentration profile of the resuspended emulsion $\phi(x_3)$ was determined based on the difference of light absorbance degree between the internal and external phase of droplets. This measurement relies on the fact that the intensity of light decreases as it travels through a liquid. This is due to absorption of light energy by medium's molecules. A large absorbance means that the light is quickly absorbed and a small absorbance means that the medium is relatively transparent to the light.

Initially since both mediums are completely transparent, there is no measurable light absorbance difference. Adding a colorant to the suspending fluid can provide a contrast in light absorbance degree between two phases. A non-fluorescent food-grade additive, E122 (Breton) used as the colorant. The idea is that the suspending fluid with a specific concentration of colorant c has an exact light absorbance degree. By inserting transparent droplets into the suspending fluid, the local concentration of the colorant c decreases and subsequently the light absorbance inclines. Thus characterizing absorbance of suspending fluid as a function of colorant concentration leads us to measure the local volume concentration of droplets ϕ .

UV-Vis spectrophotometry analysis of the colorant was performed in a quartz cuvette (Hellma Analytics) with a light path of $L = 2$ mm and a portable spectrometer (RedLite, Ocean Insight). Figure 2.10-left demonstrates the absorption spectra of the colorant dissolved in the suspending fluid with the concentration ranging from $c = 0.001\%$ to 0.04% mg/ml. The absorption spectrum was a broad band with a maximum absorbance peak at $\lambda = 520$ nm. We observe that the more colorant concentration is larger, the more absorbance intensity increases while the peak remains at the same wavelength.

To validate our experimental approach, we measured the absorbance of the colorant with a digital camera (acA2500-14gc, Basler) in Taylor-Couette Cell and compared the results with a spectrophotometer. As shown in figure 2.10-left, the wavelength related to the peak of absorbance is around $\lambda = 520$ nm, thus we used an interference bandpass filter with the center wavelength $\lambda = 525 \pm 15$ nm. Beer-Lambert law formulates the exponential decay of the light intensity passing through a solution. Thus we can relate intensities and a distance L and calculate the absorbance as:

$$A \equiv \log\left(\frac{I_0 - I_d}{I_L - I_d}\right) = \varepsilon c L \quad (2.7)$$

where I_0 is the light intensity after traveling the suspending fluid without colorant as well as the transparent container cell of sample, I_L is the traveled light intensity with contribution of the

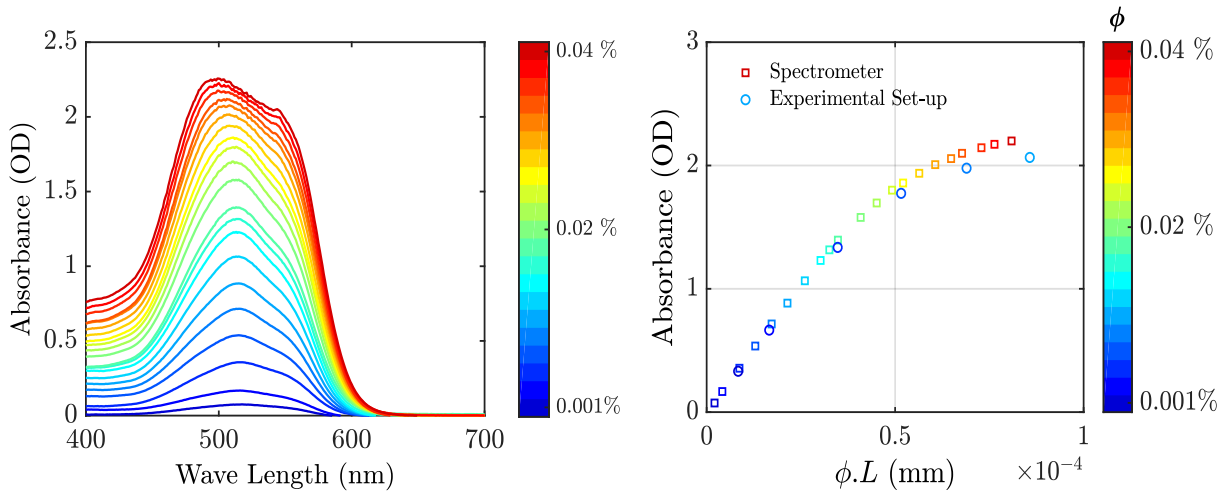


Figure 2.10: Characterization of the light absorbance of the colorant, **Left:** The light absorbance of the colorant for concentration ranging from $c = 0.001\%$ to 0.04% mg/ml. in visible light wave length measured by a spectrometer in a $L = 2$ mm cuvette, **Right:** Absorbance of the colorant at wave length $\lambda = 525$ nm as a function of $\phi.L$ where ϕ is the colorant concentration and L is the traveled length of light in the sample. The measured absorbance by the spectrometer in a cuvette with $L = 2$ mm has an excellent agreement in the linear part with measured absorbance by the experimental set-up in the Taylor-Couette cell. A bandpass filter with the center wavelength, $\lambda = 525 \pm 15$ nm was used in the experimental set-up.

colorant, I_d is the measured light intensity by the insulated camera which represents the noise and ε is the attenuation rate of light for the colorant. Contrary to the cuvette, in Taylor-Couette cell, the traveled length of the light beam through the sample is not constant. By determining the corresponding traveled length L for each pixel of the captured image, a 2D light absorbance map was obtained. As expected, for the homogeneous colorant solution in Taylor-Couette cell, we obtained an uniform 2D absorbance map. Figure 2.10-right demonstrates the absorbance of the colorant at wavelength $\lambda = 520$ nm, measured by the spectrophotometer and the experimental setup as a function of $\phi.L$ where ϕ is the colorant concentration and L is the traveled length of light in the sample. The measurements show an excellent consistency in the linear regime. The experiments were conducted in such fashion to keep the corresponding absorbance values within the linear part.

2.5.4 Tuning refractive index of droplets

Balancing the refractive index between the droplets and suspending fluid was crucial for our experimental method. Light refraction between the two phases in the emulsions could give rise to considerable errors in the measurement of the concentration profile $\phi(x_3)$. The refractive index of the oil phase was measured with precise refractometer (Abbemat 350, Anton Paar) $n = 1.44948$ nD at $T = 23$ °C and wavelength $\lambda = 589$ nm. Note that the resuspension experiments were conducted at the same temperature and a wavelength band of $\lambda = 525 \pm 15$ nm. Figure 2.11 illustrates the difference of refractive index between the droplets and suspending fluid for various glycerol volume fractions in the suspending fluid. The zero contrast was estimated with a glycerol volume fraction around $\phi = 84.68\%$ w/w. Then after preparing the solution, the contrast was refined to a precision of $\Delta n = 0.00000$ nD with drop-by-drop addition of glycerol or water. After each droplet addition to homogenize the solution it was rigorously mixed with a magnetic stirrer for an hour. After that 1 ml samples were pipetted from different sites in the solution volume. The refractive index of these samples was measured to the precision $\Delta n = 0.00000$ nD and in the case of mismatch the mixing was repeated.

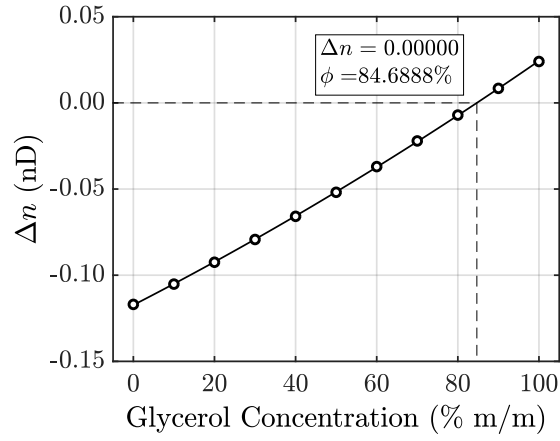


Figure 2.11: The difference of refractive index between the droplets and suspending fluid as a function of glycerol volume fraction at 23 °C and wavelength $\lambda = 589$ nm. A zero contrast of refractive index was estimated with glycerol concentration $\phi = 84.6888\%$. The final contrast was refined to a precision of $\Delta n = 0.00000$ nD by adding some drops of glycerol or water.

Chapter 3

Production and characterization of microcapsules

Membrane emulsification for the production of suspensions of uniform microcapsules with tunable mechanical properties

Mehdi Maleki^a, Clément de Loubens^{a,*}, Kaili Xie^a, Emeline Talansier^a, Hugues Bodiguel^a and Marc Leonetti^a

^aUniv. Grenoble Alpes, CNRS, Grenoble INP, LRP, 38000 Grenoble, France

ARTICLE INFO

Keywords:

membrane emulsification
microcapsules
interfacial rheology
microfluidic
capillarity
core-shell particle

ABSTRACT

A way forward for high throughput fabrication of microcapsules with uniform size and mechanical properties was reported irrespective of the kinetic process of shell assembly. Microcapsules were produced using lab-scale emulsification equipment with a micro-engineered membrane in the size range 10-100 μm . The shell of the microcapsules was assembled at the water-oil interface by complexation of polyelectrolytes or cross-linking of proteins providing two different kinetic processes. Elasticity of microcapsules was characterized with an automated extensional flow chamber. Process parameters were optimized to obtain suspensions with size variations of 15%. Some strategies were developed to obtain uniform elastic properties according to the kinetics of shell assembly. If kinetics is limited by diffusion, membrane emulsification and shell assembly have to be split into two steps. If kinetics is limited by the quantity of reactants encapsulated in the droplet, variations of elastic properties result only from size variations.

1. Introduction

Tuning the physical properties of microcapsules is of prime importance to control their stability and the delivery of encapsulated compounds in biological or industrial processes [1, 2, 3, 4]. Microcapsules' shells are ultra-thin elastic films characterized by a surface shear elastic modulus $G_s \sim Gh$, where h is the shell thickness and G the bulk shear elastic modulus. Deformation of a microcapsule of radius R in a shear flow of hydrodynamic stress σ is controlled by a capillary number $Ca = \sigma R/G_s$ that represents the ratio of viscous stress over the elastic shell response [5]. Consequently both size and shell rheology control the fate of microcapsules in processes such as break-up. Release of encapsulated compounds by osmotic pressure differences is also controlled by both shell elasticity and capsule size [6].

The simplest process for the fabrication of microcapsules is based on the emulsification with a rotor of two immiscible fluids with chemicals in each phase and their subsequent reaction at the interface leading to the formation of the shell [7, 8]. The major drawback of this process is the large variations of size and elasticity of produced microcapsules [7, 9]. Up to now, the gold standard method to control the properties of microcapsules is the layer-by-layer assembly of polyelectrolytes on dissolvable particles [10]. However this method is long and complex if several layers have to be deposited in order to stiffen the shell. Recently, several research groups have developed microfluidics techniques to generate microcapsules with highly uniform size and elasticity based on flow-focusing systems [8, 11, 12, 13, 14]. These techniques have clearly demonstrated their usefulness in understanding the relationships between the assembly of microcapsules and their interfacial rheological properties [8, 15], but were limited to research tools as their throughput was very low (a few $\mu\text{L}/\text{min}$) and were not easily scalable for industrial applications. Designing high throughput processes for the fabrication of microcapsule suspensions with uniform physical properties should open new perspectives for the optimization of microencapsulation technologies, e.g. drug delivery systems.

On the other hand, producing high-quality emulsions at pilot and industrial scales was made possible by the development of membrane emulsification systems with micro-engineered membranes [16, 17, 18]. Briefly, membrane emulsification consists in passing the dispersed phase through a membrane made of regular array of pores to form droplets that are detached by hydrodynamic stress. The pores size and surface properties have to be chosen carefully in order to produce monodisperse drops [19]. To some extent, membrane emulsification is a scaled-up version of microfluidic T-junction chips. Using this technique, suspensions of particles [20], multiple emulsions [21], soft beads [22] and liposomes [23] were produced at lab and pilot scales with an excellent control of the size uniformity.

*Corresponding author: clement.de-loubens@univ-grenoble-alpes.fr
ORCID(s): 0000-0002-4988-9168 (Clément de Loubens)

Uniform microcapsule production by emulsification

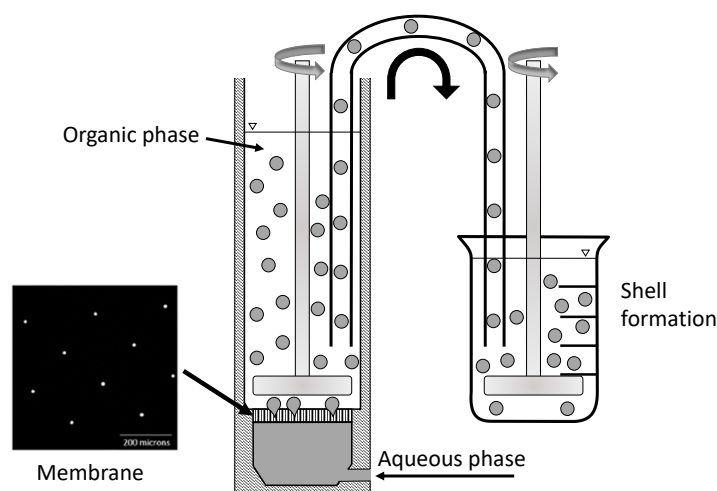


Figure 1: Sketch of the membrane emulsification system and microscopic image of the micro-engineered membrane. Aqueous droplets of BSA or CH were dispersed in the oil phase through the micro-engineered membrane. The droplets were sucked-up in a beaker that contained TC or PFAcid and stirred for several minutes in order to build the BSA/TC or CH/PFAcid shell.

However, translating membrane emulsification technologies for the high throughput production of microcapsules is not straightforward to obtain particles with uniform size and elastic properties. In fact, shell elasticity depends closely on the physico-chemical conditions of shell formation [24, 25, 26], but also on the control parameters of the fabrication process [7, 8]. Two well-studied examples can illustrate the differences in the kinetics of shell formation. The first one is based on interfacial complexation of polyelectrolytes. Two oppositely charged polyelectrolytes are dissolved in two immiscible phases and form a solid at the interface of the droplets after the emulsification step. It has been established that the kinetics of shell formation is limited by the diffusion of one of the polyelectrolytes [27, 28, 11, 29, 8]. Consequently, surface elasticity increases with the shell formation time (from a few seconds to a few hours) [8]. The second example relates to microcapsules based on interfacial cross-linking of proteins [30, 31]. In this case, proteins are dissolved in an aqueous phase and dispersed in an organic phase that contains the cross-linker. The reaction is limited to a few seconds by the quantity of proteins encapsulated in the droplet and surface elasticity greatly increases with the capsule size, whereas other parameters are kept constant (i.e. pH, concentration of proteins) [7, 9, 32]. Conversely, the surface elasticity of polyelectrolytes microcapsules does not depend on their size [8]. Both examples show that time and size have different impacts on the mechanical properties of the shell depending on its kinetics of formation. We can also anticipate that the membrane emulsification process should be controlled in different ways based on the kinetics of shell formation if elastic properties have to be controlled. The surface elasticity of the shell can be characterized by several methods: osmotic tests [6], AFM [33] or hydrodynamic methods [7]. To date, these techniques are manual and time consuming. Consequently, a small number of capsules can be analyzed. In order to quantify the shell elasticity and its variation in a sample and to conclude about the performance of membrane emulsification for capsule production, it is so required to develop also automated systems of capsule characterization.

Our objective was to show a route for high throughput fabrication of microcapsules with uniform size and elasticity. Suspensions of microcapsules were produced with a scalable membrane emulsification system [18] using a micro-engineered membrane in the size range of 10-100 μm . The effect of process parameters on the size distribution was studied. In order to optimize the process according to the kinetics of shell formation, two well-characterized microencapsulation systems were studied based on interfacial complexation of polyelectrolytes [28, 8] and cross-linking of a protein [7, 34, 9]. Based on a well-established hydrodynamic method [7], we developed a new millifluidic chamber to measure at high-throughput the distribution of the surface elasticity of a suspension. In this way, we designed different strategies to optimize the uniformity of the elastic properties according to the kinetics of shell formation.

2. Materials and Methods

2.1. Solutions for microcapsule preparation

Microcapsules were made by interfacial complexation of chitosan (CH) with phosphatidic fatty acid (PFacid) [28, 8] or by interfacial cross-linking of bovine serum albumin (BSA) with terephthaloyl chloride (TC) [35].

Chitosan is a polysaccharide carrying positively charged groups and is soluble in water at pH 3.0, whereas PFacid is a surfactant that is soluble in vegetable oil and negatively charged. Chitosan (CAS number 9012-76-4, Sigma-Aldrich) of medium molecular weight and 75-85% deacetylation was dissolved in Millipore water (Resistivity $> 18.2 \text{ m}\Omega.\text{cm}$) at a concentration of 0.25 % w/w by adjusting the pH with hydrochloric acid (1 mol/L) at 3.0. The chitosan solution was then filtered to remove undissolved particles through Minisart syringe-filters (pore size $5.0 \mu\text{m}$). PFacid was comprised of a commercial lecithin known as lecithin YN (Palsgaard 4455, food-grade, E442) which was kindly provided by Palsgaard. PFacid was dissolved in food-grade colza oil (Géant Casino, french supermarket) with concentration ranging from 0.1 to 10 % w/w.

To synthesize BSA / TC microcapsules, BSA (CAS number 9048-46-8, Sigma-Aldrich) was dissolved in phosphate buffered saline solution (Fisher Scientific) and TC (CAS number 100-20-9, Sigma-Aldrich) dissolved in a mixture of chloroform (CAS number 67-66-3, Sigma-Aldrich) : cyclohexane (CAS number 110-82-7, anhydrous, 99.5%, Sigma-Aldrich) at a ratio of 4:1 by volume. Sorbitane trioleate 85 (SPAN 85, CAS Number: 26266-58-0, Sigma-Aldrich) was used to stabilize albumin drops during emulsification.

2.2. Fabrication of suspensions of microcapsules

Suspensions of microcapsules were prepared with a lab-scale membrane emulsification system marketed by Micropore Technologies Ltd (UK) under the commercial name Micropore LDC-1. As shown in Figure 1, it included a micro-engineered emulsification membrane under a paddle-blade stirrer. The stirrer was driven by a DC motor, which controlled the rotational velocity ω . The emulsification membrane was a thin flat nickel membrane which was chemically treated to have an hydrophobic surface. It was provided by Micropore Technologies Ltd (UK). The cylindrical pores were made by laser beam with a diameter of $10 \mu\text{m}$. The pore spacing and porosity of the membrane were $200 \mu\text{m}$ and 0.23 %. The array of the pores was located in an annular narrow ring shape region on the membrane to limit variation of shear rate and minimize the polydispersity [18].

For CH / PFacid microcapsules, PFacid solution was agitated by the paddle with a rotational speed of 400 to 1200 rpm. The chitosan solution was injected for 45 s by a syringe pump (Nemesys) through the membrane. The droplets were sucked-up from the dispersion cell with a tube and collected in a beaker to improve the size uniformity of the suspension (see Results and Discussion). The capsules were kept under gentle stirring in the PFacid solution for 2 to 30 min to stiffen the shell. For BSA / TC microcapsules, solution of vegetable oil with span 85 was agitated by the paddle with a rotational speed of 400 to 1200 rpm. The BSA solution was injected by a syringe pump through the membrane during 45 s. The droplets were sucked-up from the dispersion cell and collected in a beaker containing the solution of TC. The capsules were kept under gentle stirring in the beaker for 2 min to stiffen the shell. The mean size of the capsules ranged from 10 to $100 \mu\text{m}$, according to the process parameters and viscosities of the dispersed and continuous phases.

For both encapsulation systems, the shell growth was stopped by diluting the oil phase with a large quantity of cyclohexane. The microcapsules were then suspended in silicon oil AP1000 (Wacker) for subsequent analysis.

2.3. Characterization of microcapsules

Size distribution of microcapsules was measured by bright field microscopy. A diluted suspensions of microcapsules was let to sediment in a petri dish and scanned by an inverted microscope Olympus IX-72 equipped with a 4, 10 or 20 times lens, a Marzhauser motorized stage and a camera Hamamatsu ORCA-Flash 4.0. Consequently, microcapsules were all on the same focal plane without overlap between them. The size of the microcapsules was measured with a home-made algorithm based on the image processing toolbox of Matlab (Mathworks). Due to the difference of optical indexes between oil and water, the contrast was excellent which make the detection not sensitive to the threshold or the lighting conditions. The measurements were carried out on several thousand capsules for each batch. The capsules were deposited on a glass slice (in a very diluted regime), so they were all on the same plane without overlap between them. Typically, the mean radius ranged from 10 to $100 \mu\text{m}$. The standard deviation normalized by the mean radius ranged from 15 to 50%, see Results for details.

The surface shear elasticity G_s of the microcapsules was measured in an extensional flow chamber that has been automatized to study a large number of microcapsules. In our previous work, the determination of G_s took 5 min for a

Uniform microcapsule production by emulsification

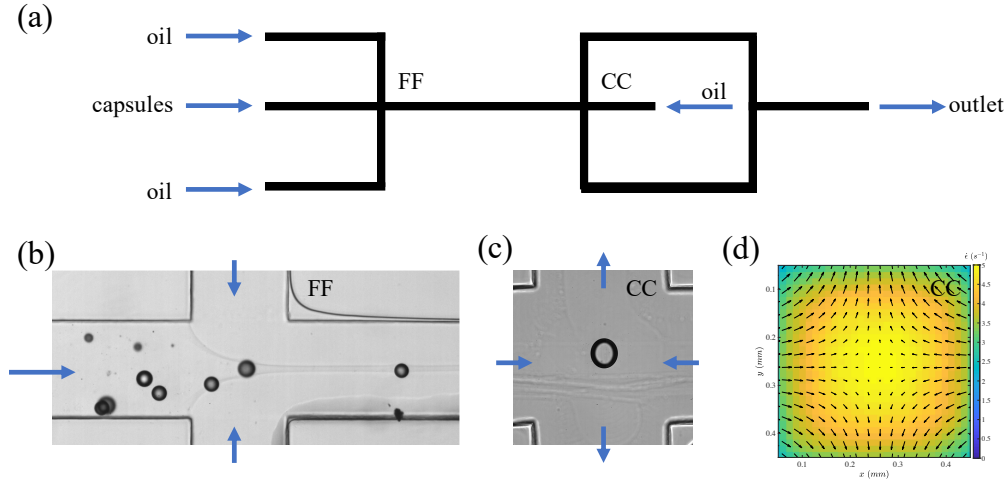


Figure 2: Automated extensional flow chamber for the characterization of microcapsules. **a:** Design of the millifluidic device. Capsules and oil are injected in a flow focusing geometry (FF) to center the capsules in the channel. Capsules are then stretched in the center of the cross-slot channel (CC). **b:** Microcapsules which have been produced by membrane emulsification being injected in the FF geometry. **c:** Deformation of a capsule in the center of the cross by extensional flow, see 2.3 for details. **d:** Colormap of the rate of elongation $\dot{\epsilon}$ in the center of the cross junction.

single capsule [7, 8, 34]. Here, we analyzed about 1,000 microcapsules in 90 min. Briefly, the device was comprised of a 2D flow-focusing geometry in serial with a cross-slot chamber, Figure 2-a. The flow-focusing geometry was used to center the capsules in the mid-plan of the channel. The cross-slot with two opposite inlets and two opposite outlets was used to generate an extensional flow in which microcapsules were deformed and analyzed. The channels of square section ($1 \times 1 \text{ mm}^2$) were engraved in PMMA and connected to four syringe pumps (Nemesys). Microcapsules were injected into the central channel of the flow focusing and were centered by the two perpendicular jets (Figure 2-b). They then reached the center of the cross-slot chamber to be deformed in the region where the hydrodynamic stress was maximal (Figure 2-c, d). The velocity \vec{u} and the elongation rate $\dot{\epsilon}$ were calibrated by particle tracking velocimetry. As expected, we found that the flow was hyperbolic: $u_x = \dot{\epsilon}x$, $u_y = \dot{\epsilon}y$ with $\dot{\epsilon}$ being the rate of elongation (Figure 1-c). $\dot{\epsilon}$ was almost constant in a zone of $200 \mu\text{m}$ radius around the stagnation point and increased linearly with the flow rate, see [7] for details. The radius of this zone has to be at least 1.5 times larger than the radius of the microcapsules to obtain an accurate result [7]. As the flow had a parabolic profile in the z direction, we discarded from the analysis the microcapsules that were not localized in a region near the mid-plane of the channel using a homemade algorithm. Microcapsules deformed as an ellipsoid with a steady-state shape. The deformation is characterized by the Taylor parameter $D = (L - S)/(L + S)$ with L and S being the major and minor axis of the ellipsoid respectively. In the regime of small deformations ($D_\infty < 0.1$), the surface elasticity G_s and the steady-state Taylor parameter D_∞ are related by [36]

$$G_s = \frac{25}{6} \frac{\eta \dot{\epsilon} R}{D_\infty} \quad (1)$$

with η being the viscosity of the continuous phase, i.e. the silicone oil, 1.18 Pa.s at 22°C.

Results on the distribution of the size and the elasticity were presented in terms of probability distribution function. If X is a variable of interest (R or G_s), its probability distribution function $P_X(X)$ is defined by

$$P_X(X) = \frac{1}{\Delta X} \frac{N(X - \frac{\Delta X}{2}, X + \frac{\Delta X}{2})}{N_T} \quad (2)$$

where N is the number of microcapsules whose variable X_i ranged between $X - \frac{\Delta X}{2}$ and $X + \frac{\Delta X}{2}$ and N_T the total number of microcapsules, so that $\int P_X dX = 1$. P_X was then smoothed with an averaged moving filter. The

Uniform microcapsule production by emulsification

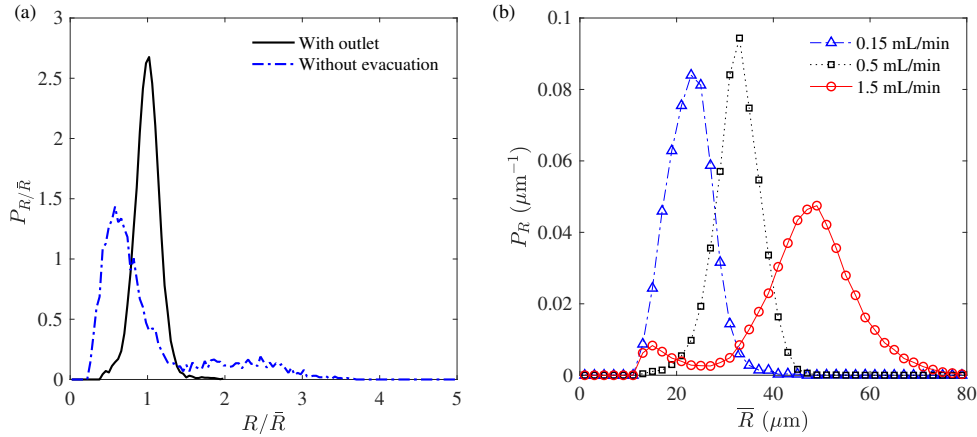


Figure 3: **a:** Probability distribution function of the size P_R for suspensions of CH / PFacid microcapsules made with (plain line) and without (dashed line) outlet. **b:** Comparison of P_R for different flow rates Q of CH solution injection.

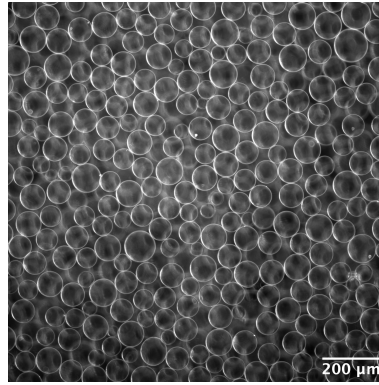


Figure 4: Fluorescence imaging of a suspension of CH / PFacid microcapsules produced by membrane emulsification.

uniformity was quantified by the coefficient of variation CV

$$CV = \frac{1}{\bar{X}} \sqrt{\frac{\sum_i (X_i - \bar{X})^2}{N_T - 1}} \times 100 \quad (3)$$

with \bar{X} being the mean value of X .

3. Results and Discussion

3.1. Size distribution of microcapsules

We investigated the effects of process parameters (paddle rotational speed ω and flow rate Q) on the mean radius \bar{R} , the probability distribution P_R and coefficient of variation CV for CH / PFacid microcapsules. First of all, the stirred emulsification cell was used as a batch process to produce monosized particles [18, 37]. For microcapsules, we observed that this batch version of the process was not suitable: CV was larger than 50 % (Figure 3-a, dashed line). As the dispersed phase had a larger density than the vegetable oil, microcapsules were not efficiently suspended in the cell by the paddle and tended to settle near the membrane where they could coalesce and/or be broken by the mechanical agitation. To overcome this limitation, microcapsules were pumped continuously at constant rate from their site of formation to outside through a tube. As shown on Figure 1, this strategy, similar to a continuous process, allowed us to minimize CV up to 15% in optimal conditions (Figure 3-a; plain line). Even with evacuation, bi-modal size distribution was observed for large injection flow rates ($Q = 1.5$ mL/min), whereas for lower Q the distribution was Gaussian with a CV that was minimized up to 15% (Figure 3-b and 4).

Uniform microcapsule production by emulsification

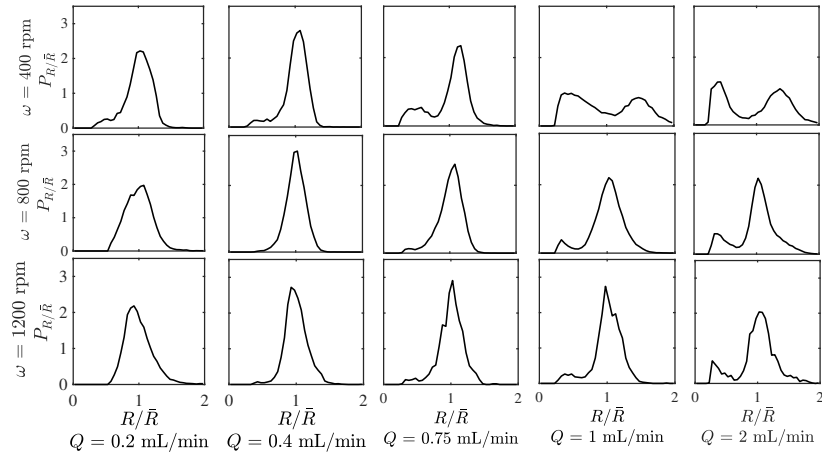


Figure 5: Size probability distribution $P_{R/\bar{R}}$ as a function of the normalized radius R/\bar{R} for different paddle rotational speeds ω and injection flow rate Q . CH / PFacid microcapsules.

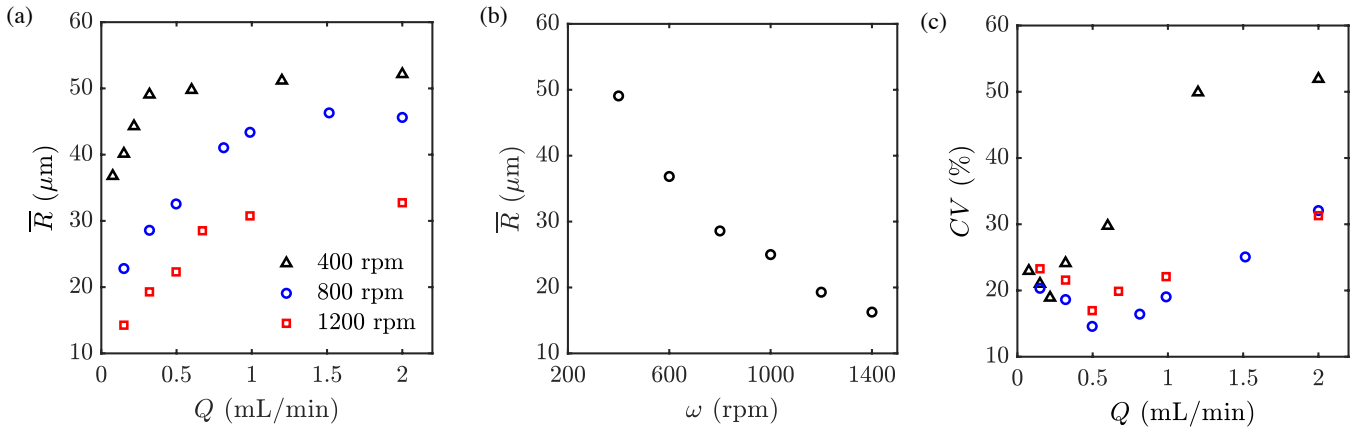


Figure 6: **a:** Mean radius \bar{R} as a function of the injection flow rate Q for different paddle rotational speed ω . **b:** \bar{R} as a function of ω , $Q=0.32$ mL/min. **c:** Coefficient of variation of size CV as a function of Q . CH / PFacid microcapsules.

Figure 5 shows the shape of P_R for systematic variations of Q and ω . We observed that, by increasing Q , the shape of P_R shifted from unimodal to bimodal form. This transition corresponded to the transition of drop generation from dripping (drop by drop) to jetting (continuous jet) regime [38, 39]. In the dripping regime (small Q), droplet detachment depends on the balance between interfacial force and hydrodynamic stress generated by the stirrer ω . It has been shown that droplets mature at the pore in a reproducible way until they are detached by hydrodynamic stress. This mechanism leads to a unimodal shape of P_R [38, 39]. In the jetting regime (large Q), the inertial force of injection exceeds the interfacial force and droplets are created by a jet. The resulting jet breaks up by the Plateau-Rayleigh instability and alternates production of small and large droplets which leads to a bimodal shape of P_R [38, 39]. Size distributions of Figure 5 are summed up in Figure 6 by plotting the variations of \bar{R} and CV with Q and ω . Figures 6-a & b show that \bar{R} increased when Q was increased and ω was decreased. At high Q (>1 mL/min), \bar{R} saturated due to the emergence of a bimodal size distribution (Figure 5). Figures 6-c show that CV had an optimum value of 15 % for 800 rpm and 0.5 mL/min. For other values of Q and ω , CV was reasonably maintained at 20-25 %, except for bimodal distribution, for which CV exceeded 50 %. This was coherent with previous results on droplets produced with a similar device [18, 37]. Note that CV was minimized up to few percents by using rotating membrane emulsification systems [23].

Uniform microcapsule production by emulsification

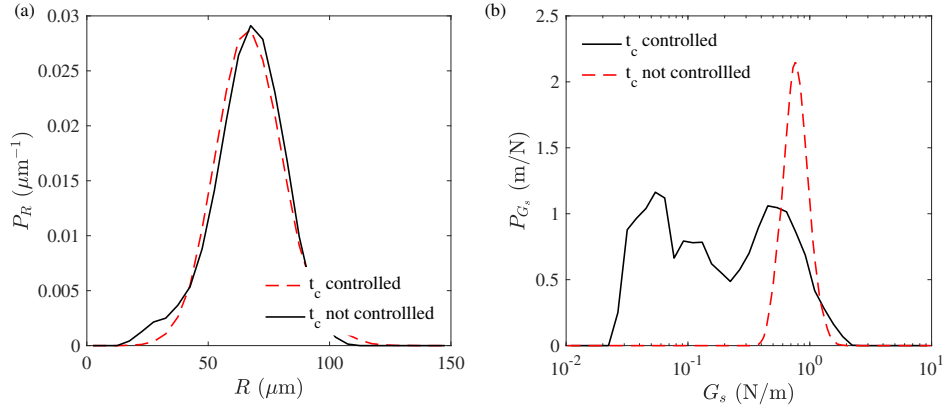


Figure 7: Comparison of uniformity of CH/PFacid microcapsules with (red dashed line) and without (black plain line) control of complexation time t_c . **a:** Probability distribution function of size P_R . CV is of 18 -19% for both conditions. **b:** Probability distribution function of surface elasticity P_{G_s} . CV is of 56% when the t_c is not controlled and reduced up to 24% when t_c is controlled.

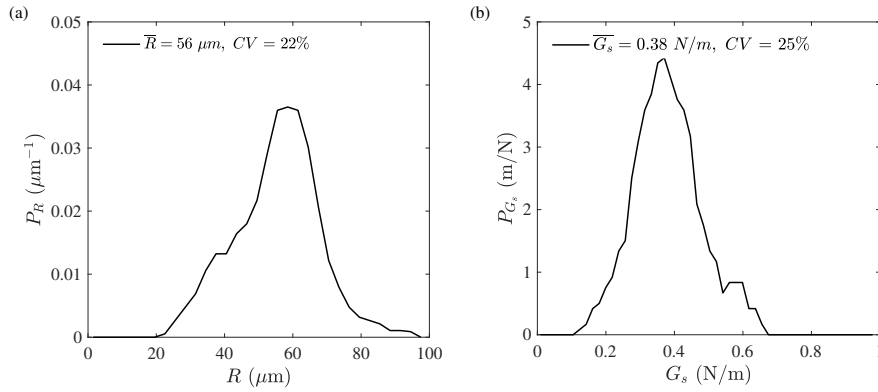


Figure 8: Fabrication and characterization of BSA/TC microcapsules. **a:** Size probability distribution P_R . **b:** Surface elasticity distribution P_{G_s} .

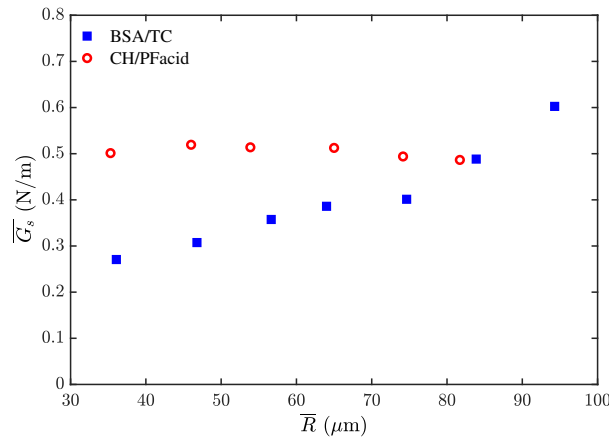


Figure 9: Mean surface elasticity \bar{G}_s as a function of the size range ($\pm 10 \mu\text{m}$).

3.2. Microcapsules with uniform elasticity

During production of uniform droplets by membrane emulsification, the emulsion was sucked up and stirred in a beaker in which the reaction took place to build the shell of the microcapsules (Figure 1). This process was designed with the initial aim of optimizing the size distribution of the droplets, Figure 3. However, splitting the process into two

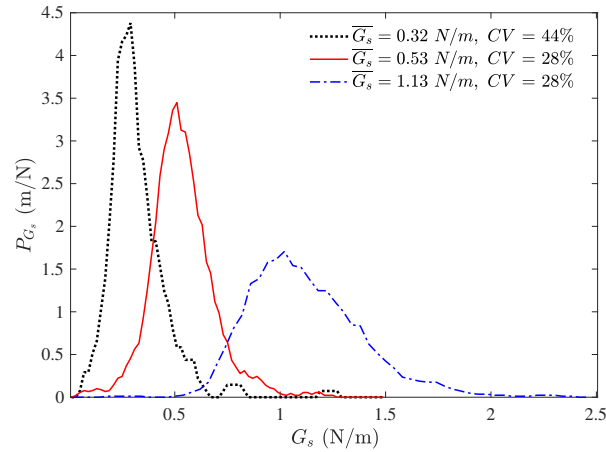


Figure 10: Probability distribution function of surface elasticity P_{G_s} for different physicochemical conditions. \bar{G}_s can be tuned with the conditions. Black dotted line: PFacid 1% w/w, CH 0.25% w/w, $t_r = 4$ min ; Red plain line: PFacid 1% w/w, CH 0.25% w/w, $t_r = 8$ min ; Blue dashed line: PFacid 21% w/w, CH 0.25% w/w, $t_r = 15$ min

steps gave also the opportunity to minimize the dispersion of elastic properties of microcapsules based on the kinetics of shell formation.

As explained in the introduction, growth of shell based on complexation of polyelectrolytes (CH/PFacid) is limited by diffusion: G_s and h increase with complexation time t_c [27, 28, 11, 29, 8]. To illustrate the consequences on production by membrane emulsification, we compared two strategies of building the shell. The naive strategy consisted in producing capsules using a concentration of PFacid of 10 % w/w in the oil phase and collecting them for 8 min in a beaker under gentle stirring containing the same continuous phase. Microcapsules were then washed to stop the reactions (see Materials and Methods). Under these conditions, the complexation time t_c was not controlled and varied between 0 and 8 min for capsules of the same batch. We expected so that capsules will have non uniform mechanical properties, because the shell of the first produced capsule should be thicker than the shell of the last produced capsule. The black lines of Figure 7-a and b show that P_R had a typical Gaussian shape ($CV = 19\%$) whereas P_{G_s} was broad and covered almost two orders of magnitude of G_s ($CV = 56\%$). We explained these variations by the time lag between production of the first and last capsules. Consequently, we designed an optimized strategy for which t_c was controlled. Microcapsules were produced with a very low concentration of PFacid (0.1 % w/w) in the emulsification system to stabilize the droplets and minimize the growth of the shell. Droplets were collected for 8 min in a beaker. When the production of droplets was finished, PFacid was added to the beaker to get 10 % w/w in the oil phase and the capsules were left under gentle stirring for 8 min. In this way, t_c was the same for all the microcapsules. Then P_{G_s} was Gaussian and CV decreased up to 24 %, dashed line of Figure 7-b. In conclusion, for shell formation limited by diffusion, one way to minimize the dispersion of shell elasticity is to dissociate droplets generation and shell formation to carefully control the reaction time.

Growth of BSA/TC capsule is limited by the mass of proteins that is encapsulated in the droplet [7, 9]. As shown in our previous studies, shell growth takes a few seconds and surface elasticity does not depend on time [32]. However, G_s increases over several orders of magnitudes with the capsule size for the same physicochemical conditions [7, 9]. In fact, a simple mass balance shows that the surface concentration of BSA available for the reaction is proportional to the radius of the capsule [7]. Then, we produced BSA droplets stabilized with a non-ionic surfactant by membrane emulsification and collected for 8 min the droplets in a beaker with the cross-linker (TC) to build the shell. CV of size distribution was about 22 % and P_{G_s} had a Gaussian shape with a mean of 0.4 N/m and a CV of 25 % (Figure 8). As expected from our previous studies [7, 9], there was an almost linear increase with the size of the mean surface elasticity \bar{G}_s (Figure 9). Note that \bar{G}_s did not varied in size for CH/PFacid capsules. We concluded that the size distribution has a strong impact on P_{G_s} for microencapsulation systems limited by the quantity of reactants that are encapsulated in the droplet.

Finally, we showed that the mean surface elasticity \bar{G}_s could also be tuned by varying the concentration of chemicals in the oil and aqueous phases or the time allowed for shell complexation after the production of the droplets (from a few seconds to several minutes or hours). Figure 10 shows P_{G_s} of CH/PFacid microcapsules for various concentrations of

PFacid and/or complexation times. \overline{G}_s and CV ranged from 0.32 to 1.13 N/m and 28 and 44 %, respectively. Details of the effects of physicochemical conditions on shell elasticity and thickness were described in our previous publications [7, 8, 9].

4. Conclusion

A lab-scale emulsification system with micro-engineered membrane was optimized to produce suspensions of microcapsules with variations in size and elasticity of 15-20 % in optimal conditions at throughput of a few mL/min. We concluded that the production of the droplets by membrane emulsification and capsule shell formation have to be split into two steps when shell growth is limited by diffusion (e.g. complexation of polyelectrolytes, CH/PFacid). If shell growth is limited by the quantity of reactants encapsulated in the droplet, variations of elastic properties are directly related to size variations (e.g. cross-linking of proteins, BSA/TC). Finally, membrane emulsification is a powerful method which can be easily scaled-up for the high throughput production of microcapsules with uniform and tunable physical properties, irrespective of the kinetics of shell formation.

5. Acknowledgments

LRP is part of the LabEx Tec21 (ANR-11-LABX-0030) and of the PolyNat Carnot Institute (ANR-11-CARN-007-01). This work has benefited from financial support from the ANR 2DVISC (ANR-18-CE06-0008).

References

- [1] S. Anandhakumar, V. Nagaraja, A. M. Raichur, Reversible polyelectrolyte capsules as carriers for protein delivery, *Colloids Surf.*, B 78 (2) (2010) 266–74. doi:10.1016/j.colsurfb.2010.03.016.
- [2] D. J. McClements, Nanoscale nutrient delivery systems for food applications: Improving bioactive dispersibility, stability, and bioavailability, *J. Food Sci.* 80 (7) (2015) N1602–N1611. doi:10.1111/1750-3841.12919.
- [3] M. A. Trojer, L. Nordstierna, J. Bergek, H. Blanck, K. Holmberg, M. Nyden, Use of microcapsules as controlled release devices for coatings, *Adv. Colloid Interface Sci.* 222 (2015) 18–43.
- [4] M. P. Neubauer, M. Poehlmann, A. Fery, Microcapsule mechanics: from stability to function, *Adv Colloid Interface Sci* 207 (2014) 65–80. doi:10.1016/j.cis.2013.11.016.
- [5] K. S. Chang, W. L. Olbricht, Experimental studies of the deformation and breakup of a synthetic capsule in steady and unsteady simple shear flow, *J. Fluid Mech.* 250 (1993) 609–633. doi:10.1017/s0022112093001582.
- [6] C. Gao, E. Donath, S. Moya, V. Dudnik, H. Möhwald, Elasticity of hollow polyelectrolyte capsules prepared by the layer-by-layer technique, *Eur. Phys. J. E: Soft Matter Biol. Phys.* 5 (1) (2001) 21–27.
- [7] C. de Loubens, J. Deschamps, M. Georgelin, A. Charrier, F. Edwards-Lévy, M. Léonetti, Mechanical characterization of cross-linked serum albumin microcapsules, *Soft Matter* 10 (25) (2014) 4561–4568.
- [8] K. Xie, C. De Loubens, F. Dubreuil, D. Z. Gunes, M. Jaeger, M. Léonetti, Interfacial rheological properties of self-assembling biopolymer microcapsules, *Soft matter* 13 (36) (2017) 6208–6217.
- [9] J. Gubspun, P.-Y. Gires, C. De Loubens, D. Barthes-Biesel, J. Deschamps, M. Georgelin, M. Léonetti, E. Leclerc, F. Edwards-Levy, A.-V. Salsac, Characterization of the mechanical properties of cross-linked serum albumin microcapsules: effect of size and protein concentration, *Colloid Polym. Sci.* 294 (8) (2016) 1381–1389.
- [10] J. J. Richardson, J. Cui, M. Björnmalm, J. A. Braunger, H. Ejima, F. Caruso, Innovation in layer-by-layer assembly, *Chemical Reviews* 116 (23) (2016) 14828–14867.
- [11] S. Sivakumar, J. K. Gupta, N. L. Abbott, F. Caruso, Monodisperse emulsions through templating polyelectrolyte multilayer capsules, *Chemistry of Materials* 20 (6) (2008) 2063–2065.
- [12] Y. Hennequin, N. Pannacci, C. P. de Torres, G. Tetradis-Meris, S. Chapuliot, E. Bouchaud, P. Tabeling, Synthesizing microcapsules with controlled geometrical and mechanical properties with microfluidic double emulsion technology, *Langmuir* 25 (14) (2009) 7857–7861.
- [13] G. Kaufman, S. Nejati, R. Sarfati, R. Boltyanskiy, M. Loewenberg, E. R. Dufresne, C. O. Osuji, Soft microcapsules with highly plastic shells formed by interfacial polyelectrolyte-nanoparticle complexation, *Soft matter* 11 (38) (2015) 7478–7482.
- [14] J. D. de Baubigny, C. Trégouët, T. Salez, N. Pantoustier, P. Perrin, M. Reyssat, C. Monteux, One-step fabrication of pH-responsive membranes and microcapsules through interfacial h-bond polymer complexation, *Scientific Reports* 7 (1) (2017) 1265.
- [15] C. Tregouët, T. Salez, C. Monteux, M. Reyssat, Microfluidic probing of the complex interfacial rheology of multilayer capsules, *Soft matter* 15 (13) (2019) 2782–2790.
- [16] S. M. Joscelyne, G. Trägårdh, Membrane emulsification—a literature review, *Journal of Membrane Science* 169 (1) (2000) 107–117.
- [17] G. Vladislavljević, I. Kobayashi, M. Nakajima, Production of uniform droplets using membrane, microchannel and microfluidic emulsification devices, *Microfluidics and nanofluidics* 13 (1) (2012) 151–178.
- [18] S. R. Kosvintsev, G. Gasparini, R. G. Holdich, I. W. Cumming, M. T. Stillwell, Liquid-liquid membrane dispersion in a stirred cell with and without controlled shear, *Industrial & Engineering Chemistry Research* 44 (24) (2005) 9323–9330. arXiv:https://doi.org/10.1021/ie0504699, doi:10.1021/ie0504699.

- [19] N. Christov, D. Ganchev, N. Vassileva, N. Denkov, K. Danov, P. Kralchevsky, Capillary mechanisms in membrane emulsification: oil-in-water emulsions stabilized by tween 20 and milk proteins, *Colloids and Surfaces A: Physicochemical and Engineering Aspects* 209 (1) (2002) 83 – 104. doi:[https://doi.org/10.1016/S0927-7757\(02\)00167-X](https://doi.org/10.1016/S0927-7757(02)00167-X).
- [20] A. Imbrogno, M. Dragosavac, E. Piacentini, G. Vladislavljević, R. Holdich, L. Giorno, Polycaprolactone multicore-matrix particle for the simultaneous encapsulation of hydrophilic and hydrophobic compounds produced by membrane emulsification and solvent diffusion processes, *Colloids and Surfaces B: Biointerfaces* 135 (2015) 116 – 125. doi:<https://doi.org/10.1016/j.colsurfb.2015.06.071>.
- [21] G. T. Vladislavljević, B. Wang, M. M. Dragosavac, R. G. Holdich, Production of food-grade multiple emulsions with high encapsulation yield using oscillating membrane emulsification, *Colloids and Surfaces A: Physicochemical and Engineering Aspects* 458 (2014) 78 – 84, formula VII: How Does Your Formulation Work? doi:<https://doi.org/10.1016/j.colsurfa.2014.05.011>.
- [22] M. P. Hanga, R. G. Holdich, Membrane emulsification for the production of uniform poly-n-isopropylacrylamide-coated alginate particles using internal gelation, *Chemical Engineering Research and Design* 92 (9) (2014) 1664 – 1673. doi:<https://doi.org/10.1016/j.cherd.2013.12.010>.
- [23] G. T. Vladislavljević, A. Laouini, C. Charcosset, H. Fessi, H. C. Bandulasena, R. G. Holdich, Production of liposomes using microengineered membrane and co-flow microfluidic device, *Colloids and Surfaces A: Physicochemical and Engineering Aspects* 458 (2014) 168 – 177, formula VII: How Does Your Formulation Work? doi:<https://doi.org/10.1016/j.colsurfa.2014.03.016>.
- [24] A. Fery, R. Weinkamer, Mechanical properties of micro- and nanocapsules: Single-capsule measurements, *Polymer* 48 (25) (2007) 7221–7235.
- [25] F. Dubreuil, N. Elsner, A. Fery, Elastic properties of polyelectrolyte capsules studied by atomic-force microscopy and ricm, *Eur. Phys. J. E: Soft Matter Biol. Phys.* 12 (2) (2003) 215–221.
- [26] A. Walter, H. Rehage, H. Leonhard, Shear-induced deformations of polyamide microcapsules, *Colloid Polym. Sci.* 278 (2000) 169–175.
- [27] D. Grigoriev, T. Bukreeva, H. Möhwald, D. Shchukin, New method for fabrication of loaded micro- and nanocontainers: emulsion encapsulation by polyelectrolyte layer-by-layer deposition on the liquid core, *Langmuir* 24 (3) (2008) 999–1004.
- [28] D. Z. Gunes, M. Pouzot, M. Rouvet, S. Ulrich, R. Mezzenga, Tuneable thickness barriers for composite o/w and w/o capsules, films, and their decoration with particles, *Soft Matter* 7 (19) (2011) 9206–9215. doi:[10.1039/c1sm05997a](https://doi.org/10.1039/c1sm05997a).
- [29] M. Rinaudo, N. Kil'deeva, V. Babak, Surfactant-polyelectrolyte complexes on the basis of chitin, *Russian Journal of General Chemistry* 78 (11) (2008) 2239–2246.
- [30] M. C. Andry, F. Edwards-Levy, M. C. Levy, Free amino group content of serum albumin microcapsules. iii. a study at low ph values, *Int. J. Appl. Pharm.* 128 (1996) 197–202.
- [31] G. Lu, Z. An, C. Tao, J. Li, Microcapsule assembly of human serum albumin at the liquid/liquid interface by the pendent drop technique, *Langmuir* 20 (19) (2004) 8401–8403.
- [32] K. Xie, Instabilities of microcapsules in flow: breakup and wrinkles, Ph.D. thesis, Centrale Marseille (2019).
- [33] A. Fery, F. Dubreuil, H. Möhwald, Mechanics of artificial microcapsules, *New journal of Physics* 6 (1) (2004) 18.
- [34] C. de Loubens, J. Deschamps, G. Boedec, M. Leonetti, Stretching of capsules in an elongation flow, a route to constitutive law, *J. Fluid Mech.* 767 (2015) R3.
- [35] F. Edwards-Lévy, M.-C. Andry, M.-C. Lévy, Determination of free amino group content of serum albumin microcapsules using trinitrobenzenesulfonic acid: effect of variations in polycondensation ph, *International Journal of Pharmaceutics* 96 (1-3) (1993) 85–90. doi:[10.1016/0378-5173\(93\)90215-2](https://doi.org/10.1016/0378-5173(93)90215-2).
- [36] D. Barthes-Biesel, H. Sgaier, Role of membrane viscosity in the orientation and deformation of a spherical capsule suspended in shear flow, *J. Fluid Mech.* 160 (1985) 119–135.
- [37] E. Egidi, G. Gasparini, R. G. Holdich, G. T. Vladislavljević, S. R. Kosvintsev, Membrane emulsification using membranes of regular pore spacing: Droplet size and uniformity in the presence of surface shear, *Journal of Membrane Science* 323 (2) (2008) 414–420.
- [38] A. Bertrandias, H. Duval, J. Casalinho, M. L. Giorgi, Dripping to jetting transition for cross-flowing liquids, *Physics of Fluids* 29 (4) (2017) 044102. doi:[10.1063/1.4979266](https://doi.org/10.1063/1.4979266).
- [39] R. F. Meyer, J. C. Crocker, Universal dripping and jetting in a transverse shear flow, *Phys. Rev. Lett.* 102 (2009) 194501. doi:[10.1103/PhysRevLett.102.194501](https://doi.org/10.1103/PhysRevLett.102.194501).

Summary

- ⇒ Development of a procedure to produce and characterize uniform microcapsules at a high rate.
- ⇒ Shell elasticity of CH/PFacid microcapsules depends on the complexation time while BSA/TC microcapsules elasticity depends on the quantity of reactants in the initial droplet.
- ⇒ To produce CH/PFacid microcapsules with uniform elasticity, production should be split in two steps: first, fabricating the initial droplet, second shell formation.

Chapter 4

Rheology of attractive suspensions of microcapsules

This chapter is dedicated to the rheological characterization of suspensions of polyelectrolytes microcapsules (CH / PF acid) with uniform size and elastic properties, which have been introduced in Chapter 3 and for which we have a knowledge of the mechanical properties of their shell [84]. This chapter is presented as a draft article.

4.1 Introduction

The primary objective is to understand the role of an elastic shell on in the rheology of dense suspensions of deformable particles. However, we show that the polyelectrolytes microcapsules used exhibit long-range attractive interactions. Their suspensions are thus an original system to study the rheology of suspensions of attractive particles at length scales as high as of few hundreds micrometers. This property leads to the emergence of a yield stress at low volume fraction for a suspension of non-Brownian particles. The objective of this paper is to understand the role of this strong attraction on the rheology of the suspension. We used classic steady-state shear rheology and shear-reversal experiments. The latter allowed us to dissociate the role of hydrodynamic interactions from the role of contact interactions in the rheology of the suspensions. We also studied the dynamics of resuspension of microcapsules to gain insights on the stability of clusters under shear. In reference to previous numerical simulations on attractive suspensions [94], we showed experimentally that two regimes can be clearly distinguished: the "attraction dominated" regime and the "shear induced rupture".

4.2 Materials and Methods

4.2.1 Chemicals and Solutions

The assembly of microcapsules was achieved by interfacial complexation of oppositely-charged polyelectrolytes [83, 84]. Chitosan, a water soluble cationic polymer, forms a complex with oil soluble anionic phosphatidicfatty acids (PFacid) at a water/oil interface.

PFacid was used in a form of a commercial lecithin known as lecithin YN (Palsgaard 4455, food-grade, E442) which was kindly provided by Palsgaard. PFacid was dissolved in food-grade rapeseed oil (Géant Casino) at a concentration of 20% at 35 °C during the night to create a stock solution. Then PFacid solution was centrifuged at 3500 g to remove the insoluble residuals. The stock solution was further diluted with rapeseed oil at required concentrations (0.1 or 5 % w/w).

Chitosan (CAS n° 9012-76-4, Sigma-Aldrich) with medium molecular weight and 75-85% deacetylation was dissolved in Millipore water (Resistivity > 18.2 mΩ.cm) at a concentration of 1 % w/w by adjusting the pH with hydrochloric acid (1 mol/L) to 3.0. The chitosan solution was then filtered to remove undissolved particles through Minisart syringe filters (pore size 5.0 μm). The solution was diluted to 0.25 % w/w with water and glycerol (99.5 % purity, VWR) mixture. The water to glycerol ratio was adjusted when needed in order to control the density of the microcapsules.

4.2.2 Production and Preparation of suspensions

Suspensions of microcapsules were prepared with a lab-scale membrane emulsification system marketed by Micropore Technologies Ltd (UK) under the commercial name Micropore LDC-1, as detailed in our previous publication [95]. Briefly, it included a hydrophobic micro-engineered emulsification membrane with 20 μm diameter pores under a paddle-blade stirrer [96]. 500 mL of PFacid solution (0.1 % w/w) were stirred by the paddle at a rotational speed of 600 rpm. 50 mL of chitosan solution was injected by a syringe pump (neMESYS, CETONI) with a flow rate of 2 mL/min through the membrane. The droplets were sucked up from the dispersion cell with a tube and collected in a beaker. Once the injection was finished, a large volume of highly concentrated PFacid was added to the suspension, bringing the overall PFacid concentration to 5 %. Then the microcapsules were kept under gentle stirring in the PFacid solution until the membrane reached the desired stiffness. The duration of chitosan / PFacid complexation process determines the elasticity of the microcapsules, [84]. Thus, two suspensions with complexation

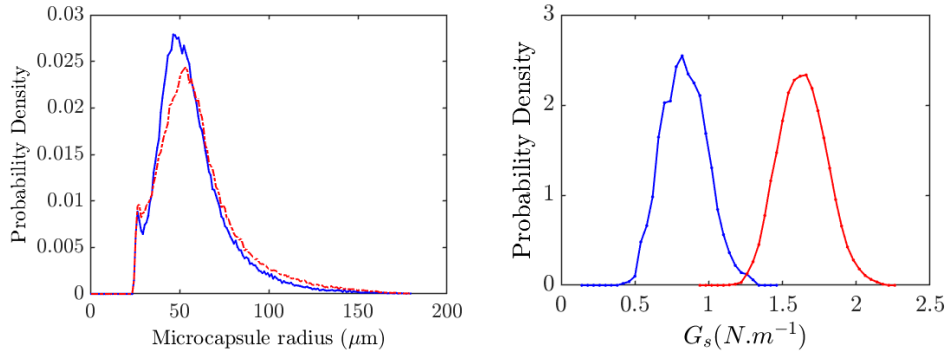


Figure 4.1: Mechanical characterization of the microcapsule suspensions, **Left:** Size distribution of both suspensions of microcapsules **Right:** Surface elastic modulus G_s distribution of both suspensions of microcapsules. Blue line: reaction time of 5 min. Red line: reaction time of 15 min.

times 5 and 15 minutes were produced to create two populations of capsules with distinct shell elasticity.

The complexation of the PFacid with chitosan was stopped by washing the oil phase with large volumes cyclohexane. The washing procedure was repeated ten times to ensure the removal of all PFacid traces. Then the microcapsules were resuspended in silicon oil AP1000 (Wacker). The residual cyclohexane in the suspending fluid was removed in a similar fashion: diluting with a large amount of AP 1000, then centrifuging the suspension and extracting AP 1000 oil. This procedure was continued until the difference in the viscosity between the extracted and pure oils was less than 1 %. This precaution was taken to ensure that there was no evaporation of residual of cyclohexane during rheometric experiments, and thus the viscosity of the continuous phase was a constant throughout the experiments.

4.2.3 Characterization of physical properties

The surface shear elasticity G_s of the microcapsule shell was measured in an extensional flow chamber that has been automatized to study a large number of microcapsules according to the methodology shown in our previous publication, see Ref. [95] for details.

Volume fraction and size distribution of microcapsule suspensions was measured by bright field microscopy. Firstly, 40 mL of the produced dense suspension of microcapsules was well mixed to be homogenized. Then at least three samples of 0.4 mL were diluted with 10 mL of suspending fluid. Microcapsules were placed on large microscope slides and scanned entirely by an inverted microscope Olympus IX-73 equipped with a 4, 10, or 20 fold objective, a Marzhauser motorized stage, and a camera Hamamatsu ORCA-Flash 4.0. The size and total volume of the microcapsules were measured with a custom written software based on the Matlab image processing toolbox (Mathworks). The volume fraction of the produced dense suspension of microcapsules was then calculated by determining the total volume of microcapsules in the three samples. Then the dense suspension was diluted by suspending fluid AP 1000 to produce suspensions with volume fraction ranging from $\phi = 0.2$ to 0.52.

The viscosity of the suspending silicon oil AP 1000 was measured by a stress-controlled rheometer (DHR3, TA) with a cone-plane geometry at 25 °C. As shown in figure 4.2, it is a Newtonian fluid with a viscosity of $\eta_0 = 1.03 \pm 0.01$ Pa.s at 25 °C. Note that all the experiments were carried out at this temperature. Additionally, it was verified that AP 1000 does not have a visco-elastic behavior. The density of AP 1000 was $\rho_0 = 1085.78$ kg/m³ at T = 25 °C which was measured by a precise densimeter (DMA 4500M, Anton Paar). As explained in 4.2.1, the volume fraction of glycerol in the chitosan solution determined the density of the microcapsules. By choosing 31.5% w/w of glycerol volume fraction, we obtained the microcapsules with density

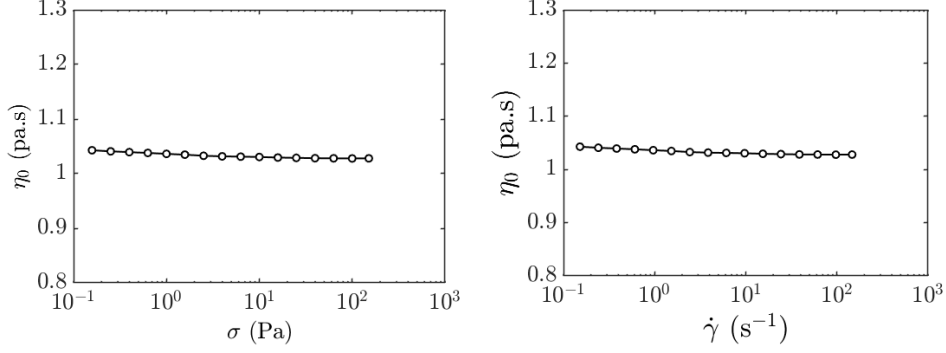


Figure 4.2: The viscosity of the suspending fluid of the microcapsules suspension, silicon oil AP1000 as a function of shear stress (left) and shear rate (right) at 25°C.

$\rho = 1074.92 \text{ kg/m}^3$ which is just 1% lower than the density of the suspending fluid. This small density contrast $\Delta\rho = 10.85 \text{ kg/m}^3$ was implemented to facilitate the washing procedure in the suspension preparation.

Finally, size and G_s distribution are shown in Figure 4.1 for both suspensions of microcapsules. The average G_s were 0.8 and 1.7 N/m with a standard deviation of 18% and 8% respectively. Both suspensions had a mean radius of 57 μm with coefficient variation of 36%.

4.2.4 Rheometer and the measurement method

The rheological measurements were carried out with a stress-controlled rheometer (DHR3, TA) with a rotating parallel plate disk geometry. The gap and the diameter of the geometry were 1.5 mm and 60 mm respectively. This gap value was chosen to accommodate 10 to 15 microcapsules in the gap. Moreover, we observed that the apparent viscosity of the suspension was independent of the gap, if the latter was larger than 1 mm. Smooth and rough surfaces were used, without any incidences on the results, meaning that there was non evidence of wall slip effects. Since in a parallel plate geometry the shear rate is not constant and varies from the center to the rim, we corrected the measured viscosity with the Mooney-Rabinovitch correction [92]:

$$\eta_s = \eta_{app} \left[1 + \frac{1}{4} \frac{d \ln(\eta_{app})}{d \ln(\dot{\gamma})} \right] \quad (4.1)$$

where η_{app} is the apparent viscosity measured by the rheometer, d the diameter of the geometry and $\dot{\gamma}$ the shear rate at the rim. The temperature was controlled with a Peltier system at 25°C.

Shear-Reversal experiments were carried out to the study the micro-structure of the suspension under a given shear stress, as proposed by Galda-Maria *et al.* [93]. The suspensions were pre-sheared with a shear stress σ of 10 Pa for 30 s. Then as shown in figure 4.3, a constant shear stress (ranging from 0.1 to 100 Pa) was imposed on the suspension until the measured viscosity achieved a steady state. Then, the imposed stress was set to zero during two seconds. The last step consisted in shearing the suspension with the same stress but in the opposite direction. The relaxation time of 2 s was chosen after different tests to have no effects of the inertia of the motor and the geometry on the measurement. then the viscosity shown a sudden drop up to increased and reach a steady state value.

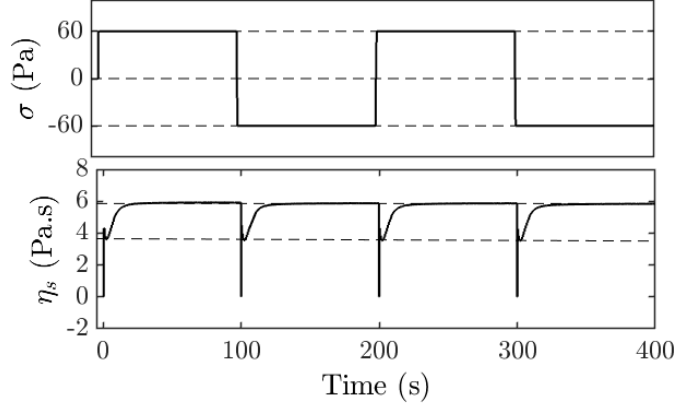


Figure 4.3: An example of Shear-Reversal experiment for a suspension of particle executed by a stress-controlled rheometer in a parallel plate geometry. **Top:** Shear stress as a function of time. **Bottom:** Apparent viscosity as a function of time.

4.3 Results

4.3.1 Steady State Rheology

Flow curve

The steady state viscosity η_s was measured for two homogeneous suspensions of microcapsule with the average surface elastic shear moduli of $G_s = 0.8$ and 1.7 N/m, figure 4.1. η_s was measured by applying a shear stress ranging from $\sigma = 10^{-2}$ to 10^2 Pa. The average size of microcapsules for both suspensions was the same $R = 57$ μm for a gap between the two plates of 1.5 mm. The volume fraction of suspensions ranged from $\phi = 20\%$ to 52% . Figure 4.4 illustrates the flow curves of the suspensions as a function of shear stress. Above a volume fraction ϕ of 25% , both suspensions of microcapsules behaved like a yield stress fluid, i.e. the viscosity diverges when σ tends to a threshold. It means that the suspension did not flow under a shear stress lower than a threshold values, called the yield stress σ_y . Both suspensions were Newtonian with a viscosity of 1.7 Pa.s for $\phi = 20\%$. Figure 4.5 shows that the data were well fitted by the Herschel-Bulkley model, $\sigma = \sigma_y + K\dot{\gamma}^n$ where K is the consistency factor and the exponent n reflects the degree to which the fluid is shear-thinning ($n < 1$) or shear-thickening ($n > 1$).

Figures 4.6 shows that n decreased from 0.97 to 0.77 when the volume fraction ϕ increased from 0.2 to 0.52 . The yield stress σ_y increased from 0.02 to 2 Pa when ϕ increased from 0.25 to 0.52 . However, the elasticity of the microcapsules in the range of $G_s = 0.8$ and 1.7 N/m did not have a significant influence on n . Moreover, the yield stress for both suspensions were the same for ϕ lower than 0.35 . Above $\phi = 0.35$, σ_y increased of a factor 1.5 when G_s was divided by 2 .

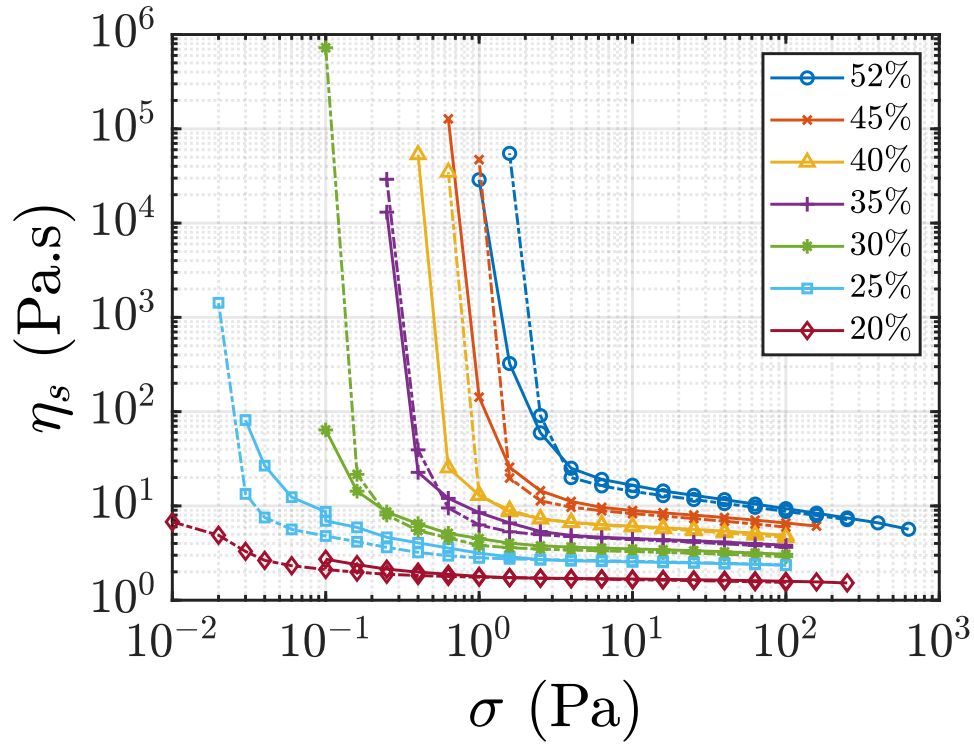


Figure 4.4: Steady state viscosity η_s of the microcapsule suspensions as a function of the shear stress σ for volume fraction ϕ in the range 0.2 and 0.52. Plain lines $G_s = 1.7$ N/m, dashed lines $G_s = 0.8$ N/m. Microcapsules were suspended in silicon oil AP 1000 with $\eta_0 = 1.03$ Pa at $T = 25^\circ\text{C}$.

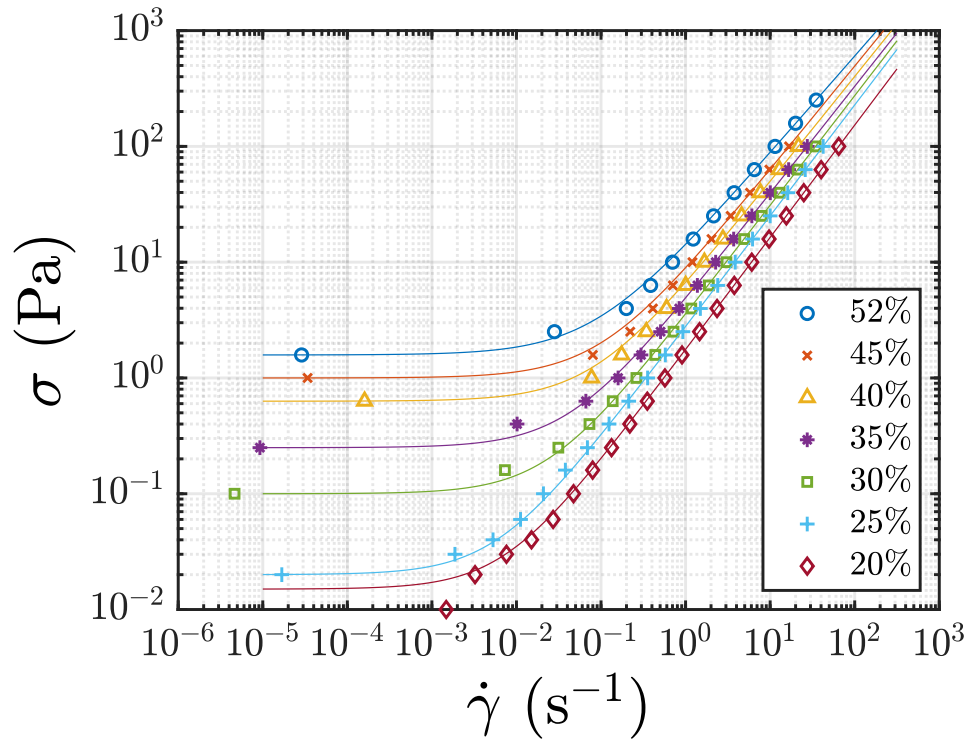


Figure 4.5: Shear stress σ as a function of shear rate $\dot{\gamma}$ for microcapsule suspensions with average $G_s = 0.8$ N/m. Plain lines : Herschel-Bulkley model.

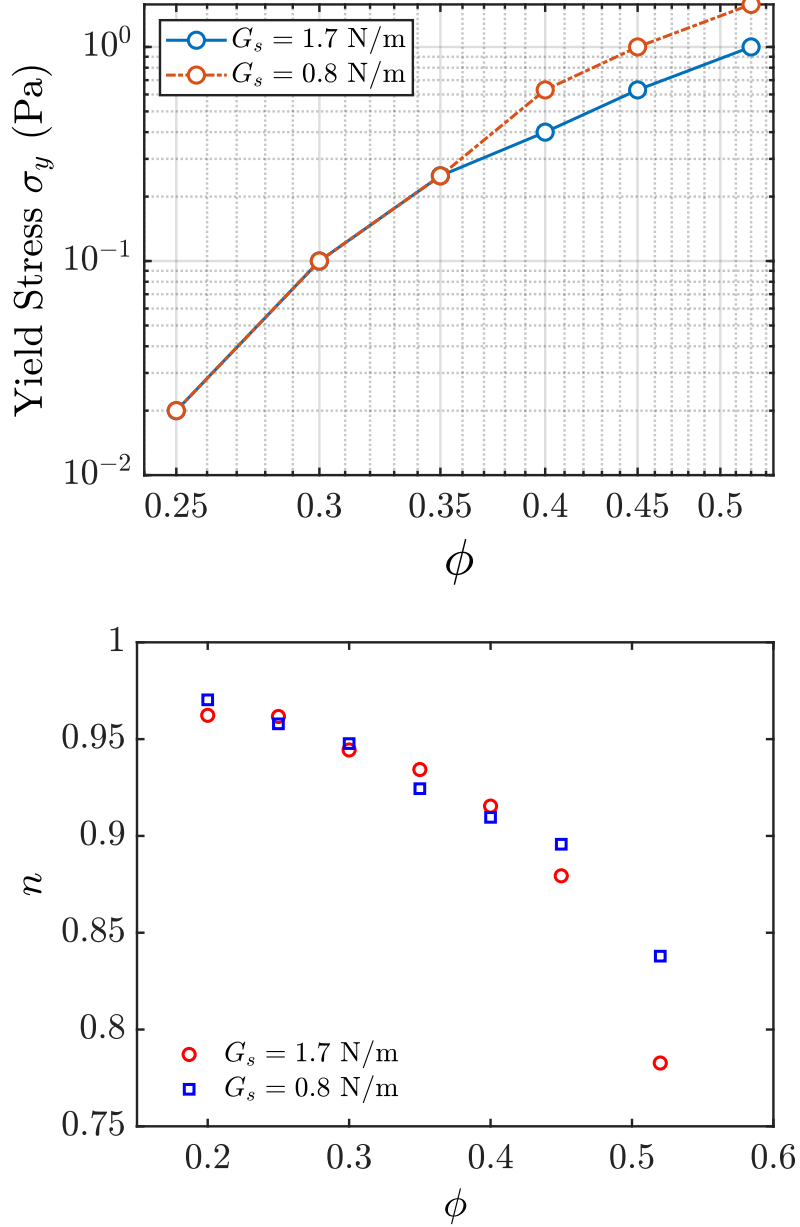


Figure 4.6: Top: Yield stress of suspensions of microcapsules as a function of volume fraction. **Bottom:** The exponent n in Herschel-Bulkley model as a function of the volume fraction of microcapsules.

Maximal volume concentration

Figure 4.7-a shows the evolution of η_s as a function of ϕ for various shear stress σ . For a given σ , η_s diverged for a given value of volume fraction, ϕ_m , referred as the maximal volume fraction. This behaviour can be fitted by Krieger–Dougherty equation $\eta_s/\eta_0 = (1 - \phi/\phi_m)^{-n_K}$. For rigid suspensions, the exponent n_K is generally equal to 2. Figure 4.7-b shows the evolution of $1/\sqrt{\eta_s}$ as a function of ϕ . We observed that the relation of Krieger–Dougherty with $n_K = 2$ was in good agreement with our experimental data. We deduced from this fitting the value of ϕ_m for each value of σ and both suspensions of microcapsules, Figure 4.7-c. ϕ_m increased from 0.25 to 0.6 when σ increased from $2 \cdot 10^{-2}$ to 2 Pa. There was no influence of the elasticity of the shell on the evolution of ϕ_m with σ .

To sum-up these first rheological analyses, we observed that suspensions of polyelectrolytes

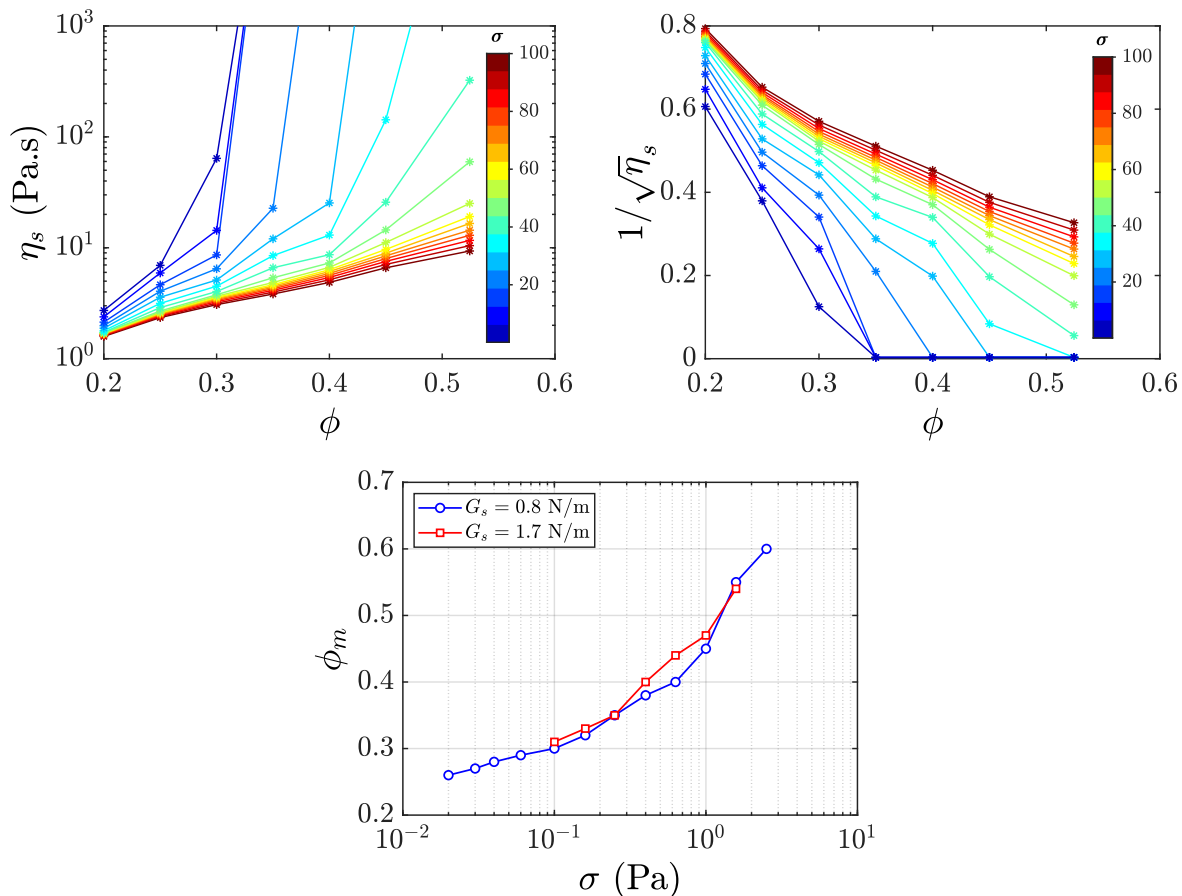


Figure 4.7: Jamming of suspensions of microcapsules. a: Steady-state viscosity η_s as a function of the volume fraction ϕ for different shear stress σ . b: $1/\sqrt{\eta_s}$ as a function of ϕ . Jamming volume fraction ϕ_m as a function of the shear stress σ .

microcapsules showed an astonishing behavior, which is the emergence of a yield stress at low volume fraction (0.25). Moreover, above a shear stress of few Pascals, the suspensions showed a quasi-Newtonian behavior up to 52 %. This behavior was quantitatively independent on the elasticity of the shell. This characterization question the nature of the interactions between the microcapsules.

Particle Interactions

In this section, some characterization and observation of the interactions between microcapsules are discussed.

As in suspensions of rigid spheres, microcapsules could be subjected to contact forces due to friction. Atomic force measurement (AFM) and scanning electron microscopy (SEM) imaging of the surface of the membrane of dried microcapsules (Figure 4.8) showed that the membrane had roughness of typical size 0.1 - 1 μm and a depth of 10-100 nm. However and more surprisingly, suspensions of microcapsules tended spontaneously to form aggregates at rest. Figure 4.9-left, shows an image of a microcapsule suspension with a volume fraction $\phi = 0.6$ after dilution in silicon oil AP1000, used as the continuous phase in rheometric experiments. We observed a big cluster of microcapsules which contains a considerable amount of particles. The size and the number of particles in such clusters varied in a wide range. It was verified that these clusters were composed of intact microcapsules and were not an aggregation of broken microcapsule shells. Figure 4.9-right shows the same cluster after being touched gently by a needle. The cluster broke down to smaller clusters and even some individual microcapsules. The clusters of microcapsules

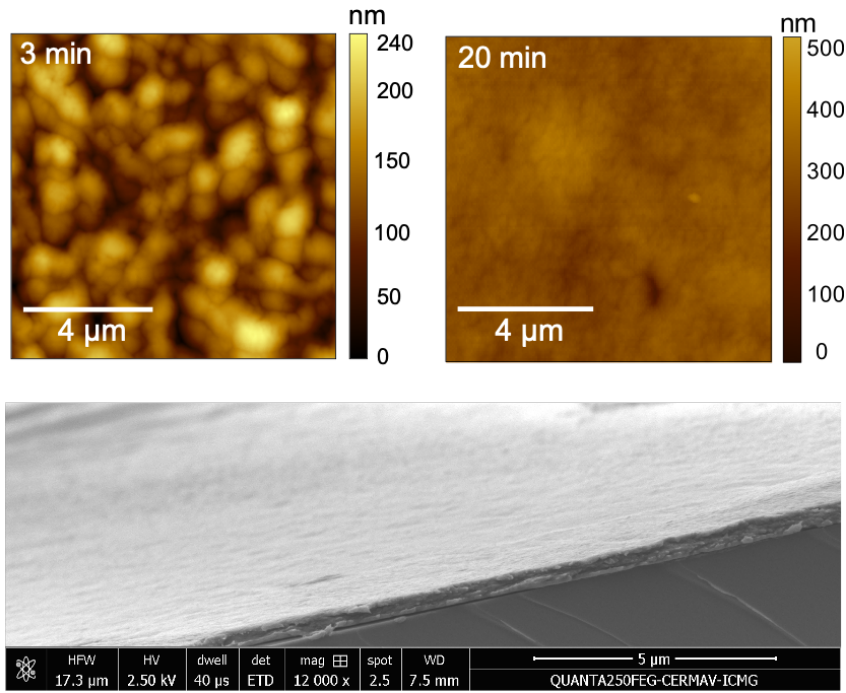


Figure 4.8: Measurement of membrane surface topology by AFM and SEM. **Top:** AFM of a membrane of CH/PFacid microcapsules for two reactions times (3 and 20 min). **Bottom:** Cross-section of a membrane visualized by SEM. Courtesy of R. Chachanidze and K. Xie.

suspended in AP 1000 silicon oil appeared at high volume fractions. The distance between the particles in high volume fraction being very small, short range attractive interactions, such as Van der Waals forces could come into play.

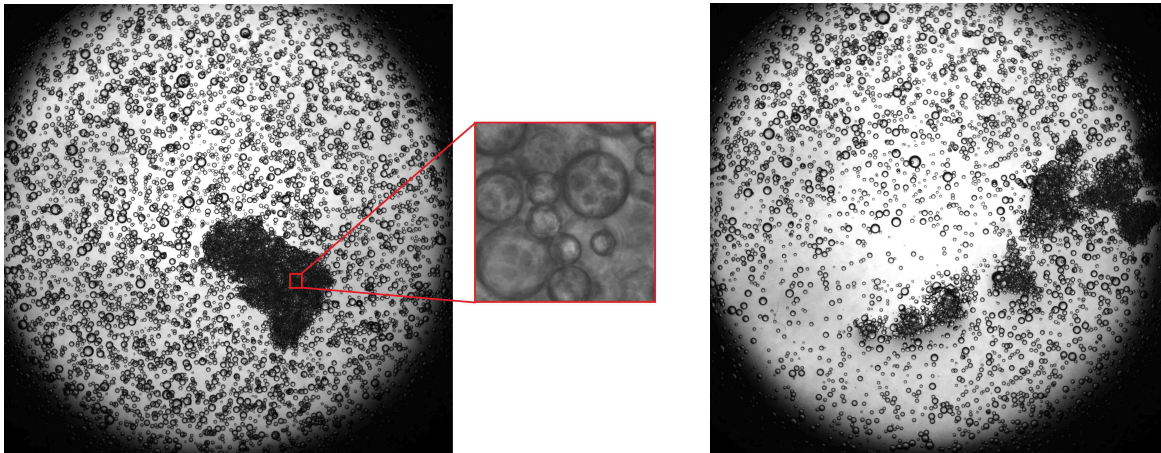


Figure 4.9: Presence of cluster in microcapsules suspension prepared in silicon oil AP1000, $\phi = 0.6$, **Left:** Initial state, **Right:** After being touched gently by a needle. It breaks down to smaller clusters and individual microcapsules.

The effect of suspending fluid on the interaction between the microcapsules at rest was investigated. The microcapsules were suspended in different silicon oils, then the suspension homogenized to have a uniform distribution of particles. Figure 4.10 illustrates the microcapsule suspensions in different suspending silicon oils after one hour at rest. The type of suspending silicon oil had a crucial role on the typical size of the clusters. Microcapsules were more strongly attracted in AK silicon oil family which was used in the resuspension experiments (Chapter 6) and less in AP family which was utilized in the rheology of dense suspensions. The criterion of choosing each type of silicon oil as the suspending fluid was based on the possibility to match

the density and the refractive index between the dispersed and continuous phase.

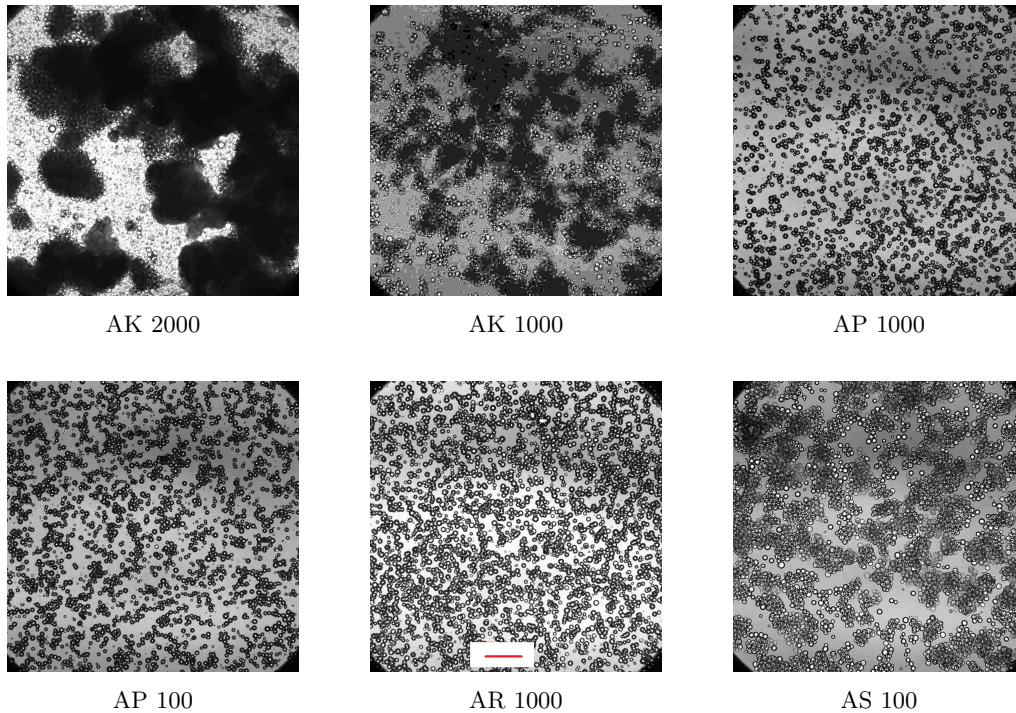


Figure 4.10: The state of microcapsule suspensions in different silicon oil after one hour without interruption. The strength of attractive interaction between microcapsules depends on the suspending silicon oil. The scale line is 1 mm.

Figure 4.11 represents a dilute microcapsule suspension in silicon oil AP 1000 after being exposed to an electric field. The microcapsules that were initially uniformly distributed, interacted with the electric field and created a network-like microstructure. Executing a shear stress by shaking the suspension breaks down a part this microstructure. However, the microcapsules reorganized again after relaxing the stress.

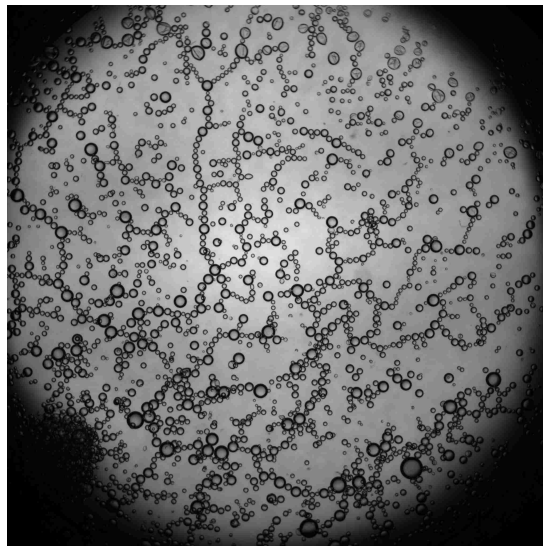


Figure 4.11: Chitosan microcapsule suspension in silicon oil AP 1000 after being exposed to an electric field creates a microstructure.

We concluded that the emergence of yield stress at low ϕ was due to long-range interactions between the particles. To study the stability of these clusters under shear, we performed resus-

pensions experiments in a Taylor-Couette flow cell, as detailed in our previous study (Chapter 5). Briefly, viscous resuspension consists of shearing a sedimented suspension of non-buoyant particles in a vertical Taylor-Couette cell. Shear flow causes a non-homogeneous distribution of normal stress on the particles which induces a migration of particles in the vertical direction. The system finally finds a balance between the gravity force and the normal stress by developing a specific vertical concentration profile of particles, with its upper limit depending on the shear rate. However, for the same system and suspension, the time-dependent dynamics of the resuspension is independent of the shear rate but is governed by the size of particles (Chapter 5). The characteristic time of resuspension experiments is the same than for sedimentation experiments and independent on the shear rate, $t_s = \eta_0/\Delta\rho gR$. Consequently, the measurement of t_s in resuspension experiments give a direct measurement of the characteristic size of the clusters of microcapsules at a given shear rate. Figure 4.12 depicts the normalized height of the suspension as a function of time for a resuspension of microcapsules in silicon oil AK 1000. We observed that the height of the suspension reached the steady state much faster with the smallest shear rate $\dot{\gamma} = 5 \text{ s}^{-1}$. As the shear rate increased to $\dot{\gamma} = 11 \text{ s}^{-1}$, it took more time to achieve the equilibrium state. This trend continued until $\dot{\gamma} = 22 \text{ s}^{-1}$. Above this value, the microcapsule suspension followed the same kinetics. This observation clearly demopnstrated that clusters of microcapsules were broken by shear for shear rate larger than 11 s^{-1} . When the shear stress overcame the attractive forces between the microcapsules, all clusters breaks apart to individual particles and the kinetic response became independent of the shear rate.

Finally, all of these observations revealed that there was long-range attractive interactions between the microcapsules within the suspension, which lead to the emergence of the yield stress at low volume fraction. Shear forces could easily overcome these attractions and broke the clusters.

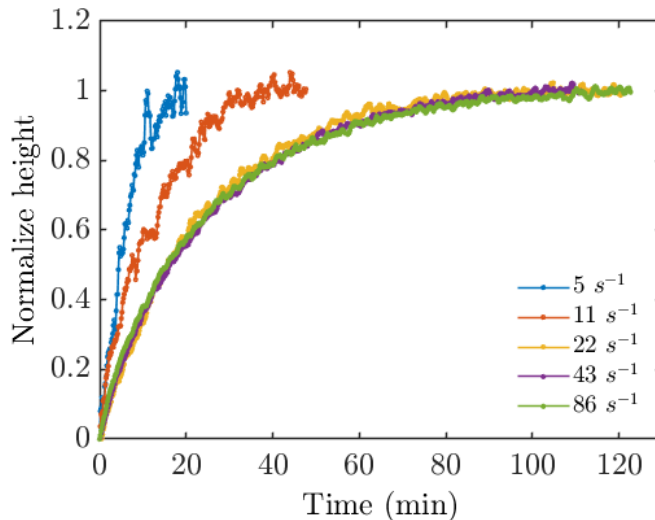


Figure 4.12: Normalized time-dependent height of microcapsule suspension in resuspension experiment.

4.3.2 Shear-reversal rheology

Long-range interactions in the suspensions of polyelectrolytes microcapsules seemed to be the salient ingredient which explained the emergence of a yield stress at low volume fraction. To gain insights on the nature of the role of these interactions on the rheology and structure of these suspensions, we detail led in this section some results obtained by shear-reversal experiments. Shear-reversal has been introduced by Galda-Maria *et al.* [93] for rigid particles to evaluate the contribution of hydrodynamic and contact viscosity to the bulk viscosity. The

physical interpretation of shear-reversal experiments for rigid suspensions, which is supported by numerical simulations [39], is that the sheared suspension develops a steady microstructure of particles. By reversing the shear direction, the microstructure is broken which correspond almost to the minimum value of viscosity η_{min} , Figure 4.3. Then the apparent viscosity increases, which corresponds to the gradual reestablishment of the microstructure of particles. η_{min} is interpreted as an approximation of steady hydrodynamic viscosity η_h for the reason that the particles move away under the effect of the inversion of the shear direction, but the lubrication forces resist to this movement. By accumulating the shear strain, the microstructure rebuilds, the contacts reestablish, and the contact viscosity regains its steady state before reversing the shear direction. When the contacts start to reestablish, the contribution of contact viscosity increases up to the steady state. The contact viscosity is defined as the difference between the steady state and the hydrodynamic viscosity, $\eta_c = \eta_s - \eta_{min}$. Numerical simulations [39], which can dissociate the contact from the hydrodynamic viscosity, confirms that the $\eta_{min} \sim \eta_h$.

Shear-Reversal for rigid particle suspensions

Firstly, we reproduced shear-reversal experiments for rigid particles to build a framework of interpretation when it will applied to the suspensions of microcapsule. Mono-size PMMA particles of 6 μm diameter were seeded in a glycerol-water mixture with a viscosity of $\eta_0 = 0.95$ Pa.s and volume fraction ranging from $\phi = 0.3$ to 0.49. The experiments were carried out as explained in section 4.2.4 with a deformation-controlled rheometer (ARES-G2, TA) in a Couette geometry with a gap of 1 mm for two shear rates $\dot{\gamma} = 0.1$ and 1 s^{-1} . As figure 4.13-left represents, the viscosity after the shear reverse sharply dropped up to a minimum value η_{min} and gradually increased up to reach the steady state viscosity of the suspension η_s . Both minimum viscosity η_{min} and steady state viscosity increased with ϕ . Figure 4.13-right shows that the strain γ necessary to reach the minimum and steady viscosities decreased when ϕ increased. These characteristics have been already reported in numerous experimental [93, 41, 92] and numeric [39, 40] studies related to the transient rheology of rigid particle suspensions. By increasing ϕ the frictional contact forces between the particles overcome the hydrodynamic interactions and become dominant. By approaching the maximum packing fraction ϕ_m the hydrodynamic contribution to the apparent viscosity can be considered negligible compare to the contact contribution [?]. This explains the deeper step of the apparent viscosity by increasing ϕ in Shear-Reversal experiments. The collapsed microstructure recreates faster by increasing ϕ because the average distance between the particles is smaller. This was observed by the steeper slope of the viscosity toward the steady state for larger ϕ in figure 4.13-right. As consequence, the minimum viscosity occurs at a smaller strain γ and the steady state is reached by a lower traveled distance when ϕ increases.

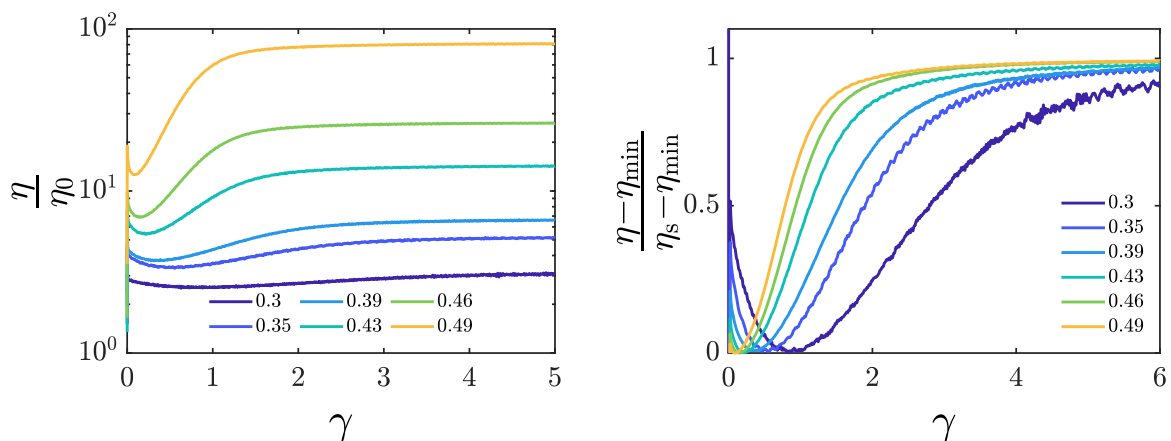


Figure 4.13: Relative transient viscosity in Shear-Reversal experiments as a function of shear strain for rigid particle suspensions for volume fractions in the range of $\phi = 0.3$ to 0.49 . The diameter of particles was $6 \mu\text{m}$, the viscosity of the suspending fluid was $\eta_0 = 0.95 \text{ Pa}\cdot\text{s}$ and experiments were carried out with shear rate $\dot{\gamma} = 1 \text{ s}^{-1}$.

The relative steady state viscosity of rigid particle suspensions as a function of volume fraction for shear rates $\dot{\gamma} = 0.1$ and 1 s^{-1} is represented in figure 4.14-left. For both shear rates, the steady viscosity increases as the volume fraction grows. The increase of the viscosity at first is moderate but after $\phi = 0.45$ drastically rises until reaching the maximum packing volume fraction ϕ_m where it diverges. The correlation of relative viscosity as a function of volume fraction proposed by Boyer *et al.* [42] plotted in solid lines. The jamming volume fractions are $\phi_m = 0.521$ and 0.535 for shear rates $\dot{\gamma} = 0.1$ and 1 s^{-1} respectively. ϕ_m represents a slight growth with shear rate, which is a well-known behavior of shear-thinning rigid particle suspensions [38]. Based on the expression of Krieger–Dougherty, $\sqrt{\eta_0/\eta_s}$ is plotted as a function ϕ in 4.14-right. The correlation is excellent, as expected for rigid particles ($n_K = 2$). However, η_{min} diverges with an exponent of $n_K = 2$. Blanc *et al.* [92] reported the same behavior of viscosity divergence by using rigid PMMA particles.

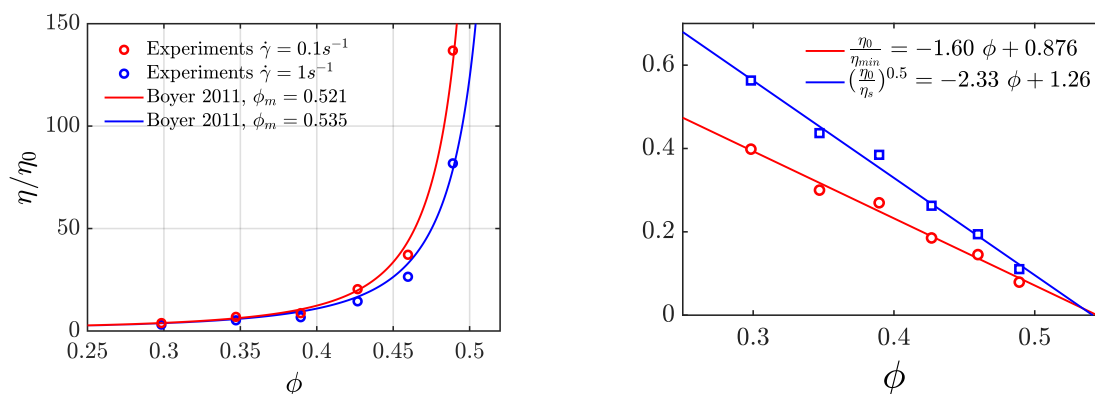


Figure 4.14: Divergence of rigid particle suspension with increasing the volume fraction: **left:** Relative steady viscosity as a function of volume fraction for $\dot{\gamma} = 1$ and 0.1 s^{-1} . The circles are the experimental results and the solid lines are the correlation proposed by Boyer *et al.* [42], **right:** Scaling of relative steady (circles) and minimum (squares) viscosity based on Krieger–Dougherty power law with $n = 2$ for steady and $n = 1$ for minimum viscosity.

The transient response of the suspension could depend on the driven nature of the flow: constant shear stress or constant shear rate. So, we performed the same experiments but with a stress-controlled rheometer. Figure 4.15 represents Shear-Reversal of two rigid particle suspensions executed by stress-controlled (left) and deformation-controlled (right) rheometers for

different shear stress / rate. Both approaches represent a minimum viscosity after the shear reverse and a gradual growth of the bulk viscosity to the steady state due to reorganization of the microstructure and contact stresses between the particles. The traveled strain to reach the minimum and steady viscosity is identical for both methods but also it remains constant by varying the shear rate or shear stress. The main difference is that the minimum viscosity in stress-controlled method has a Newtonian behavior but in deformation-controlled method has a small shear-thinning behavior. In regard to this small difference, we decided to pursue our study of shear-reversal for suspensions of microcapsules with the stress-controlled rheometer, as the constant minimal viscosity can be interpreted as the hydrodynamic viscosity.

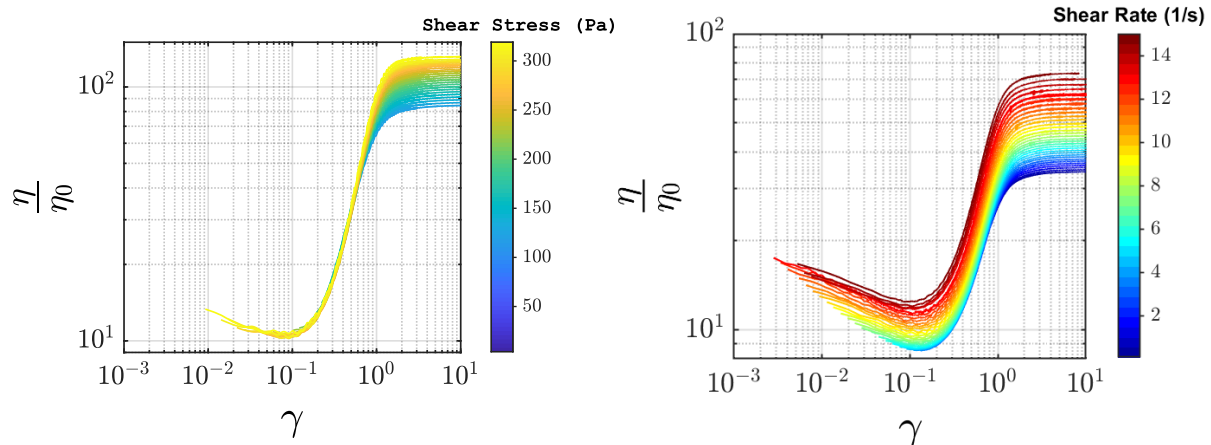


Figure 4.15: Transient viscosity of rigid particles suspensions through Shear-Reversal experiments using a stress-controlled rheometer (left) and a deformation-controlled rheometer (right).

Shear-Reversal for microcapsule suspensions

Figure 4.16 represents Shear-reversal experiments with a stress-controlled rheometer on the microcapsule suspensions. The experiments were carried on to investigate the effect of volume fraction ϕ and shear stress σ on the transient viscosity through shear reversal. Figure 4.16-left refers to a fixed volume fraction $\phi = 0.3$ with various shear stress and figure 4.16-right refers to a fixed shear stress $\sigma = 4$ Pa where the volume fraction is in the range of $\phi = 0.2$ to 0.52 . We can observe that like suspensions of rigid particles, after reversing the shear direction, the viscosity of microcapsule suspensions steps down sharply and after gaining a minimum value η_{min} , it rises to achieve a steady state η_s . As shown in figure 4.16-right, similar to rigid particles, increasing the volume fraction leads to a raise of minimum viscosity η_{min} and steady viscosity η_s . Globally the results show the same transient behavior as the rigid particle suspensions presented in figure 4.13. A difference is remarkable as shown in figure 4.16-left, contrary to the rigid particle suspensions, for a given volume fraction of microcapsules, as the shear stress increases, the minimum viscosity represents a highly shear-thinning behavior.

In fact, η_{min} as a function of σ is shown Figure 4.17-left for ϕ ranging from 0.2 to 0.52. We observe that for a given shear stress, the minimum viscosity increases as the volume fraction increases. For shear stress larger than 10 Pa, η_{min} was almost constant. The shear-thinning was marked at high volume fraction and low stress. The same behaviour was observed concerning the contact viscosity η_c but in a much more accentuated way 4.17-right. Figure 4.18 shows the ratio $(\eta_c)/\eta_{min}$ as a function of σ for different ϕ . We distinguished two regions. For stress lower than 3 Pa and ϕ larger than 0.25, the viscosity was dominated by the contact one. Above a stress of 3 Pa, the viscosity was dominated by the hydrodynamic one whatever the volume fraction was. For ϕ lower than 0.25, the hydrodynamic viscosity was always the main contributor to the total viscosity.

Finally, Figure 4.19 is the analogue of Figure 4.14 for microcapsules 4.19. We retrieved

the Krieger-Dougherty equation for the steady state viscosity, and similarly to rigid suspension η_0/η_{min} decreased linearly with ϕ in the regime of large stress (i.e. dominated by the hydrodynamic viscosity).

To conclude, shear-reversal experiments on suspensions of microcapsules revealed that the viscosity of suspension of microcapsules were dominated by the contacts at low stress and large volume fraction. If the volume fraction was too low and/or the stress above a threshold, the viscosity was governed by the hydrodynamic viscosity.

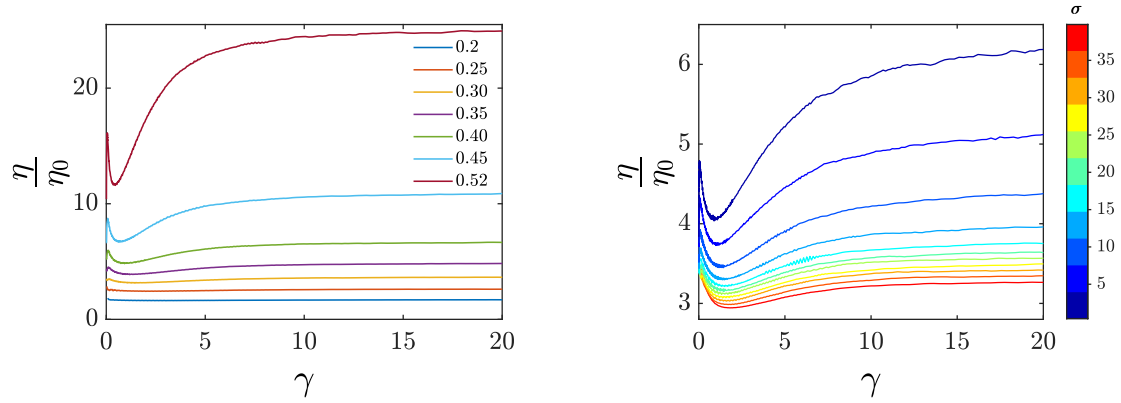


Figure 4.16: Transient viscosity of microcapsule suspensions in Shear-Reversal Experiment, performed in a stress-controlled rheometer. **Left:** Suspension with a volume fraction of $\phi = 0.3$ sheared with various shear stresses, **Right:** Suspensions with various volume fractions sheared by stress $\sigma = 4$ Pa.

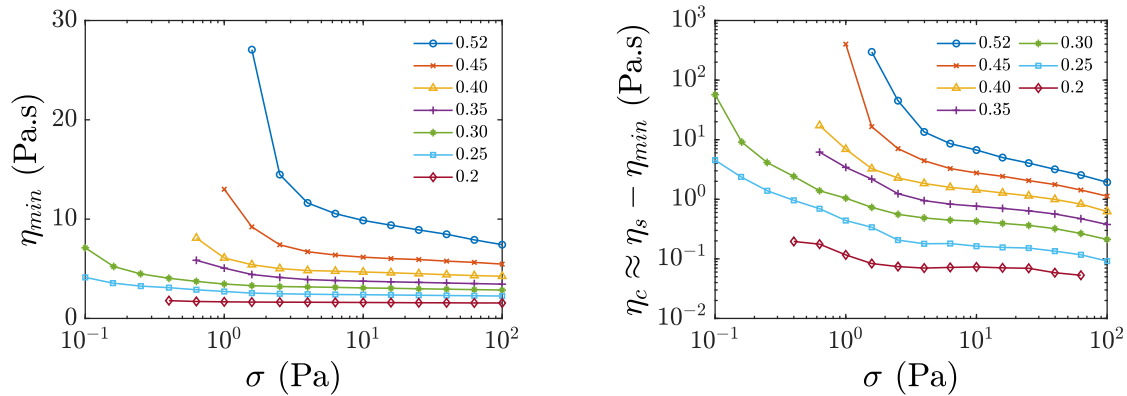


Figure 4.17: Minimum viscosity and the approximation of the contact viscosity of microcapsule suspensions with volume fraction in the range of $\phi = 0.2$ to 0.52 . **Left:** Minimum viscosity η_{min} as a function of shear stress, **Right:** Approximation of the contact viscosity $\eta_c \approx \eta_s - \eta_{min}$, as a function of shear stress.

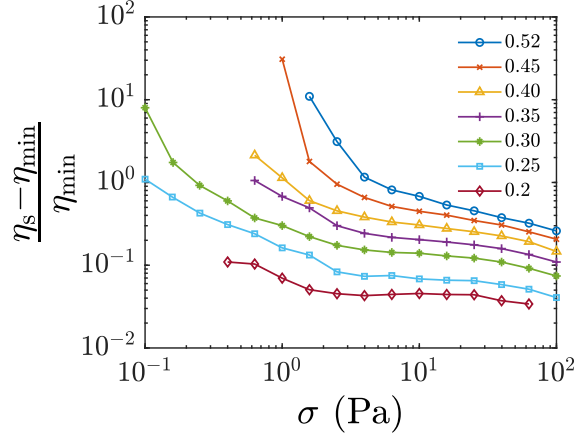


Figure 4.18: η_c/η_{min} as a function of σ for various ϕ .

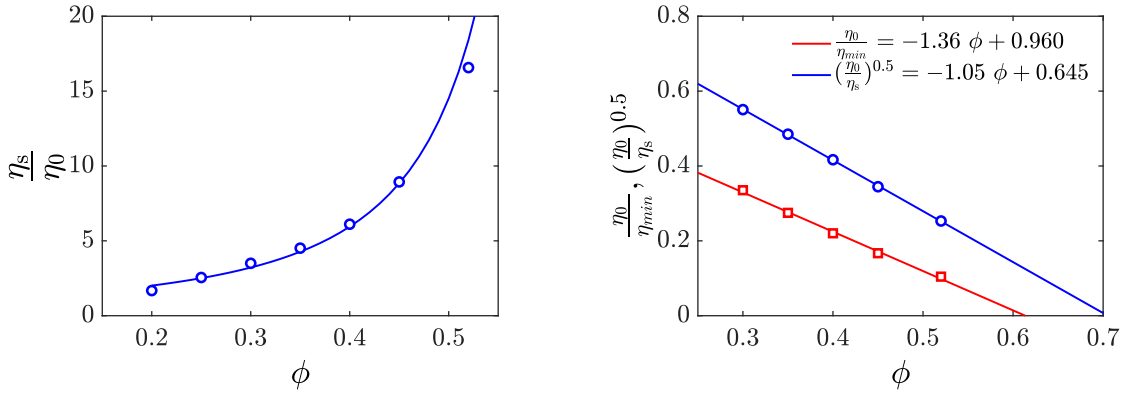


Figure 4.19: left: η_s/η_0 as a function of ϕ for suspension of microcapsules. Plain line is the fit of the Krieger-Dougherty equation. right: left: Scaling of relative steady (squares) and minimum (circles) viscosity based on Krieger-Dougherty power law with $n = 2$ for steady and $n = 1$ for minimum viscosity. $\sigma = 10$

4.3.3 Discussion

The system of polyelectrolytes microcapsules presented an intriguing features which is the emergence of a yield stress above a volume fraction of 0.25. Moreover, we distinguished two regimes. The first one was dominated by the contact between the microcapsules, and the second one by their hydrodynamic interactions. In this section, we discussed these results in regard to the deformability of the shell, the nature of the long-range attraction and simulations on the rheology of attractive suspensions.

Effect of capsule deformability

Rheology of suspensions of elastic core-shell particles has been investigated only numerically up to now in low and moderate volume fraction regime [97]. Our study is the first one to investigate experimentally the rheology of such suspensions. One numerical study focused on the dense regime [98] and showed that such suspensions are shear-thinning with n of 0.5 for highly deformable capsules. Even without aggregation, they predicted also the emergence of a yield stress for ϕ larger than 0.7. Its origin was explained by the Hertzian contacts between the particles. Our findings contrasts with these numerical results, because we observed the emergence of a yield stress from $\phi = 0.25$ and a quasi-Newtonian behavior above the yield stress,

which was independent on the elasticity of the shell.

In fact, in our experiments, the maximal capillary numbers $Ca = \sigma R/G_s$ was of the order of 10^{-3} for $\sigma = 20$ Pa. For such values of Ca , we did not expect that microcapsules could take a non-spherical shape due to the field of shear stress [76]. However, this low value of Ca did not preclude local deformation of the membrane near the contact between two microcapsules due to compressive stress, which could modify lubrication interaction in the thin film. To promote effects due to the deformability of the microcapsules, we should either reduce the G_s or reduce the size. However the lowest value of G_s with this biphasic system was limited by the water / oil surface tension, i.e. of the order of 0.1 N/m. However, these capsules break very easily under shear for low G_s values [84]. Increasing the size of the capsule will have a minor effect on the range of Ca if one want to keep the ratio of the size over the gap sufficiently small to characterize the bulk properties of the suspension. A solution could be to use microcapsules with the same inner and outer phase and then to reduce G_s values of several orders of magnitude [89]. However, such systems are very difficult to produce in mass and in a control way.

Finally, the rheology of our system of microcapsules was clearly dominated by the non-hydrodynamic interactions between the capsules.

The nature of long-range interactions

We have shown experimental evidence of long-range attractions in the suspensions of capsule at rest. Whereas depletion and van der Waals interactions can cause aggregation for sub-micrometric particles, we did not expect that such interactions play any role for particles of few hundreds of micrometers [99]. Moreover, the external phase (silicone oil) has been washed for residue of surfactant, and we cannot expect any depletion. A last hypothesis to explain these long-range interactions is the nature of the molecules used to form the capsules. Chitosan is a positively charged poly-electrolytes and was always present in the inner phase. It has been observed that such systems of polyelectrolytes can cause a strong dipolar interaction because of their large dipole moment [100, 101]. This also explain why our capsules formed chains under a moderate electric field. We can so speculate that chitosan form dipole and was so responsible of the long-range attractive interactions. These interactions can be modulated according to the kind of silicone oil, because they present different dielectric properties.

Rheology of attractive suspensions

The system of polyelectrolytes microcapsules is an original one due to its ability to interact at length scale of few hundreds of micrometer. The rheology of adhesive / attractive particles has been studied for sub-micrometer droplets [102], but to the best of our knowledge not for sub-millimetric particles. For sub-micrometric adhesive particles, it is accepted that there is no unversal flow behaivour of such jammed materials [102], as experimental results can be conflicting. However, it is expected that such materials presents slip at the wall and shear banding. Although we did not measured the velocity field, our system of attractive microcapsules obey well to the Herschel-Bulkley law and do not present non-monotonic variations of stress rate with the shear rate, which is a signature of shear banding [102]. However, without local measurement of the velocity field we cannot exclude slip at the wall and shear banding in our system.

Inrani conducts numerical simulations for attractive non-brownian suspensions [94]. Our experimental results confirms most of their findings. The general picture of the rheology of attractive particle is the presence of two regimes. The "attraction dominated" regime which leads to yield stress below the jamming volume fraction. For a given attraction strength, the yield stress increases with ϕ and for a given ϕ , the yield stress increases with the magnitude of the attraction potential. Note, that the simulations of [94] did not cover ϕ lower than 0.7,

whereas in our experiments ϕ_m was of 0.25. The second regime is the "shear-induced rupture" regime in which the clusters are broken and the viscosity collapse on a master curve for a given ϕ and whatever the strength of the attraction potential. Thus, the results of [94] shows that above a critical shear rate, the attraction do not play any role on the rheology of attractive suspensions. Our steady-state and shear reversal experiments confirms experimentally this picture of attractive suspensions. At low stress and high volume fraction, we showed that the rheology is dominated by the contact, and so the long-range attraction. Above a stress of few Pa, resuspension experiments shows that the clusters were broken and the rheology was dominated by the hydrodynamic interactions between the particles with a low shear-thinning behavior for the most concentrated suspensions. We cannot exclude also that non-Coulombian friction between the particles at high volume fraction [103, 38] or capsule deformability [98] was responsible for this small shear thinning.

Moreover, the numerical of Irani *et al.* [94] give also some insights on shear banding for such attractive systems. They showed that at high volume fraction there is no shear banding and the rheological behavior can be fitted with the Herschell-Bulkley model. At low volume fraction, shear banding and non monotonic shear stress can appear. However, shear-banding depends on the particle confinement: shear bands can be avoided if the wavelength of the unstable modes do not fit with the lateral size of the system. Due to the relatively high confinement in our system (~ 10 particles in the gap), we could expect that it precluded the formation of shear bands. Finally, in agreement with numerical simulations [94], we show that suspensions of attractive particle have a yield stress at volume fractions far below where the corresponding repulsive systems would be fluid.

4.4 Conclusion

We have studied the rheology of a suspension of non-Brownian microcapsules which presented long-range attractions. The originality of our system was to present these attractions at length scales of few hundreds of micrometers. The physical origin of this attraction is an open issue, but we can reasonably speculate, in light of the literature, that the polyelectrolyte present in the capsule was able to generate a strong dipolar moment. Such attraction has for consequence the emergence of a yield stress at volume fraction of 0.25, where the corresponding repulsive systems would be fluid. Moreover, there was no apparent sign of shear banding, which is probably due to the fact that the particles were relatively confined in the plane-plane geometry. The rheological response of this system can be depicted into two different regimes. The "attraction dominated" regime, where there is a yield stress even when we are fare from the close packing. this regime correspond to low stress value and large volume fraction. The second regime is the shear-induced rupture of the aggregates for which we have an almost Newtonian behavior and attraction do not play a significant role on the viscosity of the suspension.

Summary

- ⇒ CH/PFacid microcapsules exhibit long-range attractive interactions with a few hundred micrometers length scale resulting a yield stress at $\phi = 0.25$.
- ⇒ Rheology of microcapsule suspensions is divided into two regimes: attraction dominated regime showing a yield stress and Newtonian regime.

Chapter 5

Viscose resuspension of droplets

Viscous resuspension of droplets

Mehdi Maleki, Hugues Bodiguel,* and Clément de Loubens
Univ. Grenoble Alpes, CNRS, Grenoble INP, LRP, 38000 Grenoble, France
(Dated: February 28, 2021)

Using absorbance measurements through a Couette cell containing an emulsion of buoyant droplets, volume fraction profiles are measured at various shear rates. These viscous resuspension experiments allow a direct determination of the normal stress in the framework of the suspension balance model that have been developed for suspensions of solid particles. The results unambiguously show that the normal viscosity responsible for the shear-induced migration of the droplet is the same as for rigid particles, even at moderate capillary numbers where coalescence occurs, and independently on the polydispersity. This implies that neither the particle deformation nor the detail of contact interactions play an important role on shear-induced migration.

Flow-induced migration of suspensions of rigid particles is ubiquitous in nature and industry. The physical origin is the presence of both solid contact and long-range hydrodynamic interactions between the particles leading to an apparent diffusive behaviour of the suspension under shear [1, 2]. Inspired by margination in blood vessels [3–5], there is a growing interest to understand and model flow-induced structuration in suspensions of soft microparticles in order to design cells sorting microfluidic systems for biological analysis [6–8]. Understanding and modelling these phenomena for soft particles is considered to be a veritable challenge because of the non-linear coupling between hydrodynamic interactions and the dynamics of deformation of the particles [9, 10]. In fact, the deformability of the particle is a major ingredient to break the symmetry of inertialess flow and then generate a normal force and particle migration across the streamlines. Symmetry breaking mechanisms have been identified for isolated soft particles, such as red blood cells, vesicles or capsules by experimental and numerical studies in different canonical flows: the shear flow near a wall [11], inhomogeneous flow (e.g. Poiseuille) [12] or when two particles are crossing in a shear flow [13]. The latter phenomenon questions the role of collective interactions on the segregation in the flow of suspensions of soft particles [14]. Up to now, the problem has been addressed by full numerical simulations of a large number of particles which considers the interplay between the flow, the dynamics of deformation of the particles and their mechanical properties [10, 15, 16]. Even in a simple flow, the dynamic of deformation of soft particles is the complex result between the nature of the flow and the mechanical properties of the particle [17, 18]. The question raised in this Letter is to know in what extent all these details have to be considered or not to account for migration in suspensions of soft particles. In other words, can we describe flow-induced structuration in suspensions of soft particles by a more general framework?

Such a framework has been introduced for suspensions of rigid particles two decades ago [19, 20], referred to as

the Suspension Balance Model (SBM). SBM is a continuous hydrodynamic model that decompose the total stress into the solid and liquid phases. The flux of particle is given by a momentum balance between the divergence of the particle stress tensor, buoyancy and the mean viscous drag exerted by the fluid phase on the particle phase. The particle stress tensor is assumed to be diagonal and its normal components to scale linearly with the shear rate $|\dot{\gamma}|$,

$$\Sigma_{p,ii} = -\eta_0 \eta_{p,i}(\phi) |\dot{\gamma}| \quad (1)$$

where η_0 is the viscosity of the fluid phase and phase $\eta_{p,i}$ is the adimensional normal viscosity. It vanishes when $\phi \rightarrow 0$ and diverges at a maximal volume fraction ϕ_m , similarly to the shear viscosity. It has been determined either using direct measurement of the normal force in dedicated pressure-imposed shear experiments [21–23], either from the volume fraction profiles in non-homogeneous flow [24, 25] or from viscous resuspension experiments [23, 26–29]. All these experimental approaches lead to

$$\eta_{p,i}(\phi) = \lambda_i \frac{\phi^n}{(1 - \phi/\phi_m)^n} \quad (2)$$

where λ_i are the anisotropy coefficients. The debate concerns the value of n , 2 or 3 were used. Small variations of $\eta_{p,i}$ with $\dot{\gamma}$ were also reported and interpreted as a manifestation of non ideal Coulomb friction between the particles, in analogy with shear-thinning non-Brownian suspension at high volume fractions [28, 29]. Above these debates, one can considered SBM as a robust framework to model suspension migration at a macroscopic scale by incorporating empirically microscopic details in rheometric parameters (n , λ_i , ϕ_m), as done with usual rheological constitutive equations.

Although SBM has been developed for suspensions of rigid particles, we show in this Letter that this framework is also compatible with soft particles migration, using one of the simplest model of deformable particles, i.e. droplets. Up to our knowledge, this question has only been addressed theoretically by Ramachandran *et al.*, who derived SBM for diluted suspensions of droplets [30]. It was predicted as in earlier pioneer work on rheology of emulsions [31] that migration and normal stress

* hugues.bodiguel@univ-grenoble-alpes.fr

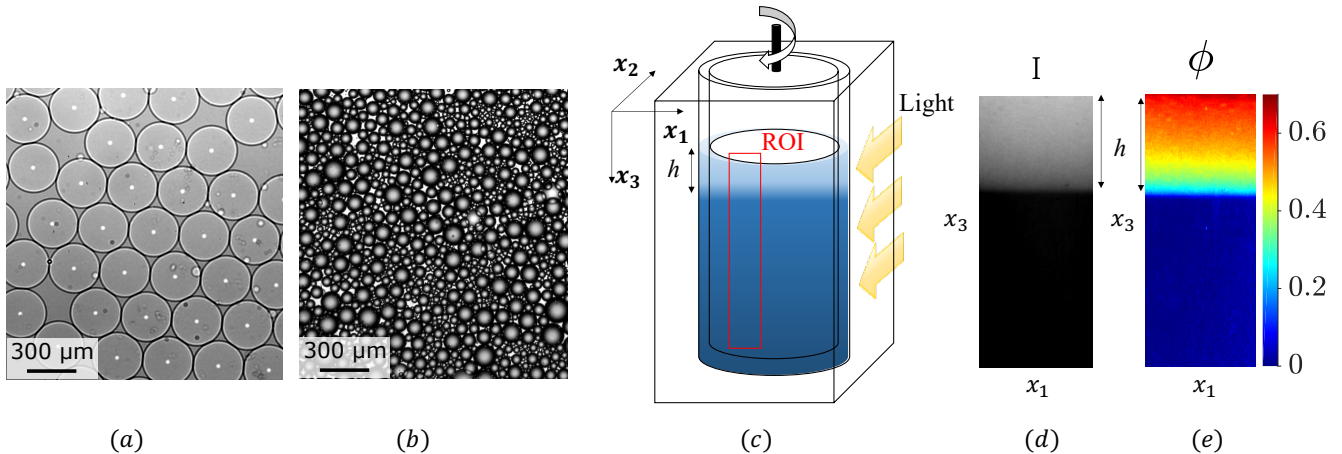


FIG. 1. (a) Monodisperse and (b) polydisperse suspensions of oil-in-water droplets. (c) The suspension was sheared between the two concentric cylinders of a Taylor-Couette cell and imaged by light transmission in the region of interest (ROI) according to \mathbf{x}_2 . h is the height of the resuspended suspension. (d) Transmitted light intensity I in the ROI. (e) Droplets volume fraction $\phi \propto \log_{10}(I_0/I)$ in the ROI.

depends on both the volume fraction and of the capillary number $Ca = \eta_0 \dot{\gamma} a / \sigma$ (a being the droplet radius and σ the surface tension), the latter accounting for the droplet deformation. Experimental data on droplet migration in the semi-dilute regime are however lacking, despite a few observations suggest that shear-induced migration in emulsions is effective [32, 33]. In this work, we aimed at filling this gap by studying the viscous resuspension of emulsions of buoyant droplets, which are the simplest model of deformable particles, in a Taylor-Couette geometry, Fig. 1-c. In this configuration, we expected a volume fraction gradient resulting from the balance between buoyancy and particle stress, similarly to the case rigid particles [28, 29]. Applied to droplets, it had two main advantages: migration is mainly the result of collective interactions between the droplets without interference of other migration mechanisms such as wall effects or gradients of shear rate; a large range of volume fraction is available simultaneously down to very small ones for a given shear rate, so that the respective dependency of η_n on ϕ and Ca could be directly tested.

Emulsions of non-Brownian droplets were made by dispersing a medium chain triglyceride oil (Nestlé, Switzerland) in an aqueous solution of glycerol (84 % w/w, CAS number 56-81-5, VWR) and were stabilized with 1% w/w sorbitan trioleate 85 (CAS number 26266-58-0, Sigma-Aldrich). Monodisperse emulsions were produced with a microfluidic T-junction, radius $a = 143 \pm 5 \mu\text{m}$ (Fig. 1-a), whereas a membrane emulsification device [34] (Micropore LDC-1, Micropore Technologies Ltd, UK) was used to produced polydisperse suspensions, $\bar{a} = 47 \mu\text{m}$ (Fig. 1-b, see Supp. Fig. 1, 2). The viscosity and density of both phases were measured with a rotational rheometer (DHR3, TA instruments) and a densimeter (DMA 4500M, Anton Paar) and were $\eta_d = 50 \text{ mPa}\cdot\text{s}$, $\eta_c = 85 \text{ mPa}\cdot\text{s}$ and $\rho_d = 943.42 \text{ kg/m}^3$, $\rho_c = 1218.52 \text{ kg/m}^3$ at

23°C , respectively. The surface tension σ between the two phases was measured by the pendant drop method and was 5 mN/m .

Resuspension experiments were carried out in home-made transparent Taylor-Couette cell in PMMA of 50 mm height (Fig. 1 -c) driven by a DHR3 rheometer (TA instruments). The inner and outer radii of the cell were $R_1 = 20$ and $R_2 = 24$ mm, respectively. The gap was large enough to accommodate at least 10 droplets, while minimizing the variations of shear rate $\dot{\gamma}$. The suspension of droplets was poured in the cell and let to cream during several hours up to get a layer of creamed droplets of height h_0 . The emulsion was sheared at different increasing steps of $\dot{\gamma}$ from 6 to 260 s^{-1} . For each step, we wait until that the concentration profile reached a steady state. The maximal value of $\dot{\gamma}$ was chosen to kept the Reynolds number $Re = \rho \Omega R_1 (R_2 - R_1) / \eta_0$ sufficiently low to avoid the emergence of Taylor vortices, i.e. $Ta = Re^2 2(R_2 - R_1) / (R_1 + R_2) < 900$. It also allowed to neglect the secondary currents which arise at higher shear rates from the combination of the centrifugal force and buoyancy [28]. This range of shear rate corresponds to a variation of Ca between 10^{-3} and 0.4. Beyond this value, break-up of droplets was expected [35]. To ensure the absence of droplet break-up and/or coalescence, we tested the repeatability of the measurement at the smaller shear rate and measured the size distribution of a sample of droplets taken in the cell after the experiment. Coalescence was furthermore avoided using surface treatment of the cell. Though these precautions were sufficient for the two monodisperse emulsions studied, we were only able to limit coalescence for the polydisperse one, but quantified it and corrected the h_0 values (see supp. mat.).

The resuspension process was imaged with a color camera (Basler, acA2500-14gc) at 0.1 fps in a $25 \times 50 \text{ mm}$ region of interest (ROI), which was centered along the axis

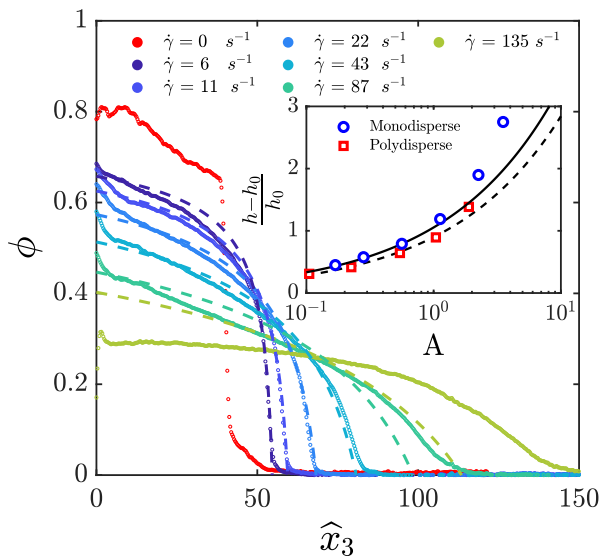


FIG. 2. Steady state concentration profiles $\phi(\hat{x}_3)$ for each shear rate step $\dot{\gamma}$ (colored dots) and Eq. 5 with $\phi_m = 0.8$ and $\lambda_3 = 1$ (colored dashed lines) for mono-dispersed suspension. In insert, the relative height increment of the resuspended layer is plotted as a function of the Acrivos number, which is simply given by $A = aSh/h_0$. The solid lines are the SBM predictions.

of rotation of the inner cylinder (Fig. 1-c). Caution was taken to minimize the parallax issue, see Spp. Mat. Fig. 3. The concentration profile $\phi(x_3)$ was deduced by light absorption technique. In this regard, the optical indexes of both phases of the emulsion were precisely matched thanks to a refractometer (Abbemat 350, Anton Paar) at a wavelength of 589 nm and temperature 23 °C, see Spp. Mat. Fig. 4. A non-fluorescent colorant (E122, Breton) was added to the continuous phase to provide light absorbance contrast (Fig. 1-d). $\phi = KA$ was then deduced from the measurement of the absorbance $A = \log_{10}(I_0/I)$ for each pixel, where I is the light intensity and I_0 the intensity of the background (Fig. 1-d,e). The coefficient of attenuation K was calibrated in the Taylor-Couette cell. The absorbance was measured in the wavelength band of 525 ± 15 nm, which corresponded to the peak of colorant light absorbance (see Spp. Mat. Fig. 5).

Fig. 2 displays the concentration profiles obtained on one of the system used. At rest, the front of ϕ showed a sharp transition between $\phi = 0$ and 0.6. However, contrarily to hard spheres, ϕ was not constant in the dense-packed zone and increased from 0.6 to 0.8. It is a signature of droplets deformation, because the droplets at the top of the layer underwent the Archimedes pressure of the layers below [36]. We analyzed this gradient (see supp. mat.) and showed that ϕ is at rest a unique function of the Laplace number $La = \Sigma_{p,33}a/\sigma$ (which typical values were up to 0.3 in the conditions tested). This result highlights that equation 1 is not valid for very small

shear rates and high volume fractions, but this range falls out of the scope of the present letter.

Increasing shear rate $\dot{\gamma}$, the height h of the suspended layer increased whereas the mean value of ϕ was decreasing, due to volume conservation. Integration of ϕ showed that the volume of droplets was conserved all along the experiment, which validated its measurement (see Spp. Mat.). In the SBM framework, the steady state volume fraction profiles results from the momentum balance in the particle phase, i.e. $\phi\Delta\rho g + \nabla \cdot \Sigma_p = 0$. Simplifying the latter with the definition of the normal components of Σ_p (Eq. 1), we obtain

$$\frac{\phi}{Sh} = -\frac{d\eta_{p,3}}{d\phi} \frac{d\phi}{d\hat{x}_3} \quad (3)$$

where $\hat{x}_3 = x_3/a$ and $Sh = \eta_0\dot{\gamma}/\Delta\rho ga$ is the Shields number. Thus, integrating Eq. 3 along the resuspended height provides a measurement of $\eta_{p,3}$ over a range of ϕ which depends on Sh (or $\dot{\gamma}$)

$$\eta_{p,3} = \frac{1}{Sh} \int_{\hat{x}_3}^{h/a} \phi(u) du. \quad (4)$$

The results of this integration are presented in Fig. 3. Unambiguously, most of the data fall on the same master-curve. Deviations observed for the smallest shear rates at low ϕ are not relevant since the corresponding volume fraction profiles tends to zero very sharply, over a distance that is about the droplet size. For the highest shear rates, a deviation could also be seen at the very top of the resuspended layer.

Moreover, this evolution of $\eta_{p,3}(\phi)$ is very well fitted by Eq. 3 with n equal 2, as observed for rigid particles [20, 21, 28]. The main difference is the value of the maximal volume fraction ϕ_m which is comprises between 0.53-0.63 for rigid particles, and is found to be as high as 0.8 for the emulsion tested. λ_3 of the order of unity, similarly to the rigid case. The validity of these fits was also tested directly on the volume fraction profiles which are more sensitive to the values of the coefficients. In the case of $n = 2$, the concentration profile can be calculated analytically and is given by [28]

$$\frac{\phi(\hat{x}_3)}{\phi_m} = 1 - \left[1 + \frac{\phi_m}{\lambda_3 Sh} (\hat{h} - \hat{x}_3) \right]^{-1/2} \quad (5)$$

where the normalized height of the suspension in the steady state \hat{h} is

$$\hat{h} = \hat{h}_0 + 2\sqrt{\frac{\lambda_3 \hat{h}_0}{\phi_m} Sh}. \quad (6)$$

The experimental and analytical profiles of $\phi(\hat{x}_3)$ are in very good agreement (see Fig. 2, and supp. mat. for the polydisperse case), except for the highest value of $\dot{\gamma}$ (135 s^{-1} , $Ca = 0.33$). The relative height increment, displayed in insert in Fig. 2 also show a very good agreement with equation 6.

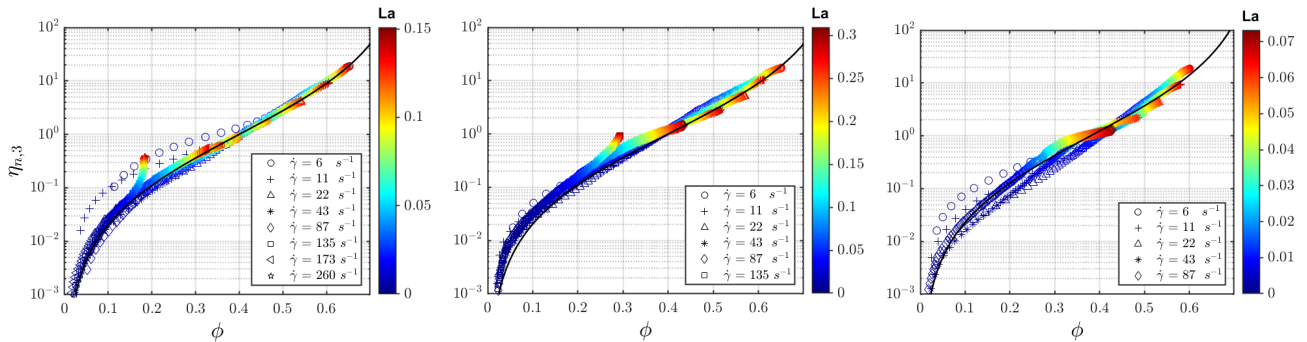


FIG. 3. Relative normal viscosity $\eta_{n,3}$ as a function of the local droplet concentration ϕ for shear rates in the range of $\dot{\gamma} = 6$ to 260 s^{-1} . $\eta_{n,3}$ is deduced by integration of the concentration profile, Eq. 4. The solid lines are the best fit of Eq. 2. **Left:** Monodisperse emulsion with $a = 185 \text{ }\mu\text{m}$, $h_0 = 3.6 \text{ mm}$, $\phi_m = 0.8$ and $\lambda_3 = 1$ **Middle:** Monodisperse emulsion with $a = 143 \text{ }\mu\text{m}$, $h_0 = 5.4 \text{ mm}$, $\phi_m = 0.8$ and $\lambda_3 = 1$ **Right:** Polydisperse emulsion with $\bar{a} = 47 \text{ }\mu\text{m}$, $h_0 = 4$ to 6 mm , $\phi_m = 0.76$ and $\lambda_3 = 0.69$. The color stands for the Laplace number which denotes particle deformation.

The deviations observed for the highest shear rates can have several origins. While it is difficult to exclude some possible contribution of Ca , inertia might also start play a role, as the particle Reynolds number exceeds 0.1. However, and comparing the two set of results monodisperse systems studied, we noticed that the deviation is delayed in the case h_0 was smaller, leading to a lower maximum value of the Laplace number. It thus seems that the observed deviations only concerns high Laplace number and small volume fractions.

This set of result shows that a simple constitutive equation of $\eta_{p,3}$ for a suspension of deformable droplets is sufficient to catch migration phenomena without further sophistication of the SBM. Strikingly, even when droplet deformation cannot be neglected at rest, i.e. for Laplace number above 0.05, it does not affect the normal viscosity under shear up to $La \sim 0.3$. The linear dependency with respect to the shear rate rules out some significant contribution of migration mechanisms due to drop deformability.

The polydisperse emulsion exhibited a very similar behavior, with only small differences in the coefficients. This result is rather surprising as one might expect some size segregation of the droplet under shear. Our results indicate that such kind of behaviour affects neither the macroscopic particle viscosity nor the maximal volume fraction. We believe that it would be interesting to investigate the particle size spatial distribution.

Let us eventually discuss the dynamics of resuspension. Momentum balance in the direction x_3 and mass conservation of the particulate phase read

$$\frac{\partial \Sigma_{p,33}}{\partial x_3} - \frac{9}{2} \frac{\eta_0}{a^2} \frac{\phi}{f(\phi)} (u_{p,3} - u_3) + \Delta \rho g \phi = 0 \quad (7)$$

$$\frac{\partial \phi}{\partial t} + \frac{\partial \phi u_{p,3}}{\partial x_3} = 0 \quad (8)$$

where u_p and u are the velocities of the particle phase and suspension phase, respectively. The second term in Eq. 8 corresponds to the viscous drag on the par-

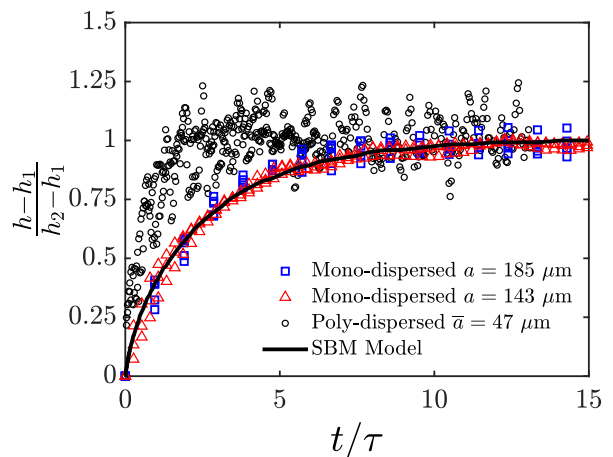


FIG. 4. Kinetics of viscous resuspension. Variation of the total height h of resuspended layer, when the shear rate is suddenly changed from $\dot{\gamma}_1$ to $\dot{\gamma}_2$. The corresponding steady states heights are h_1 and h_2 , respectively. Data are plotted as function of time normalized by $\tau = \eta_0 h_0 / \Delta \rho g a^2$. Several experiments are plotted together for each system (typical shear rates values are between 10 and 100 s^{-1}), and collapse on a single curve. The solid lines are the calculated solutions of the SBM (see text) for the various shear rate steps tested and using the normal viscosity determined in steady state. In the tested range, neither the shear rate nor the amplitude of the step has a significant effect.

ticle phase. f is the hindered settling factor which is given by $(1 - \phi)^5$ [37]. For suspensions of droplets, f depends also on the viscosity ratio between the dispersed and continuous phases κ . Several expressions were proposed in Zichenko *et al.* [38] and Ramachandran *et al.* [30] in the limit of small ϕ and Ca . The simplest expression was $f_0 = (2\kappa + 2) / (9\kappa + 6)$. In this letter, we extend their results to not vanishing ϕ and Ca by writing $f = f_0 (1 - \phi)^5$ which is a combination of f expressions

given for suspensions of solid particles and droplets in the dilute regime. The system of equation 8 was solved for $u_3 = 0$ and using the normal viscosity determined in steady state. They are compared to the experimental results displayed in Fig. 4. An excellent agreement is found for monodisperse emulsions. In the range of parameters investigated, the kinetics is governed by a single characteristic time, given by $\tau = \eta_0 h_0 / \Delta \rho g a^2$ and does not significantly depend on the shear rate. For the poly-disperse case, the kinetics is about two times faster, but this is not surprising as it is very sensitive to the particle size.

In conclusion, the results reported in this letter unambiguously show that the SBM quantitatively accounts for the viscous resuspension of droplets, both in transient and steady state. Moreover, the particle normal stress is linear with respect to the shear rate, and is strikingly very similar to that of rigid particles, but with a higher maximal volume fraction. This result has important consequences. The first one concerns the role of the droplet deformability. The normal stress, which is in principle a function of ϕ and Ca, does not depend on Ca up to 0.4. This implies that the other migration mechanisms due to the coupling between particle shape

and the flow are weak as compared collective effects associated to shear-induced migration which we find to scale as ϕ^2 , down to volume fractions on the order of 5%. The second consequence concerns the role of contact forces in shear-induced migration of particles. If one put aside the small shear-thinning that have recently been reported for suspension of rigid particles [28, 29], it is striking to observe than switching from rigid particles where frictional contacts dominate the rheology to droplets where short range interactions are very different does not have any other impacts than modifying the maximal volume fraction. As a consequence, the SBM together with a normal viscosity proportional to $\phi^2 / (1 - \phi / \phi_m)^2$ appear to be very robust to account for shear induced migration in very different systems, independently on the details of interparticle interactions.

ACKNOWLEDGMENTS

LRP is part of the LabEx Tec21 (ANR-11-LABX-0030) and of the PolyNat Carnot Institute (ANR-11-CARN-007-01).

-
- [1] A. Acrivos, G. Batchelor, E. Hinch, D. Koch, and R. Mauri, Longitudinal shear-induced diffusion of spheres in a dilute suspension, *Journal of fluid mechanics* **240**, 651 (1992).
 - [2] F. Da Cunha and E. Hinch, Shear-induced dispersion in a dilute suspension of rough spheres, *Journal of fluid mechanics* **309**, 211 (1996).
 - [3] R. Fahraeus and T. Lindqvist, The viscosity of the blood in narrow capillary tubes, *American Journal of Physiology-Legacy Content* **96**, 562 (1931).
 - [4] L. L. Munn and M. M. Dupin, Blood cell interactions and segregation in flow, *Annals of biomedical engineering* **36**, 534 (2008).
 - [5] A. R. Pries, T. W. Secomb, P. Gaehtgens, and J. Gross, Blood flow in microvascular networks. experiments and simulation., *Circulation research* **67**, 826 (1990).
 - [6] H. L. Goldsmith and S. Spain, Margination of leukocytes in blood flow through small tubes, *Microvascular research* **27**, 204 (1984).
 - [7] S. S. Shevkoplyas, T. Yoshida, L. L. Munn, and M. W. Bitensky, Biomimetic autoseparation of leukocytes from whole blood in a microfluidic device, *Analytical chemistry* **77**, 933 (2005).
 - [8] E. Henry, S. H. Holm, Z. Zhang, J. P. Beech, J. O. Tegenfeldt, D. A. Fedosov, and G. Gompper, Sorting cells by their dynamical properties, *Scientific reports* **6**, 34375 (2016).
 - [9] A. Kumar and M. D. Graham, Margination and segregation in confined flows of blood and other multicomponent suspensions, *Soft Matter* **8**, 10536 (2012).
 - [10] J. B. Freund, Numerical simulation of flowing blood cells, *Annual review of fluid mechanics* **46**, 67 (2014).
 - [11] N. Callens, C. Minetti, G. Couplier, M.-A. Mader, F. Dubois, C. Misbah, and T. Podgorski, Hydrodynamic lift of vesicles under shear flow in microgravity, *EPL (Europhysics Letters)* **83**, 24002 (2008).
 - [12] B. Kaoui, G. Ristow, I. Cantat, C. Misbah, and W. Zimmermann, Lateral migration of a two-dimensional vesicle in unbounded poiseuille flow, *Physical Review E* **77**, 021903 (2008).
 - [13] P.-Y. Gires, A. Srivastav, C. Misbah, T. Podgorski, and G. Couplier, Pairwise hydrodynamic interactions and diffusion in a vesicle suspension, *Physics of Fluids* **26**, 013304 (2014).
 - [14] X. Grandchamp, G. Couplier, A. Srivastav, C. Minetti, and T. Podgorski, Lift and down-gradient shear-induced diffusion in red blood cell suspensions, *Physical review letters* **110**, 108101 (2013).
 - [15] H. Zhao, E. S. Shaqfeh, and V. Narsimhan, Shear-induced particle migration and margination in a cellular suspension, *Physics of Fluids* **24**, 011902 (2012).
 - [16] D. A. Fedosov and G. Gompper, White blood cell margination in microcirculation, *Soft matter* **10**, 2961 (2014).
 - [17] J. Deschamps, V. Kantsler, and V. Steinberg, Phase diagram of single vesicle dynamical states in shear flow, *Physical review letters* **102**, 118105 (2009).
 - [18] C. de Loubens, J. Deschamps, F. Edwards-Levy, and M. Leonetti, Tank-treading of microcapsules in shear flow, *Journal of Fluid Mechanics* **789**, 750 (2016).
 - [19] P. R. Nott and J. F. Brady, Pressure-driven flow of suspensions: simulation and theory, *Journal of Fluid Mechanics* **275**, 157 (1994).
 - [20] J. F. Morris and F. Boulay, Curvilinear flows of noncolloidal suspensions: The role of normal stresses, *Journal of rheology* **43**, 1213 (1999).

- [21] F. Boyer, O. Pouliquen, and É. Guazzelli, Dense suspensions in rotating-rod flows: normal stresses and particle migration, *Journal of Fluid Mechanics* **686**, 5 (2011).
- [22] F. Boyer, É. Guazzelli, and O. Pouliquen, Unifying suspension and granular rheology, *Physical Review Letters* **107**, 188301 (2011).
- [23] I. E. Zarraga, D. A. Hill, and D. T. Leighton Jr, The characterization of the total stress of concentrated suspensions of noncolloidal spheres in newtonian fluids, *Journal of Rheology* **44**, 185 (2000).
- [24] M. Lyon and L. Leal, An experimental study of the motion of concentrated suspensions in two-dimensional channel flow. part 1. monodisperse systems, *Journal of Fluid Mechanics* **363**, 25 (1998).
- [25] B. Snook, J. E. Butler, and É. Guazzelli, Dynamics of shear-induced migration of spherical particles in oscillatory pipe flow, *Journal of Fluid Mechanics* **786**, 128 (2016).
- [26] D. Leighton and A. Acrivos, Viscous resuspension, *Chemical engineering science* **41**, 1377 (1986).
- [27] A. Acrivos, R. Mauri, and X. Fan, Shear-induced resuspension in a couette device, *International journal of multiphase flow* **19**, 797 (1993).
- [28] B. Saint-Michel, S. Manneville, S. Meeker, G. Ovarlez, and H. Bodiguel, X-ray radiography of viscous resuspension, *Physics of Fluids* **31**, 103301 (2019).
- [29] E. d'Ambrosio, F. Blanc, and E. Lemaire, Viscous resuspension of non-brownian particles: determination of the concentration profiles and particle normal stresses, *Journal of Fluid Mechanics* **911**, A22 (2021).
- [30] A. Ramachandran, M. Loewenberg, and D. T. Leighton Jr, A constitutive equation for droplet distribution in unidirectional flows of dilute emulsions for low capillary numbers, *Physics of Fluids* **22**, 083301 (2010).
- [31] W. Schowalter, C. Chaffey, and H. Brenner, Rheological behavior of a dilute emulsion, *Journal of colloid and interface science* **26**, 152 (1968).
- [32] K. Hollingsworth and M. Johns, Droplet migration in emulsion systems measured using mr methods, *Journal of colloid and interface science* **296**, 700 (2006).
- [33] M. Abbas, A. Pouplin, O. Masbernat, A. Liné, and S. Décarre, Pipe flow of a dense emulsion: Homogeneous shear-thinning or shear-induced migration?, *AIChE Journal* **63**, 5182 (2017).
- [34] S. R. Kosvintsev, G. Gasparini, R. G. Holdich, I. W. Cumming, and M. T. Stillwell, Liquid-liquid membrane dispersion in a stirred cell with and without controlled shear, *Industrial & engineering chemistry research* **44**, 9323 (2005).
- [35] B. Bentley and L. G. Leal, An experimental investigation of drop deformation and breakup in steady, two-dimensional linear flows, *Journal of Fluid Mechanics* **167**, 241 (1986).
- [36] M. Henschke, L. H. Schlieper, and A. Pfennig, Determination of a coalescence parameter from batch-settling experiments, *Chemical Engineering Journal* **85**, 369 (2002).
- [37] J. Richardson and W. Zaki, Sedimentation and fluidisation: Part i, *Chemical Engineering Research and Design* **75**, S82 (1997).
- [38] A. Zinchenko, Effect of hydrodynamic interactions between the particles on the rheological properties of dilute emulsions, *Journal of Applied Mathematics and Mechanics* **48**, 198 (1984).

Supplementary material for: Resuspension of droplets

Mehdi Maleki, Hugues Bodiguel,* and Clément de Loubens
Univ. Grenoble Alpes, CNRS, Grenoble INP, LRP, 38000 Grenoble, France
(Dated: February 28, 2021)

CONTENTS

I. Droplet production	1
II. Size Distribution	1
III. Parallax issue	2
IV. Tuning refractive index	3
V. Characterizing the absorbance	3
VI. Coalescence issue	4
VII. Concentration profiles at rest	6
VIII. Concentration profile of polydisperse suspension	7
IX. Suspension height evolution	7
References	7

I. DROPLET PRODUCTION

The oil-in-water emulsions were produced with two different methods: microfluidics and membrane emulsification. Monodisperse emulsions were fabricated by microfluidics method while polydisperse emulsions were produced by membrane emulsification. The aqueous phase consisted of water-glycerol mixture (glycerol 84 % w/w, CAS number 56-81-5, VWR) and added food grade colorant (0.001% w/w, E122, Breton). The oil phase was composed of medium chain triglyceride oil (Nestlé, Switzerland) with sorbitan trioleate 85 (1% w/w, CAS number 26266-58-0, Sigma-Aldrich). Table I demonstrates the physical properties of oil and water phases of the emulsions.

TABLE I. Physical properties of oil and water phases of the emulsions at 23 °C.

Phase	Density kg.m^{-3}	Viscosity mPa.s	Refractive Index nD
Oil Phase	943.42	50	1.44948
Water Phase	1218.52	85	1.44948

* hugues.bodiguel@univ-grenoble-alpes.fr

Monodisperse oil-in-water emulsions were produced with a custom-made PMMA T-junction microfluidic chip with a cross-section 1×1 mm. The inside of the chip was treated with acetone in order to render the surface hydrophilic. As shown in figure 1-right, the continuous aqueous phase was injected through the main channel while the dispersed oil phase was introduced through the perpendicular branch via a round glass capillary (CM Scientific Ltd) of $300 \mu\text{m}$ inner diameter. The flow rates were controlled by two syringe pumps (neMSYS, CETONI). To improve the production rate, T-junction chip was modified by narrowing the intersection area to strength shear forces. Two monodisperse emulsions with different droplet sizes were generated at volumetric flow rates of oil phase 0.2 and 0.3 ml/min while the flow rate of aqueous phase 2 ml /min in both cases.

The lab-scale membrane emulsification system was purchased from Micropore Technologies Ltd (UK) under the commercial name Micropore LDC-1. The system includes a micro-engineered emulsification membrane with $20 \mu\text{m}$ cylindrical laser etched pores under a paddle-blade stirrer (Figure 1-left). The rotational velocity of the stirrer was controlled by a DC motor. The thin flat nickel emulsification membrane was chemically treated on one side to have a hydrophilic surface. The pore spacing and porosity of the membrane were $200 \mu\text{m}$ and 0.91% respectively. The array of pores was located in a narrow annular region on the membrane to limit the variation of shear rate and thus homogenize the droplet size distribution [1]. The aqueous phase was stirred with the paddle at 500 rpm and the oil phase was injected by a syringe pump (neMSYS, CETONI) through the membrane with a flow rate of 2 ml/min.

II. SIZE DISTRIBUTION

The estimation of the droplet size distribution was based on bright field microscopy images. A large amount of droplets was placed on wide microscope slides and put under an inverted microscope (IX-73, Olympus) equipped with 4, 10, and 20 fold objectives. The motorized stage (Marzhauser) was automatized to perform a tile scan on the entire specimen and the pictures were acquired with a digital camera (ORCA-Flash 4.0, Hamamatsu). The droplet size was measured with a custom written software based on the Matlab (The MathWorks, Inc.) image processing toolbox. The average radius of the monodisperse droplets are $a = 143$ and $185 \mu\text{m}$ and polydisperse droplets $a = 47 \mu\text{m}$ with a sampling

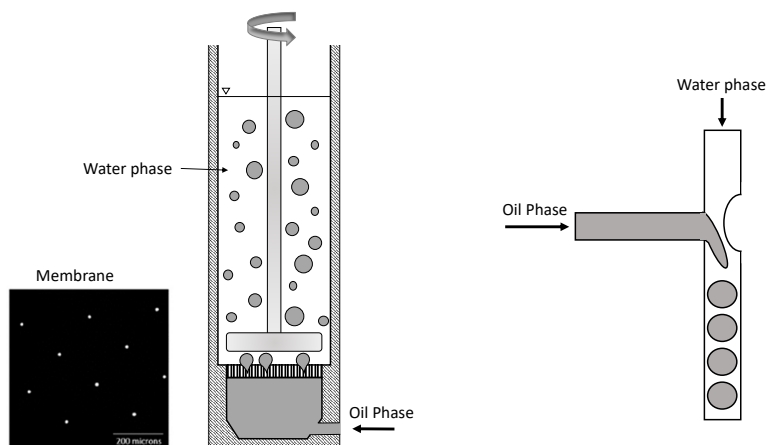


FIG. 1. Production of droplet emulsions. **Left:** Membrane emulsification system to produce poly dispersed droplets, **Right:** Microfluidic T-junction chip to produce monodispersed droplets

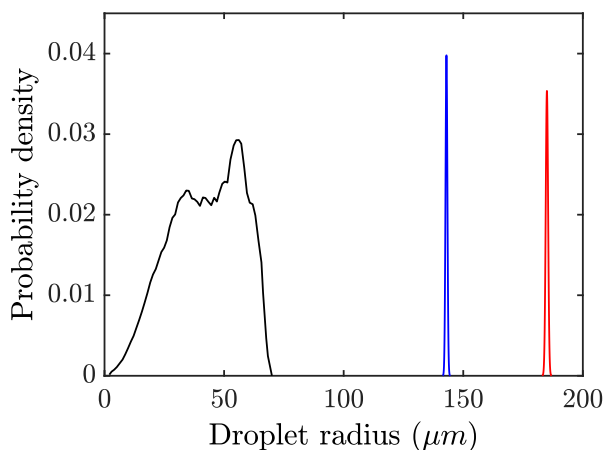


FIG. 2. Probability density of volumic size distribution of droplets. Polydisperse emulsion is resulted from membrane emulsification system and monodisperse emulsion is produced by microfluidic system.

rate over several thousand. The size distribution of the monodisperse and polydisperse emulsions is shown in Figure 2.

III. PARALLAX ISSUE

In this section, we analyze the parallax issue raised by the finite distance between the camera and Taylor-Couette geometry. In the experimental setup, the light source was a 2D LED panel with a homogeneous and stable light intensity. It was placed parallel to the Taylor-Couette geometry with 10 cm of distance. As shown in

figure 3-right, light beams traveled through the suspension and geometry, then they were collected by a camera (Basler, acA2500-14gc), located at a distance of L from the geometry.

By considering a finite value of L , the camera receives the incident light beams within an angle of 0 to α relative to the horizontal direction. This leads to a smoothing effect on the concentration profile in the vertical direction x_3 through a length of l (figure 3-right). This means that the measurement of the droplet concentration is vertically averaged in this length. Consequently, the errors induced by smoothing can be considerable where the vertical concentration sharply shifts to zero at the nose of the suspension as shown in figure 7. Note that, measurement of normal viscosity $\eta_{n,3}$ and determining exponent n in SBM model depends strongly on the provided precision to detect the curvature of the concentration transition to zero.

By increasing the distance L between the camera and geometry, the angle α and the vertical averaging length l reduce. Consequently, the spatial smoothing of the concentration profile in the vertical direction becomes less effective. The experiments were performed with a distance of L up to 5 m, whereas the height of the suspension in the measurement zone was 2 cm. To have high resolution images (5 pixels for a droplet diameter) we used a lens with a large focal length. Figure 3-left represents an image of the geometry with two similar rulers placed at two sides of the geometry. We can observe that the parallax in the measurement zone is negligible however by approaching to the bottom of geometry, it becomes more decisive. In such configuration of the experimental setup, we estimate $\alpha = 0.11$ degree and vertical averaging length $l = 96 \mu\text{m}$. The ratio of l to the diameter of monodisperse and polydisperse droplets is $l/a = 1/3$ and 1 respectively. These small ratios indicate a negligible

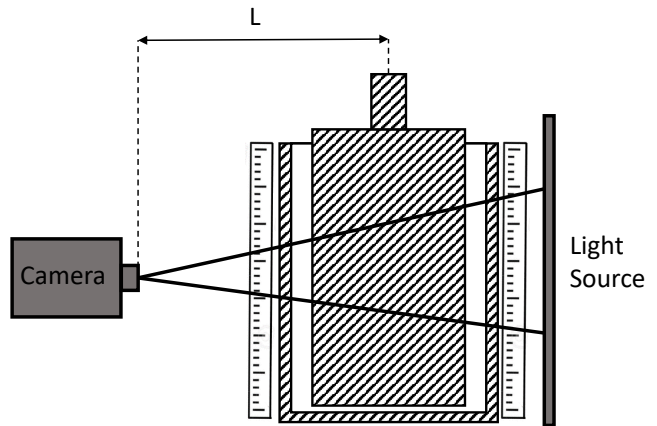
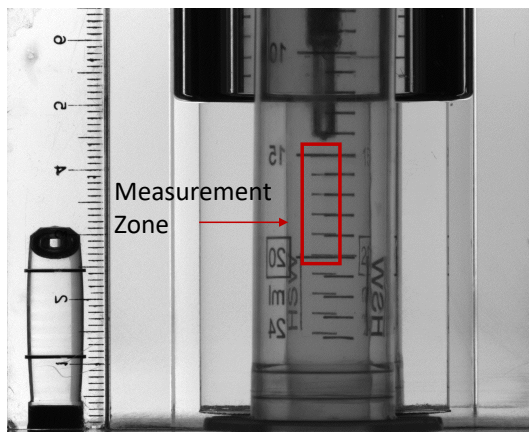


FIG. 3. Parallax issue along the vertical direction solved by increasing the distance L between the camera and Taylor-Couette cell up to five meters. To have high resolution pictures of measurement zone a lens with a large focal length has been used. A ruler behind and front of the Taylor-Couette cell indicates a negligible parallax issue.

effect of the parallax on the concentration profile measurement where it experiences a sharp transition to zero. Consequently, the parallax does not impact the comparison of our measurements with SBM model.

IV. TUNING REFRACTIVE INDEX

Balancing the refractive index between the droplets and suspending fluid was crucial for our experimental method. Light refraction between the two phases in the emulsions could give rise to considerable errors in the measurement of the concentration profile $\phi(x_3)$. The refractive index of the oil phase was measured with precise refractometer (Abbemat 350, Anton Paar) $n = 1.44948$ nD at $T = 23$ °C and wavelength $\lambda = 589$ nm. Note that the resuspension experiments were conducted at the same temperature and a wavelength band of $\lambda = 525 \pm 15$ nm. Figure 4 illustrates the difference of refractive index between the droplets and suspending fluid for various glycerol volume fractions in the suspending fluid. The zero contrast was estimated with a glycerol volume fraction around $\phi = 84.68\%$ w/w. Then after preparing the solution, the contrast was refined to a precision of $\Delta n = 0.00000$ nD with drop-by-drop addition of glycerol or water. After each droplet addition in order to homogenize the solution it was rigorously mixed with a magnetic stirrer for an hour. After that 3 ml samples were pipetted from different sites in the solution volume. The refractive index of these samples was measured to the precision $\Delta n = 0.00000$ nD and in the case of mismatch the mixing was repeated.

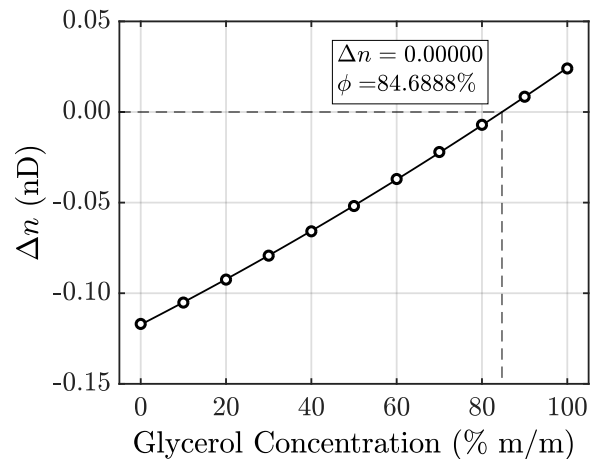


FIG. 4. The difference of refractive index between the droplets and suspending fluid as a function of glycerol volume fraction at 23 °C and wavelength $\lambda = 589$ nm. A zero contrast of refractive index was estimated with glycerol concentration $\phi = 84.6888\%$. The final contrast was refined to a precision of $\Delta n = 0.00000$ nD by adding some drops of glycerol or water.

V. CHARACTERIZING THE ABSORBANCE

The vertical concentration profile of the resuspended emulsions $\phi(x_3)$ was obtained by the light absorption technique. Since the droplets and suspending fluid were both completely transparent, adding a colorant to the suspending fluid provided a contrast in the light absorbance degree between the two phases. A non-fluorescent food-grade additive, E122 (Breton) was used as the colorant. UV-Vis spectrophotometry analysis of the colorant was performed in a quartz cuvette (Hellma Analytics) with a light path of $L = 2$ mm and a portable

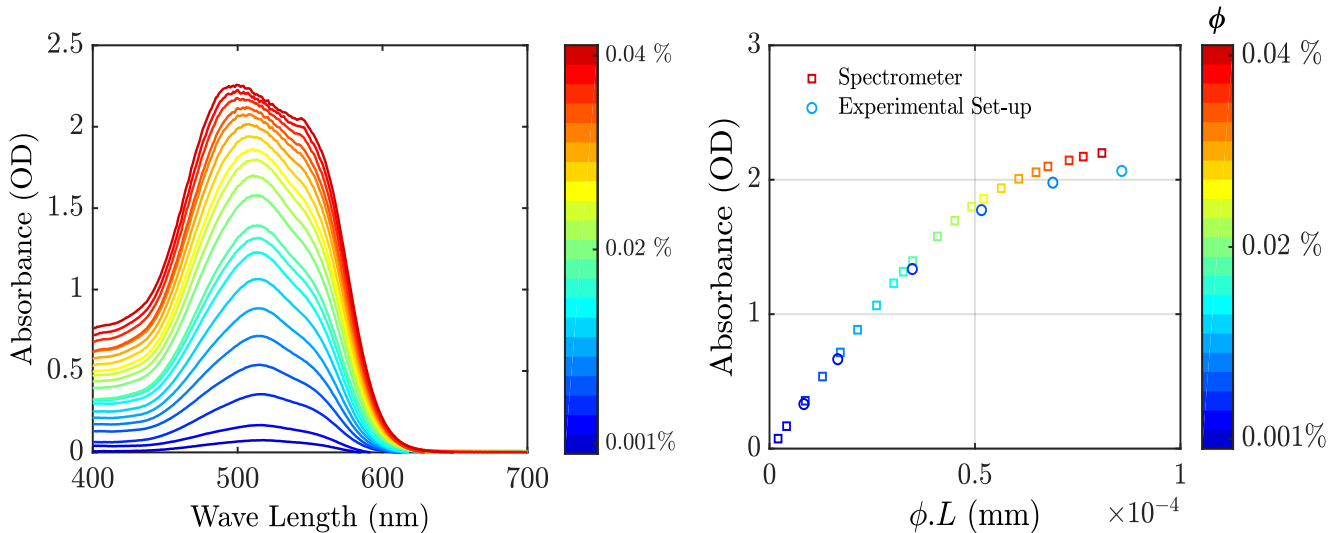


FIG. 5. Characterization of the light absorbance of the colorant, **Left:** The light absorbance of the colorant for concentration ranging from $c = 0.001\%$ to 0.04% mg/ml. in visible light wave length measured by a spectrometer in a $L = 2$ mm cuvette, **Right:** Absorbance of the colorant at wave length $\lambda = 525$ nm as a function of $\phi.L$ where ϕ is the colorant concentration and L is the traveled length of light in the sample. The measured absorbance by the spectrometer in a cuvette with $L = 2$ mm has an excellent agreement in the linear part with measured absorbance by the experimental set-up in the Taylor-Couette cell. A bandpass filter with the center wavelength, $\lambda = 525 \pm 15$ nm was used in the experimental set-up.

spectrometer (RedLite, Ocean Insight). Figure 5-left demonstrates the absorption spectra of the colorant dissolved in the suspending fluid with the concentration ranging from $c = 0.001\%$ to 0.04% mg/ml. The absorption spectrum was a broad band with a maximum absorbance peak at $\lambda = 520$ nm.

To validate our experimental approach, we measured the absorbance of the colorant with a digital camera (acA2500-14gc, Basler) in Taylor-Couette Cell and compared the results with a spectrophotometer. As shown in figure 5-left, the wavelength related to the peak of absorbance is around $\lambda = 520$ nm, thus we used an interference bandpass filter with the center wavelength $\lambda = 525 \pm 15$ nm. Beer-Lambert law formulates the exponential decay of the light intensity passing through a solution. Thus we can relate intensities and a distance L and calculate the absorbance as:

$$A \equiv \log\left(\frac{I_0 - I_d}{I_L - I_d}\right) = \varepsilon c L \quad (1)$$

where I_0 is the light intensity after traveling the suspending fluid without colorant as well as the transparent container cell of sample, I_L is the traveled light intensity with contribution of the colorant, I_d is the measured light intensity by the insulated camera which represents the noise and ε is the attenuation rate of light for the colorant. Contrary to the cuvette, in Taylor-Couette cell, the traveled length of the light beam through the sample is not constant. By determining the corresponding traveled length L for each pixel of the captured image, a 2D light absorbance map was obtained. As expected, for the homogeneous colorant solution in Taylor-Couette

cell, we obtained an uniform 2D absorbance map. Figure 5-right demonstrates the absorbance of the colorant at wavelength $\lambda = 520$ nm, measured by the spectrophotometer and the experimental setup as a function of $\phi.L$ where ϕ is the colorant concentration and L is the traveled length of light in the sample. The measurements show an excellent consistency in the linear regime. The experiments were conducted in such fashion to keep the corresponding absorbance values within the linear part.

VI. COALESCENCE ISSUE

As the droplets are less dense than the suspending fluid, they cream on top of the Taylor-Couette cell. The droplets can be deformed under the buoyant force, which causes them to coalesce [2]. The droplet coalescence was inhibited with a surface treatment of the geometry for monodisperse suspensions. However, this surface treatment proved to be inefficient for polydisperse suspensions. Figure 6-a shows the concentration map of the polydisperse droplets in $x_1 - x_3$ plane for shear rates ranging from $\dot{\gamma} = 0$ to 87 s^{-1} in steady state. It illustrates the emergence and then stabilization of the oil layer caused by coalescence at the top of the geometry. Additionally, we observed that the creamed suspension undergoes a similar transformation over a short period of time even at rest. However, under a shear stress this process slows down. We had to make a correction in the experimental data in order to discard the coalesced part and take into account only the true quantity of droplets in the suspension. This was necessary since the migration

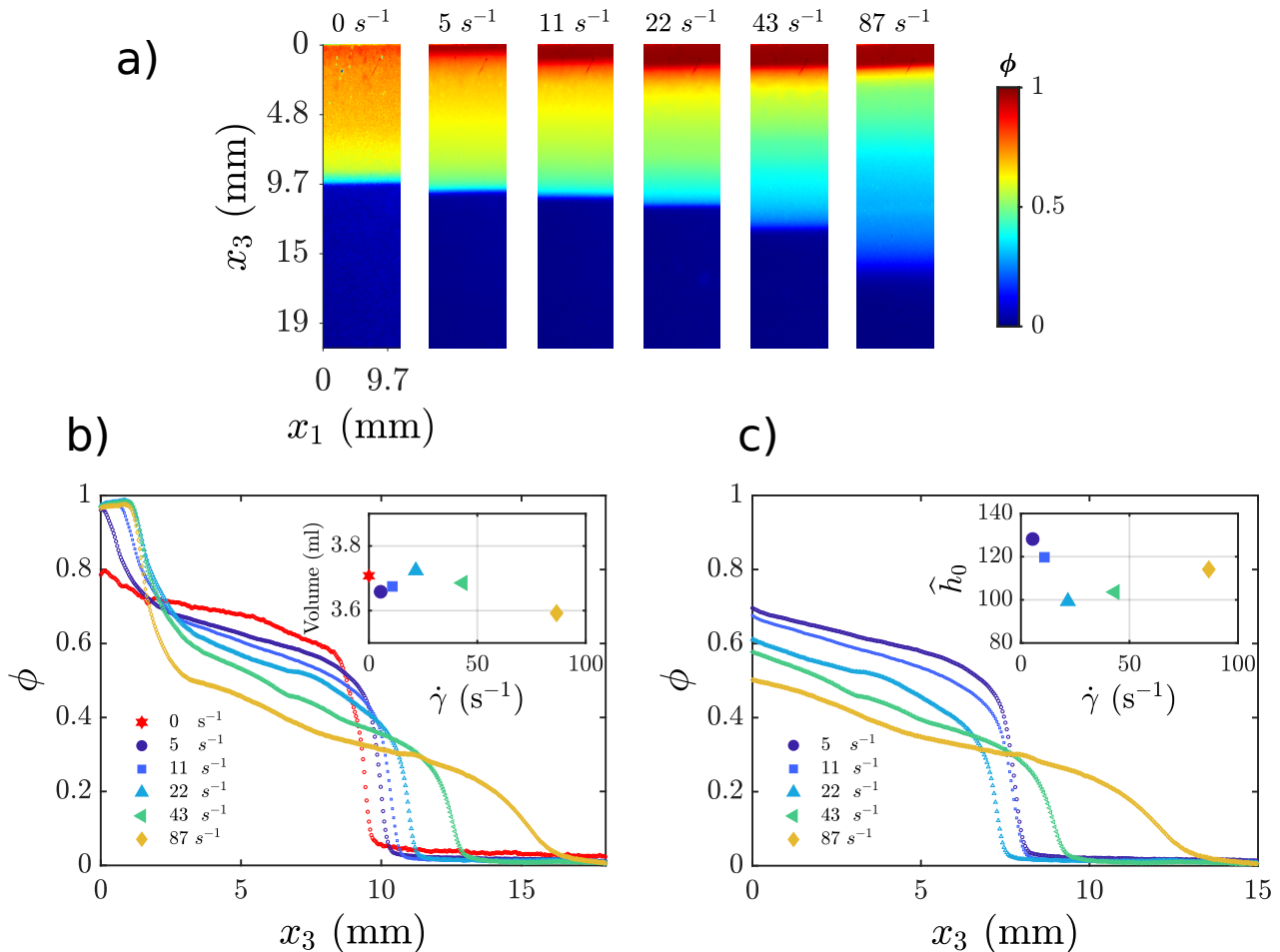


FIG. 6. Coalescence issue for polydisperse suspensions despite surface treatment, **a**: 2D concentration profile of droplets in $x_1 - x_3$ plane and presence of an oil layer at the top of the Taylor-Couette cell resulted from coalescence of droplets, **b**: The concentration profile of droplets in steady state along the resuspension direction x_3 for shear rates ranging from $\dot{\gamma} = 0$ to 87 s^{-1} . The coalesced part can be detected by sharp increase of the concentration. Inset figure is the total volume of oil phase calculated by equation 2. **c**: Corrected concentration profile of droplets as a function of x_3 . Inset figure is normalized height of the creamed suspension at rest $\hat{h}_0 = h/a$ calculated by the equation 3 as a function of shear rate. h is the height of resuspension in the steady state and a is the average size of the droplets.

phenomenon in the resuspension experiments depends on the droplet quantity. Moreover, comparing the migration rate in the same suspension as a function of shear rate is possible only if the non-coalesced droplet quantity is taken into account.

Figure 6-b shows the vertical steady state concentration profile of droplets $\phi(x_3)$ for shear rates ranging from $\dot{\gamma} = 0$ to 87 s^{-1} . The total volume of the oil phase (droplets and coalesced part) can be calculated by integrating $\phi(x_3)$ over x_3 :

$$V = \pi(R_2^2 - R_1^2) \int_0^H \phi(x_3) dx_3 \quad (2)$$

where $R_1 = 20$, $R_2 = 24$ and $H = 50$ mm are the inner, outer radii and height of the Taylor-Couette cell respectively. The total volume of oil phase (inset figure 6-b) is

$V = 3.691 \pm 0.033$ ml for shear rates up to $\dot{\gamma} = 43 \text{ s}^{-1}$ which corresponds to a relative standard deviation from 2.7 % up to = 5.2 % at $\dot{\gamma} = 87 \text{ s}^{-1}$. This variation increment originates from the optical issues at the surface of oil layer with the air. The coalesced part can be detected by a sharp increase in the concentration profile near $x_3 = 0$. Figure 6-c shows the same concentration profiles after eliminating the part related to the coalescence. Consequently, each concentration profile is a representation of the droplets migration as a response to the shear rate but with different quantities of particles in the suspension. Based on the mass conservation, by integrating the concentration profile over the normalized length $\hat{x}_3 = x_3/a$, we can estimate the normalized height of the creamed suspension at rest \hat{h}_0 for each concentration

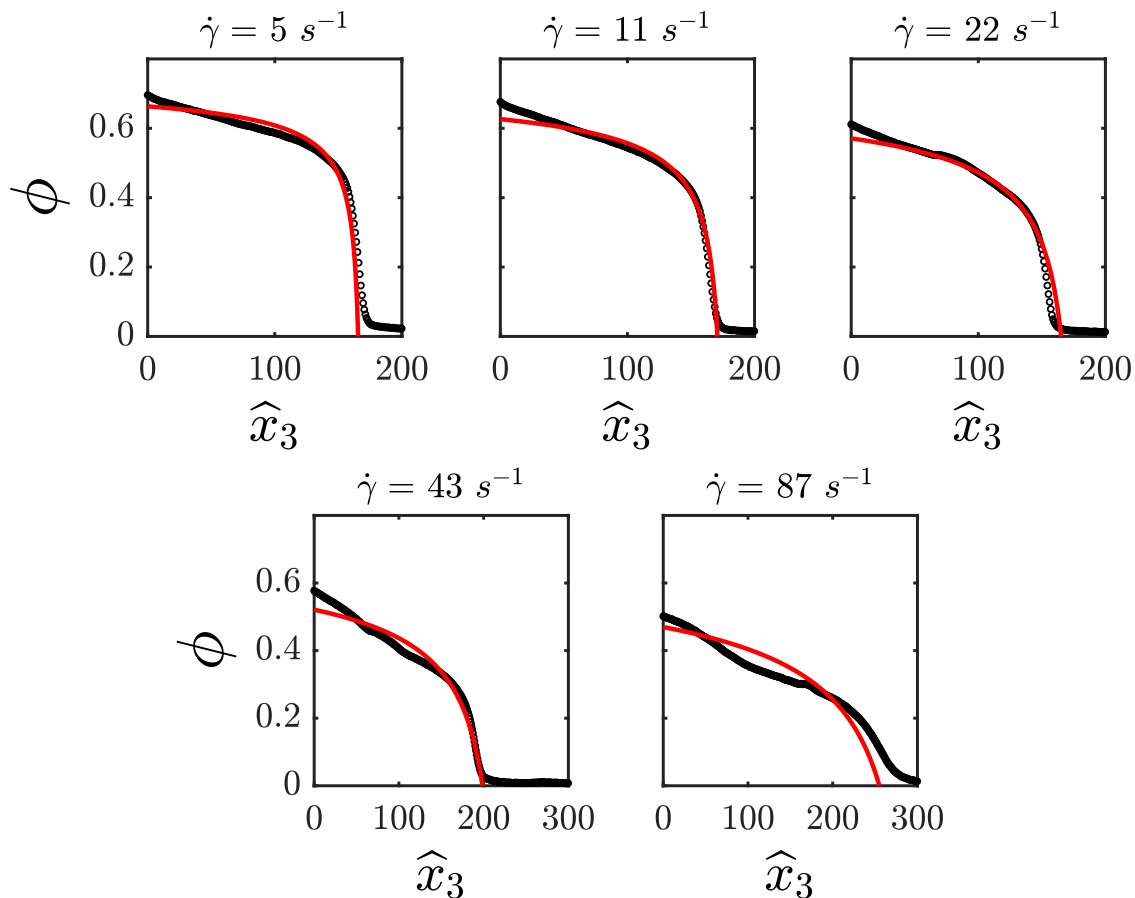


FIG. 7. Corrected concentration profile of polydisperse suspension of droplets for shear rates in the range of $\dot{\gamma} = 5$ to 87 s^{-1} . The circles are the experimental data from section VI and solid lines are the analytical profiles based on the Suspension Balance Model with $n = 2$ and calculated from equation 4 with $\phi_m = 0.76$ and $\lambda_3 = 0.69$.

profile:

$$\hat{h}_0 \phi_m = \int_0^{\hat{h}} \phi(\hat{x}_3) d\hat{x}_3 \quad (3)$$

where \hat{h} is the normalized height of the suspension in steady state. Jamming concentration was considered (CONSIDERED BASED ON WHAT?) $\phi_m = 0.76$ for all droplet quantities. The inset of figure 6-c shows the calculated \hat{h}_0 for each concentration profile which is in the range of 100 to 128. The increase of \hat{h}_0 for shear rates $\dot{\gamma} = 43$ and 87 s^{-1} can be attributed to the break-up of the large oil pockets which did not coalesce with the oil layer located at the top of the geometry. To compare our results, such as the normal viscosity $\eta_{n,3}$, the evolution of suspension height \hat{h} and concentration profile $\phi(\hat{x}_3)$, to Suspension Balance Model (SBM) we used the corrected data.

VII. CONCENTRATION PROFILES AT REST

At rest and after creaming during about 12h, the volume fraction is not uniform but exhibits a gradient from about 0.6 at the bottom of the emulsion layer up to 0.8 at the top. This effect is the signature of droplet deformability, since - at least for monodisperse systems - a volume fraction of 0.8 cannot be obtained with spherical droplets. When comparing the particle stress, given by $\Sigma_{p,33} = \int \Delta \rho g \phi dx_3$ with the Laplace pressure, we indeed find that the particle stress is a non negligible fraction of Laplace pressure, which allows significant deformation of the droplet.

In Fig. 8, the volume fraction at rest is plotted for the three systems studied as a function of the Laplace number, $La = \Sigma_{p,33}/(\gamma/a)$. The two monodisperse systems nicely collapse on a master curve, which is roughly an affine function of La . This validates the above hypothesis that the droplet deform due to the buoyant mass of the layer underneath. The polydisperse system slightly deviates from this behaviour in the bottom of the layer,

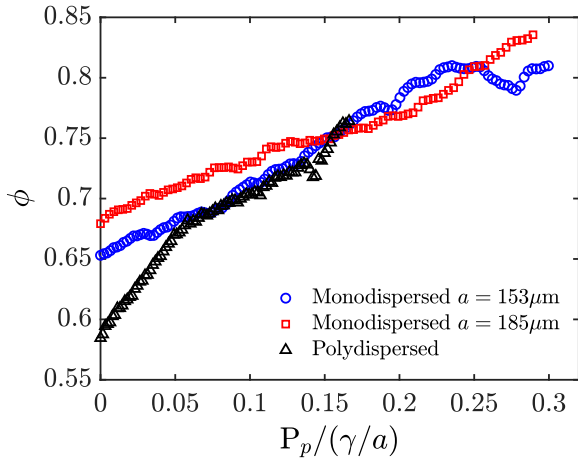


FIG. 8. Concentration profiles at rest ($\dot{\gamma} = 0$) as a function of the Laplace number L_A for monodispersed and polydispersed suspensions of droplets.

which might indicate that a size segregation exists in this case.

VIII. CONCENTRATION PROFILE OF POLYDISPERSE SUSPENSION

Based on the theoretical framework of the Suspension Balance Model (SBM), in the case of $n = 2$, the concentration profile of the droplets can be calculated analytically as [3]:

$$\frac{\phi(\hat{x}_3)}{\phi_m} = 1 - \left[1 + \frac{\phi_m}{\lambda_3 Sh} (\hat{h} - \hat{x}_3) \right]^{-1/2} \quad (4)$$

where the normalized steady state height of the suspension \hat{h} is

$$\hat{h} = \hat{h}_0 + 2\sqrt{\frac{\lambda_3 \hat{h}_0}{\phi_m} Sh} \quad (5)$$

Figure 7 represents the corrected concentration profiles of the polydisperse suspension and the analytical profile calculated by equation 4 for shear rates ranging from $\dot{\gamma} = 5$ to 87 s^{-1} . Jamming concentration was $\phi_m = 0.76$ and the best fit was found with free parameter $\lambda_3 = 0.69$. The experimental results for shear rates $\dot{\gamma} = 5$ to 43 s^{-1} are in good agreement with the theoretical

prediction in equation 4. In the case of $\dot{\gamma} = 87 \text{ s}^{-1}$ the inertia effects can come into play. Furthermore, the discrepancies between the experimental and theoretical results can be originated from the structuration of the droplets caused by size polydispersity.

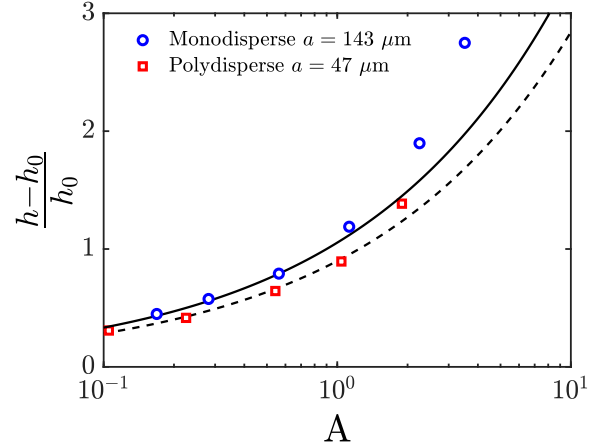


FIG. 9. Variation of the normalized height of resuspended monodisperse and polydisperse suspensions as a function of Acrivos number. Solid line is the correlation with $n = 2$, $\phi_m = 0.8$ and $\lambda_3 = 1$ for monodisperse droplets and dashed line with $n = 2$, $\phi_m = 0.76$ and $\lambda_3 = 0.69$ for monodisperse and polydisperse droplets respectively.

IX. SUSPENSION HEIGHT EVOLUTION

Normalized height of the suspensions for shear rates in the range of $\dot{\gamma} = 5$ to 135 s^{-1} is presented in figure 9 as a function of Acrivos number. Acrivos number is defined:

$$A = \frac{\eta_0 \dot{\gamma}}{\Delta \rho g h_0} \quad (6)$$

which is the ratio of viscous force to buoyancy force as Shields number Sh but with h_0 for the characteristic length. The analytical correlation presented in equation 5 is traced for monodisperse droplets (solid line) with $n = 2$, $\phi_m = 0.8$ and $\lambda_3 = 1$ and for polydisperse droplets (dashed line) with $n = 2$, $\phi_m = 0.76$ and $\lambda_3 = 0.69$. We can observe that the experimental results for both monodisperse and polydisperse suspensions are in excellent agreement with the theoretical correlation in the range of $0.1 < A < 1$. In contrast, a divergence is found for higher values of A which can be due to the inertial effects.

[1] S. R. Kosvintsev, G. Gasparini, R. G. Holdich, I. W. Cumming, and M. T. Stillwell, *Industrial & Engineering Chemistry Research* **44**, 9323 (2005), <https://doi.org/10.1021/ie0504699>.

[2] M. Henschke, L. H. Schlieper, and A. Pfennig, *Chemical Engineering Journal* **85**, 369 (2002).

[3] B. Saint-Michel, S. Manneville, S. Meeker, G. Ovarlez, and H. Bodiguel, *Physics of Fluids* **31**, 103301 (2019).

Summary

- ⇒ Shear-induced migration of monodisperse and polydisperse droplet suspensions was investigated in viscose resuspension in the framework of Suspension Balance Model (SBM).
- ⇒ Particle normal stress was calculated by measuring the concentration profile thanks to light absorption method.
- ⇒ Particle normal stress scales linearly with shear rate up to Capillary $Ca < 0.4$ similar to rigid particles which implies negligible effects of deformability compare to collective effects.

Chapter 6

Viscous resuspension of attractive microcapsules

6.1 Introduction

Suspension Balance Model (SBM) was originally proposed to account for the migration of monodisperse rigid particles in a suspension under shear. In Chapter 5 we showed that this theoretical framework can be extended to the deformable particles (droplets) without taking extra precautions, and even for a polydisperse system. It is interesting to examine this framework for a more complex system of deformable particles as microcapsules which in top of deformability presents long-range attractive interactions and for which solid contact between particles can occur (contrary to droplets).

6.2 Materials and methods

The experimental approach to measure the vertical concentration of particles, which was developed for droplet suspensions, can not be directly implemented for microcapsules. The measurements for droplets were based on light absorption of a dye dissolved in the suspending fluid. The droplets were completely transparent since the refractive indices of both medias were matched precisely to avoid refraction and related errors. In contrast, the microcapsules have an elastic solid shell with a thickness of 10-100 nm, which cannot be index-matched and which partly absorb visible light. As a consequence, the system becomes opaque if its thickness is above a few millimeters, even though both inner and outer phases are index-matched. Although a true absorption technique cannot be used as for the emulsion system, we empirically found that the light absorption is monotonically related to the capsule volume fraction. Consequently, concentration profile measurements for microcapsules could be achieved after calibration. To calibrate the light absorption as a function of microcapsule volume fraction, a large amount of concentrated suspension $\phi = 0.63$ was produced. This concentration was obtained by centrifuging the suspension, however it was verified that the particles were not damaged. Then it was diluted to various concentrations ranging from $\phi = 0.05$ to 0.63 and their light absorbance degree were measured by a camera where the suspensions were placed in a 3 mm cell.

The average size of the particles was $a = 115 \mu\text{m}$ in radius and they were suspended in AK 1000 silicon oil with $\eta_0 = 0.905 \text{ Pa}\cdot\text{s}$ and $\Delta\rho = 155 \text{ kg}/\text{m}^3$ at 25°C . Note that the microcapsule system studied in the Chapter 4 is suspended in silicon oil AP 1000 which induces less attractive interaction between the microcapsules.

Microcapsule suspension was poured into the Taylor-Couette geometry and enough time has been given to the suspension to reach a steady state settled height h_0 . We observed that the

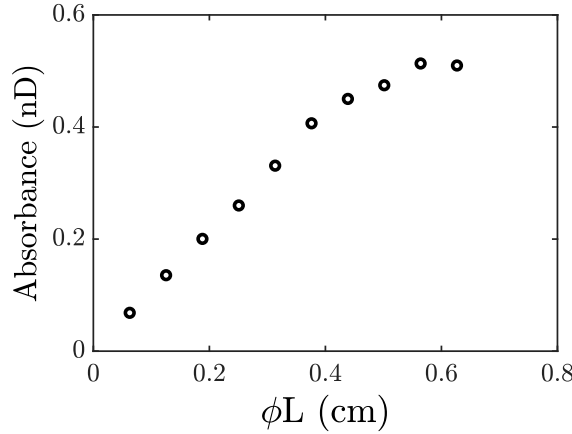


Figure 6.1: Light absorbance of the microcapsules as a function of the concentration of particles multiplied by the light path length

concentration of the particles in the settled layer at the bottom of the geometry was unexpectedly ranging from $\phi = 0.38$ to 0.45 . This is far below the random close packing of hard sphere (0.63) [104] and even below the so-called random loose packing obtained after sedimentation. It is worth noting that we found $\phi_m = 0.80$ for monodisperse droplets. Bright field microscopy measurements of the sedimented microcapsules concentration proved this low values. However, by centrifuging the microcapsules, we could obtain $\phi = 0.63$ thanks to the deformability of the particles. Actually, this phenomenon can be explained by the attractive interactions between the particles (see Chapter 4 for details) which create a sort of branch-like microstructure in the settled layer as shown in figure 6.2.

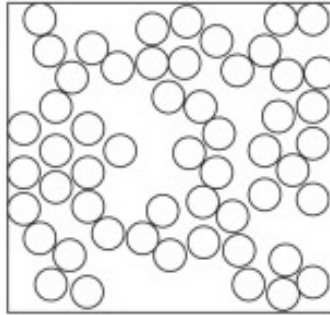


Figure 6.2: Schematic representation of branch like microstructure of sedimented attractive microcapsules [105]

6.3 Results

The normal viscosities $\eta_{n,3}(\hat{x}_3)$ for shear rates ranging from $\dot{\gamma} = 2.7$ to $43.3s^{-1}$ were calculated using the methodology detailed in Chapter 5, i.e. by direct intergration of the volume fraction profiles. They are illustrated in figure 6.3-left as a function of $\phi(\hat{x}_3)$. Additionally, the correlations proposed by Boyer *et al.* with $\phi_m = 0.45$ and $\lambda_3 = 0.3$ (dashed line) and Zarraga *et al.* with $\phi_m = 0.45$ and $\lambda_3 = 0.26$ (solid line) are presented. We observe that contrary to droplets, $\eta_{n,3}$ curves for different shear rates do not collapse in a master curve and by increasing the shear rate systematically it shifts downward. This means that for a given ϕ the normal viscosity depends on the shear rate and exhibits a shear-thinning behavior. It seems that the variation of $\eta_{n,3}$ with $\dot{\gamma}$ is nonlinear and follows a power law with an exponent equal to 0.7 . Rescaling the experimental data by $0.31Sh^{0.3}$ brings to gather $\eta_{n,3}$ curves and they collapse to

a master curve for whole range of ϕ as shown in figure 6.3-right. Note that the parallax issue in experimental setup was completely solved and the averaging of the concentration profiles in the sharp transition to zero was avoided. For more details about parallax issues, see 5. Recently, Sanit-Michel *et al.* [106] and D'Ambrosio *et al.* [107] reported the same behavior for rigid particles where $\eta_{n,3}$ varies non-linearly with $\dot{\gamma}$ and follows a power law with 0.7 for the exponent. However Sanit-Michel *et al.* found a good agreement of $\eta_{n,3}$ with the correlation proposed by Boyer *et al.* while D'Ambrosio *et al.* turned up with Zarraga *et al.* correlation. In our case for deformable attractive microcapsules, the correlation proposed by Boyer *et al.* predicts rescaled $\eta_{n,3}$ accurately in the whole range of ϕ while the correlation of Zarraga *et al.* underestimates the experimental data.

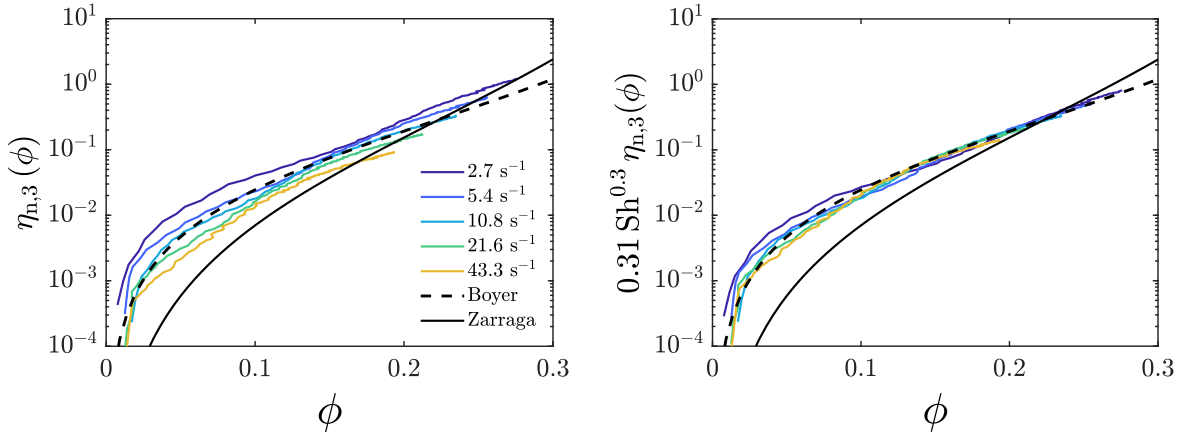


Figure 6.3: **Left:** Normal viscosity $\eta_{n,3}$ as a function microcapsules volume fraction ϕ for shear rates ranging from $\dot{\gamma} = 2.7$ to 43.3 s^{-1} . The dashed line is the correlation proposed by Boyer *et al.* with $\phi_m = 0.45$ and $\lambda_3 = 0.3$ and the solid line corresponds to the correlation proposed by Zarraga *et al.* with $\phi_m = 0.45$ and $\lambda_3 = 0.26$, **Right:** The same data where the normal viscosity has been rescaled by a factor of $0.31 \text{Sh}^{0.3}$.

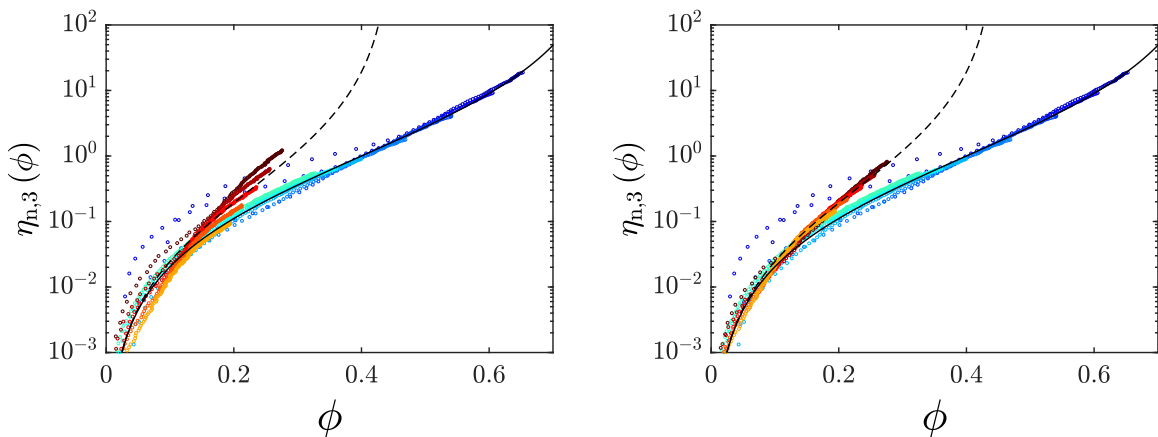


Figure 6.4: Particle normal viscosity as a function of particle volume fraction for droplets (Chapter 5) in cold color code and microcapsules in warm color code. For droplets the shear rate was in the range of $\dot{\gamma} = 6$ to 173 s^{-1} and for microcapsules $\dot{\gamma} = 2.7$ to 43.3 s^{-1} . The lines represent the Boyer correlation with $\phi_m = 0.8$ and $\lambda_3 = 1$ for droplets (solid line) and $\phi_m = 0.45$ and $\lambda_3 = 0.3$ for microcapsules (dashed line). **Left:** Normal viscosity of microcapsules shows a shear thinning where for droplets $\eta_{n,3}$ scales linearly with $\dot{\gamma}$. **Right:** The same data after rescaling of microcapsules $\eta_{n,3}$ by a factor of $0.31 \text{Sh}^{0.3}$.

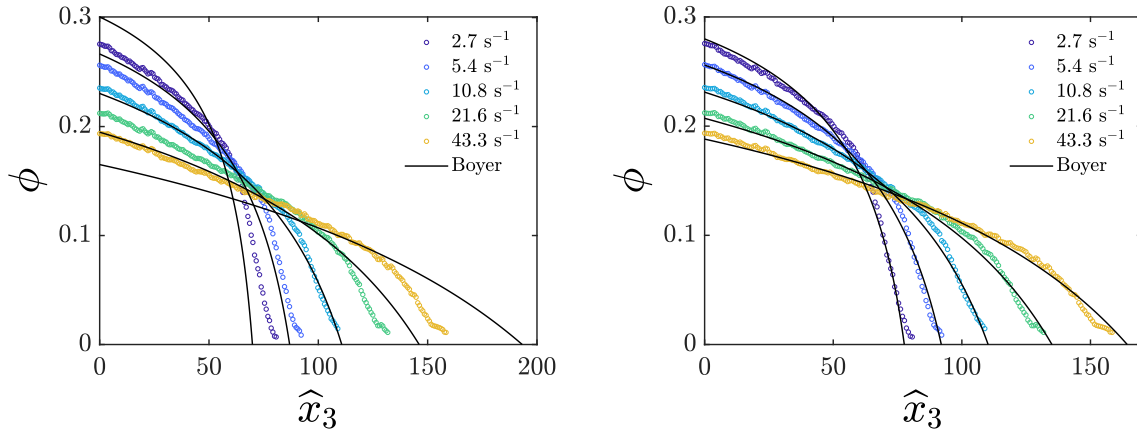


Figure 6.5: **Left:** Vertical concentration profile of resuspended microcapsules as a function of normalized height \hat{x}_3 . The markers are the experimental data and solid line is the correlation proposed by Boyer with $\phi_m = 0.45$ and $\lambda_3 = 0.3$. **right:** Same data where the correlation of Boyer is rescaled by a factor of $0.31 \text{ Sh}^{0.3}$

6.4 Discussion and concluding remarks

The results presented in this chapter show that, similarly to that of viscous resuspension of droplets, the shear-induced migration of micro-capsules is very well accounted by the SBM.

Though deformable, the main characteristic of the system of microcapsules is the presence of long range attraction which results in a yield stress above 45%. Dynamics of resuspension shows that the clusters that forms at rest and at low stress are broken due to shear in the range of shear stress investigated.

We found that the particle normal stress in the vorticity direction is well accounted by a normal viscosity proportional to $\phi^2/(1-\phi/\phi_m)^2$, i.e. Boyer's correlation, in very good agreement with the results we obtained on emulsions, and with the results of Saint-Michel *et al.*. The value of ϕ_m changes drastically from a system to another. It equals 0.8 for droplets, 0.58 for rigid particles and 0.45 for micro-capsules. It is tempting to conclude that the microscopic details of the inter-particle interactions could be mainly hidden in the value of the maximal volume fraction, and that the normal stress form remains otherwise unchanged. Note that this conclusion is not consistent with the set of experimental results recently reported in reference [107]. This discrepancy ask probably for some additional work and in-depth checks of experimental details.

The above conclusion, i.e. the fact the microscopic details of the interparticle interactions only affect ϕ_m is only a rough approximation. Indeed, a significant difference is evidenced between to kinds of systems. Only the normal stress of the suspension of droplet exhibit a linear dependency with respect to the shear rate, as the one of suspension of microcapsules together with the one of rigid spheres are better accounted by a power-law which exponent is about 0.7. The similarity between the systems of microcapsule and the one of rigid particle is striking. Thanks to the study of viscous resuspension of droplet, we can discard the possible role of the microcapsule deformability. The non linear behavior observed might have the same origin as for rigid sphere, since the elastic shell of the capsule is solid-like. A non-coulombian frictional contact might explain this apparent shear-thinning of the normal stress, and we believe that direct studies of these contacts should be interesting to perform in order to clarify this issue.

Summary

- ⇒ Shear-induced migration of deformable attractive microcapsules was investigated in the framework of Suspension Balance Model (SBM).
- ⇒ Particle normal stress exhibits a small shear-thinning, which can be scaled by a power law with an exponent 0.7 as for rigid particles.
- ⇒ Long-range attractive interparticle interaction apparently does not play a role in shear-induced migration and frictional contacts may be the origin of non-linearity of particle normal stress.

Chapter 7

Conclusion and Perspectives

This thesis is mainly dedicated to experimental study of the collective behavior of deformable particles in a dense suspension under shear. Non-Brownian droplets and microcapsules were used as deformable particles. The thesis consists of three main axes: **1.** High throughput production and mechanical characterization of microcapsules, **2.** Shear-induced migration of droplets and microcapsules in viscous resuspension by measuring the particle normal stress, **3.** Steady state and transient rheology of dense microcapsule suspensions.

We developed a method to produce monodisperse microcapsule suspensions in large quantities with tunable size and shell elasticity. The microcapsules were produced by a membrane emulsification system and their shell elasticity were measured in a microfluidic extensional flow. The shell of the microcapsules was assembled at the water-oil interface by complexation of polyelectrolytes or cross-linking of proteins providing two different kinetic processes. The method has two important characteristics: first, a high production rate up to 2 ml/min and a fully automatized measurement of shell elasticity which is capable of treating 1000 microcapsules in one hour, second, the capacity of coupling the production and characterization steps to develop an in-line procedure in order to tune the shell elasticity and studying different kinetics of shell formation. We concluded that the production of the droplets containing chemicals and microcapsule shell formation have to be split into two steps when shell growth is limited by diffusion (e.g. complexation of polyelectrolytes, CH/PFacid). If shell growth is limited by the quantity of reactants encapsulated in the droplet, the variations of elastic properties are directly related to size variations (e.g. cross-linking of proteins, BSA/TC).

Shear-induced migration of droplets and microcapsules was investigated in viscous resuspension which simply consists of shearing a settled suspension in a Taylor-Couette geometry. In such flow, the migration is related to collective effects while other migration mechanisms like wall effect and shear rate gradient are discarded. It allows a precise determination of the particle normal stress, since the volume fraction gradient which appears under shear directly balances buoyancy. Though very simple in principle, this experimental approach needed to be conducted with great care. First, the physical properties of the system should be chosen in a narrow range in order to be able to neglect inertial effects, secondary currents, but also to limit viscous dissipation which tend to increase the temperature, and to limit the duration of the experiments. Second, and when applied to soft systems such as emulsions or capsules, additional requirements were to be taken into account. Not only the system needed to be index matched in order to determine directly the local volume fraction, but also to prevent early coalescence of the particles. The results were consistent both in transient and steady state and with the Suspension Balance Model (SMB) which was originally proposed for rigid particles. We found that the particle normal stress is linear with shear rate for droplets, but microcapsules showed a non-linearity with a power law equal to 0.7, exactly as what was recently reported for rigid particles [107, 106]. These results lead to several conclusions. First, up to Ca 0.4, particle deformability does not play any significant role since the particle normal stress is perfectly linear

with the shear rate for droplets. To our point of view, it would be very difficult to increase Ca further as coalescence or droplet break up would then occur. Second, the same scaling of the particle normal stress found for droplets, microcapsules and rigid particles with $\phi^2/(1 - \phi/\phi_m)^2$ suggests that the exact nature of the short range interparticle interactions do not have a major role in shear-induced migration. The SBM, together with Boyer's correlation for the normal stress, appear to be a very robust framework. Looking into more details, the differences concerning the particle normal stress between those systems are twofolds. On the one hand, they all exhibit a different maximal volume fraction ϕ_m . This was already the conclusions of some simulations on rigid particles where the friction coefficient was varied [108]. This concept might thus be pushed further: the details of interparticle interaction mainly influence the value of ϕ_m . On the other hand, this conclusion is only a rough approximation since both microcapsules and rigid particles exhibit a small but non-negligible shear thinning behavior. The similarity between those systems might come from non-Coulombian friction between the particles.

We have also studied the rheology of a suspension of non-Brownian microcapsules. Similarly to shear-induced migration, we did not observe any influence of particle deformability by varying the shell elasticity. However, we realized that this is likely due to the fact that the system investigated exhibit strong long-range attraction between particles, which clearly dominate the rheological properties. The length scale of these interactions is strikingly huge, a few hundreds of nanometers, and is an originality of the system studied. The physical origin of this attraction remains an open issue, but we can reasonably speculate, in light of the literature and of the spectacular response of the capsules to any electric field, that the polyelectrolyte present in the capsule was able to generate a strong dipolar moment. Such attraction has for consequence the emergence of a yield stress at a volume fraction as low of 0.25, a concentration where any suspension of non-interacting particles would very easily flow. There was no evidence of shear banding, which is probably due to the fact that the particles were relatively confined in the plane-plane geometry. The rheological response of this system can be depicted into two main regimes. An "attraction dominated" regime at low stress is found, where the magnitude of the interparticle interaction dominates the viscous stress, and where big clusters of capsules percolate. The second regime is the shear-induced rupture of the aggregates for which we have an almost Newtonian behavior and where attraction does not play a significant role on the viscosity of the suspension.

In the thesis, we answered many questions, but several others remain unanswered. Additionally, it also opens numerous perspectives. A few are listed below.

1. We focused on viscous resuspension in the vorticity direction, and thus determined $\Sigma_{p,33}$. It would be interesting to investigate with a similar approach viscous resuspension in the shear direction. This could be done thanks to an annular Couette geometry, as in the pioneer work of Leighton and Acrivos. However, the experimental difficulty would then be to determine the volume fraction gradient as accurately as in the Couette cell where direct observation is easier. A possible alternative approach would be to use a shear cell mounted on a confocal microscope.
2. We found that shear-induced migration of deformable particles in a simple flow can be explained in the framework of Suspension Balance Model (SBM) without taking caution of deformability effects. However, other mechanisms for migration exist for deformable particle, such as migration due to the vicinity of a wall in a simple shear, and migration due to shear rate gradients, such as in Poiseuille flow. This rises a question: In a flow of dense deformable suspensions where shear rate gradient is present, do the collective effects dominate yet the effects of the other mechanism ? This will probably depend on the volume fraction. It would be interesting to study droplet migration in a Poiseuille flow for example.
3. In viscous resuspension we could measure the concentration profile of a polydisperse sus-

pension of droplets. We found that shear induced-migration of such suspension is in agreement with SBM predictions in steady state. However we did not have access to spatial size distribution of particles induced by the flow. This rise another question: A suspension with a polydisperse size distribution does show a particle-size structuration under shear ? An extension of the experimental approach used in this thesis would be interesting to develop in that regard. Adding a dye which preferentially goes at the interface between the two phase and with a different wavelength would allow to combine measurement of the volume fraction together with the amount of interface, and thus to a mean particle size. Other experimental approaches could also possible, using high resolution and tomography or confocal imaging.

4. The long-range interaction we evidence for the micro-capsule system clearly asks for more in-depth studies as we were able to observe it directly only qualitatively. Direct force measurements would be interesting and one could reuse the various approach used in biophysics to measure forces : suction with a pipette, optical tweezers ...
5. We were able to characterize the strength of the interaction using rheology (yield stress VS volume fraction, dynamics of the viscous resuspension ...). We limit ourselves to one system, but observed that the interaction can be controlled rather simply by varying the dielectric properties of the suspending fluid. It would therefore be interesting to investigate the rheology of these systems, where the strength of the long-range interaction could be varied. Since some shear-banding and slippage at the wall might happen for attractive systems, it would be important to couple rheometry with some velocimetry techniques, in order to verify these issues.
6. The effect of an electric field on the microcapsules made with a polyelectrolyte are spectacular. We observed some alignments, some odd flow patterns, and huge electric mobilities. These effects were out of the scope of the thesis but are certainly a rich subject of investigations that might deserve some attention.

Bibliography

- [1] A Karnis, HL Goldsmith, and SG Mason. The kinetics of flowing dispersions: I. concentrated suspensions of rigid particles. *Journal of Colloid and Interface Science*, 22(6):531–553, 1966.
- [2] RG Cox and SG Mason. Suspended particles in fluid flow through tubes. *Annual Review of Fluid Mechanics*, 3(1):291–316, 1971.
- [3] Jason E Butler, Paul D Majors, and Roger T Bonnecaze. Observations of shear-induced particle migration for oscillatory flow of a suspension within a tube. *Physics of Fluids*, 11(10):2865–2877, 1999.
- [4] Jason E Butler and Roger T Bonnecaze. Imaging of particle shear migration with electrical impedance tomography. *Physics of fluids*, 11(8):1982–1994, 1999.
- [5] MK Lyon and LG Leal. An experimental study of the motion of concentrated suspensions in two-dimensional channel flow. part 1. monodisperse systems. *Journal of Fluid Mechanics*, 363:25–56, 1998.
- [6] MK Lyon and LG Leal. An experimental study of the motion of concentrated suspensions in two-dimensional channel flow. part 2. bidisperse systems. *Journal of Fluid Mechanics*, 363:57–77, 1998.
- [7] Martin Frank, Douglas Anderson, Eric R Weeks, and Jeffrey F Morris. Particle migration in pressure-driven flow of a brownian suspension. *Journal of Fluid Mechanics*, 493(493):363–378, 2003.
- [8] Denis Semwogerere, Jeffrey F Morris, and Eric R Weeks. Development of particle migration in pressure-driven flow of a brownian suspension. *Journal of Fluid Mechanics*, 581:437, 2007.
- [9] David Leighton and Andreas Acrivos. The shear-induced migration of particles in concentrated suspensions. *Journal of Fluid Mechanics*, 181:415–439, 1987.
- [10] JR Abbott, N Tetlow, AL Graham, SA Altobelli, Eiichi Fukushima, LA Mondy, and TS Stephens. Experimental observations of particle migration in concentrated suspensions: Couette flow. *Journal of rheology*, 35(5):773–795, 1991.
- [11] François Boyer, Olivier Pouliquen, and Élisabeth Guazzelli. Dense suspensions in rotating-rod flows: normal stresses and particle migration. *Journal of Fluid Mechanics*, 686:5, 2011.
- [12] B Chapman. *shear-induced migration phenomena in concentrated suspensions*. PhD thesis, University of Notre Dame, 1990.
- [13] Andrea W Chow, Steven W Sinton, Joseph H Iwamiya, and Thomas S Stephens. Shear-induced particle migration in couette and parallel-plate viscometers: Nmr imaging and stress measurements. *Physics of Fluids*, 6(8):2561–2576, 1994.
- [14] Jeffrey F Morris and Fabienne Boulay. Curvilinear flows of noncolloidal suspensions: The role of normal stresses. *Journal of rheology*, 43(5):1213–1237, 1999.
- [15] Young Won Kim and Jung Yul Yoo. The lateral migration of neutrally-buoyant spheres transported through square microchannels. *Journal of Micromechanics and Microengineering*, 18(6):065015, 2008.
- [16] Adam Zrehen and Arun Ramachandran. Demonstration of secondary currents in the pressure-driven flow of a concentrated suspension through a square conduit. *Physical review letters*, 110(1):018306, 2013.
- [17] Arun Ramachandran and DAVID T LEIGHTON. The influence of secondary flows induced by normal stress differences on the shear-induced migration of particles in concentrated suspensions. *Journal of Fluid Mechanics*, 603:207, 2008.
- [18] BK Chapman and DT Leighton Jr. Dynamic viscous resuspension. *International journal of multiphase flow*, 17(4):469–483, 1991.
- [19] HL Goldsmith and SG Mason. The movement of single large bubbles in closed vertical tubes. *Journal of Fluid Mechanics*, 14(1):42–58, 1962.
- [20] D Ausserre, J Edwards, J Lecourtier, H Hervet, and F Rondelez. Hydrodynamic thickening of depletion layers in colloidal solutions. *EPL (Europhysics Letters)*, 14(1):33, 1991.
- [21] US Agarwal, A Dutta, and RA Mashelkar. Migration of macromolecules under flow: the physical origin and engineering implications. *Chemical Engineering Science*, 49(11):1693–1717, 1994.

- [22] Lin Fang, Hua Hu, and Ronald G Larson. Dna configurations and concentration in shearing flow near a glass surface in a microchannel. *Journal of rheology*, 49(1):127–138, 2005.
- [23] Amit Kumar and Michael D Graham. Margination and segregation in confined flows of blood and other multicomponent suspensions. *Soft Matter*, 8(41):10536–10548, 2012.
- [24] Vincent Mansard. *Non-local rheology of soft glassy materials*. PhD thesis, Bordeaux 1, 2012.
- [25] Jonathan R. Clausen, Daniel A. Reasor, and Cyrus K. Aidun. The rheology and microstructure of concentrated non-colloidal suspensions of deformable capsules. *Journal of Fluid Mechanics*, 685:202–234, 2011.
- [26] Jeffrey F Morris and Bhavana Katyal. Microstructure from simulated brownian suspension flows at large shear rate. *Physics of Fluids*, 14(6):1920–1937, 2002.
- [27] JJJ Gillissen and HJ Wilson. Modeling sphere suspension microstructure and stress. *Physical Review E*, 98(3):033119, 2018.
- [28] S. Mueller, E. W. Llewellyn, and H. M. Mader. The effect of particle shape on suspension viscosity and implications for magmatic flows. *Geophysical Research Letters*, 38(13):1–5, 2011.
- [29] Debra J Audus, Ahmed M Hassan, Edward J Garboczi, and Jack F Douglas. Interplay of particle shape and suspension properties: a study of cube-like particles. *Soft matter*, 11(17):3360–3366, 2015.
- [30] Howard A Barnes. *Handbook of elementary rheology*. University of Wales, 2000.
- [31] Paul F Luckham and Michael A Ukeje. Effect of particle size distribution on the rheology of dispersed systems. *Journal of colloid and interface science*, 220(2):347–356, 1999.
- [32] Sidhant Pednekar, Jaehun Chun, and Jeffrey F Morris. Bidisperse and polydisperse suspension rheology at large solid fraction. *Journal of Rheology*, 62(2):513–526, 2018.
- [33] Élisabeth Guazzelli and Olivier Pouliquen. Rheology of dense granular suspensions. *Journal of Fluid Mechanics*, 852:P11–P173, 2018.
- [34] A. Einstein. Eine neue bestimmung der moleküldimensionen. *Annalen der Physik*, 324(2):289–306, 1906.
- [35] G. K. Batchelor and J. T. Green. The hydrodynamic interaction of two small freely-moving spheres in a linear flow field. *Journal of Fluid Mechanics*, 56(2):375–400, 1972.
- [36] G. K. Batchelor and J. T. Green. The determination of the bulk stress in a suspension of spherical particles to order c^2 . *Journal of Fluid Mechanics*, 56(3):401–427, 1972.
- [37] Jetin E Thomas, Kabir Ramola, Abhinendra Singh, Romain Mari, Jeffrey F Morris, and Bulbul Chakraborty. Microscopic origin of frictional rheology in dense suspensions: Correlations in force space. *Physical review letters*, 121(12):128002, 2018.
- [38] Laurent Lobry, Elisabeth Lemaire, Frédéric Blanc, Stany Gallier, and François Peters. Shear thinning in non-brownian suspensions explained by variable friction between particles. *Journal of Fluid Mechanics*, 860:682–710, 2019.
- [39] François Peters, Giovanni Ghigliotti, Stany Gallier, Frédéric Blanc, Elisabeth Lemaire, and Laurent Lobry. Rheology of non-brownian suspensions of rough frictional particles under shear reversal: A numerical study. *Journal of Rheology*, 60(4):715–732, 2016.
- [40] Christopher Ness and Jin Sun. Two-scale evolution during shear reversal in dense suspensions. *Physical Review E*, 93(1):1–7, 2016.
- [41] Neil Y.C. Lin, Ben M. Guy, Michiel Hermes, Chris Ness, Jin Sun, Wilson C.K. Poon, and Itai Cohen. Hydrodynamic and Contact Contributions to Continuous Shear Thickening in Colloidal Suspensions. *Physical Review Letters*, 115(22):1–5, 2015.
- [42] François Boyer, Élisabeth Guazzelli, and Olivier Pouliquen. Unifying suspension and granular rheology. *Physical Review Letters*, 107(18):1–5, 2011.
- [43] Y. Forterre B. Andreotti and O. Pouliquen. *Granular Media: Between Fluid and Solid*. Cambridge University Press, 2013.
- [44] Anaël Lemaître, Jean-Noël Roux, and François Chevoir. What do dry granular flows tell us about dense non-brownian suspension rheology? *Rheologica acta*, 48(8):925–942, 2009.
- [45] Ronald J Phillips, Robert C Armstrong, Robert A Brown, Alan L Graham, and James R Abbott. A constitutive equation for concentrated suspensions that accounts for shear-induced particle migration. *Physics of Fluids A: Fluid Dynamics*, 4(1):30–40, 1992.
- [46] Prabhu R Nott and John F Brady. Pressure-driven flow of suspensions: simulation and theory. *Journal of Fluid Mechanics*, 275:157–199, 1994.
- [47] Zhiwu Fang, Andrea A Mammoli, John F Brady, Marc S Ingber, Lisa A Mondy, and Alan L Graham. Flow-aligned tensor models for suspension flows. *International journal of multiphase flow*, 28(1):137–166, 2002.

- [48] François Boyer, Élisabeth Guazzelli, and Olivier Pouliquen. Unifying suspension and granular rheology. *Physical review letters*, 107(18):188301, 2011.
- [49] Jeffrey F. Morris. A review of microstructure in concentrated suspensions and its implications for rheology and bulk. *Rheologica Acta*, 48(8):909–923, 2009.
- [50] Ryan M Miller, John P Singh, and Jeffrey F Morris. Suspension flow modeling for general geometries. *Chemical Engineering Science*, 64(22):4597–4610, 2009.
- [51] Daniel Lhuillier. Migration of rigid particles in non-brownian viscous suspensions. *Physics of Fluids*, 21(2):023302, 2009.
- [52] Prabhu R Nott, Elisabeth Guazzelli, and Olivier Pouliquen. The suspension balance model revisited. *Physics of Fluids*, 23(4):043304, 2011.
- [53] JF Richardson and WN Zaki. The sedimentation of a suspension of uniform spheres under conditions of viscous flow. *Chemical Engineering Science*, 3(2):65–73, 1954.
- [54] Ryan M Miller and Jeffrey F Morris. Normal stress-driven migration and axial development in pressure-driven flow of concentrated suspensions. *Journal of non-newtonian fluid mechanics*, 135(2-3):149–165, 2006.
- [55] Isidro E Zarraga, Davide A Hill, and David T Leighton Jr. The characterization of the total stress of concentrated suspensions of noncolloidal spheres in newtonian fluids. *Journal of Rheology*, 44(2):185–220, 2000.
- [56] P. Mills and P. Snabre. Apparent viscosity and particle pressure of a concentrated suspension of non-Brownian hard spheres near the jamming transition. *European Physical Journal E*, 30(3):309–316, 2009.
- [57] Anugrah Singh and Prabhu R Nott. Experimental measurements of the normal stresses in sheared stokesian suspensions. *Journal of Fluid Mechanics*, 490:293, 2003.
- [58] Étienne Couturier, François Boyer, Olivier Pouliquen, and Élisabeth Guazzelli. Suspensions in a tilted trough: second normal stress difference. *Journal of Fluid Mechanics*, 686:26, 2011.
- [59] S Garland, G Gauthier, Jérôme Martin, and JF Morris. Normal stress measurements in sheared non-brownian suspensions. *Journal of Rheology*, 57(1):71–88, 2013.
- [60] Angélique Deboeuf, Georges Gauthier, Jérôme Martin, Yevgeny Yurkovetsky, and Jeffrey F Morris. Particle pressure in a sheared suspension: A bridge from osmosis to granular dilatancy. *Physical review letters*, 102(10):108301, 2009.
- [61] Robin Fahraeus and Torsten Lindqvist. The viscosity of the blood in narrow capillary tubes. *American Journal of Physiology-Legacy Content*, 96(3):562–568, 1931.
- [62] Axel R Pries, Timothy W Secomb, P Gaehtgens, and JF Gross. Blood flow in microvascular networks. experiments and simulation. *Circulation research*, 67(4):826–834, 1990.
- [63] Harry L Goldsmith and Samira Spain. Margination of leukocytes in blood flow through small tubes. *Microvascular research*, 27(2):204–222, 1984.
- [64] John C Firrell and Herbert H Lipowsky. Leukocyte margination and deformation in mesenteric venules of rat. *American Journal of Physiology-Heart and Circulatory Physiology*, 256(6):H1667–H1674, 1989.
- [65] Dmitry A Fedosov and Gerhard Gompper. White blood cell margination in microcirculation. *Soft matter*, 10(17):2961–2970, 2014.
- [66] Jonathan B Freund. Numerical simulation of flowing blood cells. *Annual review of fluid mechanics*, 46:67–95, 2014.
- [67] Rafael G Henríquez Rivera, Xiao Zhang, and Michael D Graham. Mechanistic theory of margination and flow-induced segregation in confined multicomponent suspensions: Simple shear and poiseuille flows. *Physical Review Fluids*, 1(6):060501, 2016.
- [68] Koohyar Vahidkhah and Prosenjit Bagchi. Microparticle shape effects on margination, near-wall dynamics and adhesion in a three-dimensional simulation of red blood cell suspension. *Soft Matter*, 11(11):2097–2109, 2015.
- [69] Jules Dupire, Marius Socol, and Annie Viallat. Full dynamics of a red blood cell in shear flow. *Proceedings of the National Academy of Sciences*, 109(51):20808–20813, 2012.
- [70] Thomas M Fischer, M Stohr-Lissen, and Holger Schmid-Schonbein. The red cell as a fluid droplet: tank tread-like motion of the human erythrocyte membrane in shear flow. *Science*, 202(4370):894–896, 1978.
- [71] Vasily Kantsler and Victor Steinberg. Transition to tumbling and two regimes of tumbling motion of a vesicle in shear flow. *Physical review letters*, 96(3):036001, 2006.
- [72] David Abreu, Michael Levant, Victor Steinberg, and Udo Seifert. Fluid vesicles in flow. *Advances in colloid and interface science*, 208:129–141, 2014.
- [73] Sai K Doddi and Prosenjit Bagchi. Lateral migration of a capsule in a plane poiseuille flow in a channel. *International Journal of Multiphase Flow*, 34(10):966–986, 2008.

- [74] Y Sui, HT Low, YT Chew, and P Roy. Tank-treading, swinging, and tumbling of liquid-filled elastic capsules in shear flow. *Physical Review E*, 77(1):016310, 2008.
- [75] J Walter, A-V Salsac, D Barthès-Biesel, and Patrick Le Tallec. Coupling of finite element and boundary integral methods for a capsule in a stokes flow. *International journal for numerical methods in engineering*, 83(7):829–850, 2010.
- [76] Clément de Loubens, Julien Deschamps, Florence Edwards-Lévy, and Marc Leonetti. Tank-treading of microcapsules in shear flow. *Journal of Fluid Mechanics*, 789:750–767, 2016.
- [77] Alireza Yazdani and Prosenjit Bagchi. Influence of membrane viscosity on capsule dynamics in shear flow. *Journal of Fluid Mechanics*, 718:569, 2013.
- [78] Natacha Callens, Mauricio Hoyos, Pascal Kurowski, and Carlo S Iorio. Particle sorting in a mini step-split-flow thin channel: influence of hydrodynamic shear on transversal migration. *Analytical chemistry*, 80(13):4866–4875, 2008.
- [79] Pierre-Yves Gires, Aparna Srivastav, Chaouqi Misbah, Thomas Podgorski, and Gwennou Coupier. Pairwise hydrodynamic interactions and diffusion in a vesicle suspension. *Physics of Fluids*, 26(1):013304, 2014.
- [80] FR Da Cunha and EJ Hinch. Shear-induced dispersion in a dilute suspension of rough spheres. *Journal of fluid mechanics*, 309:211–223, 1996.
- [81] G Plantard, H Saadaoui, P Snabre, and B Poulligny. Surface-roughness-driven segregation in a granular slurry under shear. *EPL (Europhysics Letters)*, 75(2):335, 2006.
- [82] Michael Levant, Julien Deschamps, Eldad Afik, and Victor Steinberg. Characteristic spatial scale of vesicle pair interactions in a plane linear flow. *Phys. Rev. E*, 85:056306, May 2012.
- [83] Deniz Z. Gunes, Matthieu Pouzot, Martine Rouvet, Stéphane Ulrich, and Raffaele Mezzenga. Tuneable thickness barriers for composite o/w and w/o capsules, films, and their decoration with particles. *Soft Matter*, 7(19):9206–9215, 2011.
- [84] Kaili Xie, Clément De Loubens, Frédéric Dubreuil, Deniz Z Gunes, Marc Jaeger, and Marc Léonetti. Interfacial rheological properties of self-assembling biopolymer microcapsules. *Soft matter*, 13(36):6208–6217, 2017.
- [85] F. Edwards-Lévy, M.-C. Andry, and M.-C. Lévy. Determination of free amino group content of serum albumin microcapsules using trinitrobenzenesulfonic acid: effect of variations in polycondensation ph. *International Journal of Pharmaceutics*, 96(1-3):85–90, Jul 1993.
- [86] Serguei R. Kosvintsev, Gilda Gasparini, Richard G. Holdich, Iain W. Cumming, and Michael T. Stillwell. Liquid-liquid membrane dispersion in a stirred cell with and without controlled shear. *Industrial & Engineering Chemistry Research*, 44(24):9323–9330, 2005.
- [87] D Barthes-Biesel and H Sgaier. Role of membrane viscosity in the orientation and deformation of a spherical capsule suspended in shear flow. *J. Fluid Mech.*, 160:119–135, 1985.
- [88] DOMINIQUE BARTHÈS-BIESEL, ANNA DIAZ, and EMMANUELLE DHENIN. Effect of constitutive laws for two-dimensional membranes on flow-induced capsule deformation. *Journal of Fluid Mechanics*, 460:211–222, 2002.
- [89] Clément de Loubens, Julien Deschamps, Marc Georgelin, Anne Charrier, Florence Edwards-Lévy, and Marc Leonetti. Mechanical characterization of cross-linked serum albumin microcapsules. *Soft Matter*, 10(25):4561–4568, 2014.
- [90] Clement de Loubens, Julien Deschamps, Gwenn Boedec, and Marc Leonetti. Stretching of capsules in an elongation flow, a route to constitutive law. *J. Fluid Mech.*, 767:R3, 2015.
- [91] E. LAC, D. BARTHÈS-BIESEL, N. A. PELEKASIS, and J. TSAMOPOULOS. Spherical capsules in three-dimensional unbounded stokes flows: effect of the membrane constitutive law and onset of buckling. *Journal of Fluid Mechanics*, 516:303–334, 2004.
- [92] Frédéric Blanc, Enzo D’Ambrosio, Laurent Lobry, François Peters, and Elisabeth Lemaire. Universal scaling law in frictional non-Brownian suspensions. *Physical Review Fluids*, 3(11):1–12, 2018.
- [93] F. Gadala-Maria and Andreas Acrivos. Shear-Induced Structure in a Concentrated Suspension of Solid Spheres. *Journal of Rheology*, 24(6):799–814, 1980.
- [94] Ehsan Irani, Pinaki Chaudhuri, and Claus Heussinger. Impact of attractive interactions on the rheology of dense athermal particles. *Physical review letters*, 112(18):188303, 2014.
- [95] Mehdi Maleki, Clément de Loubens, Kaili Xie, Emeline Talansier, Hugues Bodiguel, and Marc Leonetti. Membrane emulsification for the production of suspensions of uniform microcapsules with tunable mechanical properties. *arXiv preprint arXiv:2102.05909*, 2021.
- [96] Serguei R. Kosvintsev, Gilda Gasparini, Richard G. Holdich, Iain W. Cumming, and Michael T. Stillwell. Liquid-liquid membrane dispersion in a stirred cell with and without controlled shear. *Industrial & Engineering Chemistry Research*, 44(24):9323–9330, 2005.

- [97] Roland G Winkler, Dmitry A Fedosov, and Gerhard Gompper. Dynamical and rheological properties of soft colloid suspensions. *Current opinion in colloid & interface science*, 19(6):594–610, 2014.
- [98] Markus Gross, Timm Krüger, and Fathollah Varnik. Rheology of dense suspensions of elastic capsules: normal stresses, yield stress, jamming and confinement effects. *Soft matter*, 10(24):4360–4372, 2014.
- [99] Shirley C Tsai and Kamel Zammouri. Role of interparticular van der waals force in rheology of concentrated suspensions. *Journal of Rheology*, 32(7):737–750, 1988.
- [100] Chen Shi, Bin Yan, Lei Xie, Ling Zhang, Jingyi Wang, Atsushi Takahara, and Hongbo Zeng. Long-range hydrophilic attraction between water and polyelectrolyte surfaces in oil. *Angewandte Chemie International Edition*, 55(48):15017–15021, 2016.
- [101] Lei Xie, Chen Shi, Xin Cui, and Hongbo Zeng. Surface forces and interaction mechanisms of emulsion drops and gas bubbles in complex fluids. *Langmuir*, 33(16):3911–3925, 2017.
- [102] Lydiane Bécu, Sébastien Manneville, and Annie Colin. Yielding and flow in adhesive and nonadhesive concentrated emulsions. *Physical review letters*, 96(13):138302, 2006.
- [103] Adolfo Vázquez-Quesada, Roger I. Tanner, and Marco Ellero. Shear thinning of noncolloidal suspensions. *Phys. Rev. Lett.*, 117:108001, Aug 2016.
- [104] Andrew P. Shapiro and Ronald F. Probst. Random packings of spheres and fluidity limits of monodisperse and bidisperse suspensions. *Phys. Rev. Lett.*, 68:1422–1425, Mar 1992.
- [105] Sümer M. Peker, Şerife Ş. Helvacı, H. Banu Yener, Berrin İkizler, and Alp Alparslan. Solid-liquid two phase flow. pages 167–243. Elsevier, Amsterdam, 2008.
- [106] Brice Saint-Michel, Sébastien Manneville, Steven Meeker, Guillaume Ovarlez, and Hugues Bodiguel. X-ray radiography of viscous resuspension. *Physics of Fluids*, 31(10), 2019.
- [107] Enzo D’Ambrosio, Frédéric Blanc, and Elisabeth Lemaire. Viscous resuspension of non-Brownian particles: Determination of the concentration profiles and particle normal stresses. *Journal of Fluid Mechanics*, 911:1–25, 2021.
- [108] William Chèvremont, Bruno Chareyre, and Hugues Bodiguel. Quantitative study of the rheology of frictional suspensions: Influence of friction coefficient in a large range of viscous numbers. *Physical Review Fluids*, 4(6):1–17, 2019.